New design proposal to mimic the joint structure between bone and hyaline cartilage

Anna Mas Vinyals

UNIVERSITAT RAMON LLULL

DOCTORAL THESIS

Title	New design proposal to mimic the joint structure between bone and hyaline cartilage
Presented by	Anna Mas Vinyals
Centre	IQS School of Engineering
Department	Bioengineering
Directed by	Dr. Salvador Borrós Gómez

C. Claravall, 1-3 | 08022 Barcelona | Tel. 93 602 22 00 | Fax 93 602 22 49 | info@url.edu | www.url.edu

This page left blank intentionally

A la meva família

This page left blank intentionally

Eighty percent of success is showing up.

Woody Allen

This page left blank intentionally

Acknowledgments

Primer de tot, vull donar les gràcies al meu director de tesi, el Dr. Salvador Borrós, qui ara ja fa 7 anys em va donar l'oportunitat de formar part de la gran família GEMAT. Salvador, durant tot aquest temps t'has convertit en molt més que el meu director de tesi. Hem compartit molts bons moments i d'altres que no ho han estat tant. No hi ha paraules per agrair el teu suport sempre, per deixar-me equivocar i ajudar-me a rectificar. Al teu costat he pogut créixer a nivell professional i el que crec més important, a nivell personal. La teva passió pel que fas aconsegueix enganxar-nos, i puc dir amb molta seguretat que no vull que la meva aventura acabi aquí. Se'm fa molt difícil imaginar el moment de dir adeu, i és per això que espero que segueixis sent un dels protagonistes d'aquesta nova etapa que estic apunt de començar. Gràcies per tant!!

Víctor, moltes i moltes gràcies per tot. Has estat sempre disposat a ajudar-me quan m'he encallat i he necessitat escoltar altres punts de vista. Quanta paciència per aconseguir que entengués la química de polímers! Gràcies per aguantar les nostres tonteries i riure sempre que veníem a molestar-te a mode "*suricato*" a la porta del despatx.

I would also like to thank Dr. April Craft from Boston Children's Hospital, Harvard Medical School. Although we haven't had the opportunity to meet in person yet, I am honored for the interest that you have shown towards this work, and sincerely grateful for your support in all our project applications.

També ha fet possible la realització d'aquesta tesi, Bioibérica, S.A.U. Vull agrair a la Dra. Laia Montell Bonaventura, haver-nos proporcionat tot l'àcid hialurònic i el condroitin sulfat que hem necessitat, i per haver mostrat interès en la nostra feina i haver escoltat els nostres avenços.

Com ja he dit abans, a GEMAT som una gran família i aquesta tesi no hagués estat possible sense tots i cadascun de vosaltres. Després d'acabar les pràctiques d'estiu que em van fer arribar a GEMAT vaig decidir quedar-m'hi i fer la tesi de màster. Un cop acabada, com que no n'havia tingut prou, vaig prendre la decisió que m'ha portat a estar escrivint aquestes línies. Evidentment, soc totalment responsable de les meves decisions, però estic segura que no haguessin estat les mateixes si no m'hagués trobat amb tots vosaltres. Núria, Marina, formeu part de l'ànima del grup!! Moltíssimes gràcies a les dues. Núria, al teu costat les llargues estones al DMA i al BOSE han estat més divertides, i Marina...quanta feina a l'AFM! Gràcies al teu esforç vaig poder veure per primera vegada les fibres del meu estimat col·lagen. Un trosset d'aquesta tesi és vostre.

Potser ja és hora de començar a parlar dels meus socis de triumvirat o p*** màfia. Joan, em moro de ganes d'escriure: Moltes gràcies al Gran Dr. Joan Gilabert, però no puc resumir tant. Des del primer dia que vaig posar un peu al laboratori has estat com el meu "germà gran". M'has cuidat molt des del principi, tant a nivell professional com a nivell personal, i has estat sempre al meu costat per ajudar-

me a tirar endavant quan no ho veia gens clar. Per això i molt més, t'has convertit en una persona molt important per mi, sento que tot aquest temps m'ha fet guanyar un gran amic. Robert, ara és l'hora de dir-te que les teves tàctiques de "micro-bullying" funcionen. Pel que dius, el "micro-bullying" és la teva manera de mostrar apreci cap a les persones que t'envolten i sembla mentida però, així t'has convertit en una peça clau del meu dia a dia. Els dies que no hi ets al laboratori, tot i que no he de suportar els teus crits, mai són tant divertits. No sé on serem d'aquí 20 anys (potser serem filòsofs?), ni quin serà el teu despatx, però espero que la connexió que ens permet parlar només mirant-nos als ulls no es perdi mai. Gràcies per haver-te convertit en un amic tant especial.

I aquesta tesi ja no té sentit sense parlar de la Laura. Laura, ara farà un any que et vas incorporar al projecte i ha estat més que suficient per veure que amb tu, està en bones mans. Em fa molt feliç saber que hem aconseguit "abduir-te". T'agraeixo molt la teva capacitat d'esforç, les teves incomptables ganes d'aprendre, la teva passió, la teva humilitat i, sobretot, la paciència per aguantar-me en els moments més difícils. Estic segura que el camí que aviat començaràs estarà ple d'èxits, t'ho mereixes! Tampoc puc oblidar-me de l'Ignasi, que amb el seu TFG, va tenir un paper clau en els meus inicis!

Alba, como alguien dijo una vez..."ets com un raig de llum". Este último año ha sido especialmente difícil, pero gracias a tu sonrisa cada mañana y a todo tu cariño has hecho que cada día fuera más fácil que el anterior. Polete! Què he de dir de tu? A part de que em deus com a mínim 4 costelles per cada cop que em vas aixafar contra la taula amb les teves extremitats descontrolades? Gràcies per totes les discussions filosòfiques i polítiques, per fer-me riure i ser el millor company de "*bacon-queso*" i *jaggers* que algú pugui tenir. Aii, Peri!! Com et trobem a faltar! Ets una persona increïble, m'has ajudat incondicionalment sempre que ho he necessitat, has convertit el meu llenguatge en "Bor-enc" (Ha! Quin paio) i m'emporto per sempre el moment a Can Ruti quan em vas dir: Au va *pamorta*, aparta que ja t'ho faig jo! Laura, Núria, quin bon tàndem de marixoxes! Sort que vau decidir quedar-vos a fer la tesi...voleu ser els nous *sheriffs* de Biomat? *Macarronet*, Nunu, aquests anys compartits amb vosaltres m'han regalat dues bones amigues, sou genials, gràcies!! Mira Mire! M'encanta la teva vitalitat, les teves ganes de fer coses i com has estat capaç de liar-me (totalment contra la meva voluntat) més d'un dijous. Cris, eres la clara demostración de que perseguir nuestros sueños tiene recompensa. Tienes una fuerza envidiable y consigues transmitir tu alegría a los demás. Manu, lo prometido es deuda, ¿cómo no ibas a aparecer? Te has convertido en uno más, y aunque no trabajes con nosotros, siempre apareces en los momentos más divertidos. I ara arriba el torn dels calvos. Tito, ¿quién nos iba a decir cuando éramos compañeros de promoción que compartiríamos la etapa de redacción de tesis? Muchas gracias por estar ahí cuando es más necesario. ¿Ahora me vas a contar tu secreto o aún no? Germán, les teves excentricitats et fan únic i el bon rotllo que desprens ho fa tot més fàcil, gràcies!! Mario, un poco como Manu, haces tu aparición estelar en los mejores momentos. Gracias por estar siempre dispuesto a ayudar y por decir: ¡Quilombo! y alegrar la noche. Pau, encara que no haguem coincidit tant pel lab, quan ho hem fet m'has al·lucinat amb les teves idees i el do tant especial que tens per la ciència. Ara arriba el torn dels més jovenets del grup: Patri, Tony quins bons fitxatges! Per descomptat sou carn de GEMAT…espero poder seguir compartint moments amb vosaltres. I el grup no seria el mateix sense l'Anna, la Carloteta i l'Ari. Tenir TFM's com vosaltres és genial, però ens ho

feu passar malament quan marxeu! I dit això, vull agrair també a la Teresa el seu pas pel lab. Teresa!! Tenemos ganas de verte...esto ya no es lo mismo sin la vasca. Óscar, amb tu vaig compartir els inicis a Biomaterials i quin equip més perillós que fèiem. Gràcies per tot el que em vas ensenyar, i sobretot per haver contribuït a que avui estigui escrivint aquestes línies.

També m'agradaria donar les gràcies al *team* Sagetis. Elena, siempre serás "la mama". ¡¡Cómo nos cuidaste cuando aterrizamos en el grupo como jovencitos confusos...Muchas gracias por todo!! Irene, amb tu vaig conèixer el meravellós món de les cèl·lules. Vas estar al meu costat ensenyant-m'ho tot fins que vaig ser capaç de treballar jo sola. Gran part d'aquesta tesi també és teva, gràcies! Cris, tot i anar sempre atabalada amunt i avall, sempre ets allà quan t'hem necessitat, t'has convertit en una peça clau del lab! Anna, moltes gràcies pel teu suport, per haver-me ajudat a dissenyar els meus primers experiments amb cèl·lules i haver-me ajudat a patir menys els *Westerns*...Miguel Ángel, gracias por estar siempre dispuesto a resolver cualquier duda. No puc oblidar-me de Teixits, especialment de la Cate i la Cris Castells. Noies, moltíssimes gràcies per haver estat sempre disposades a ajudar-me, haver-me explicat els "truquillos" dels cultius 3D i de l'anàlisi de PCR.

Encara que a vegades no ho sembli, també hi ha vida fora d'IQS. És per això que m'agradaria agrair a l'Alba, la Sandra, la Laia, la Laura, la Mireia, la Pati, la Valeria, la Vero, l'Emma, i la Maria el seu suport incondicional. Aquest últim any ha estat ple de canvis, i més d'una de nosaltres hem hagut de superar algun entrebanc. Tot i així, hem demostrat que som una gran família i que juntes podem amb tot i més. Gràcies per estar sempre al meu costat i valorar d'una manera tant especial el que faig. Em sento molt orgullosa de totes i cadascuna de vosaltres, de la vostra força i de la passió amb la que viviu cada dia.

Cris, a tu també t'he d'agrair haver estat tots aquests anys al meu costat. Vam patir moltes hores d'estudi, però sobretot al teu costat vaig viure els moments més divertits i bojos de la carrera. La teva amistat és una de les millors coses que m'emporto d'IQS.

Finalment m'agradaria donar les gràcies a la meva família. A la meva mare, per ser-hi sempre i per viure les nostres vides com si fossin la seva. Admiro la teva gran força i el teu esperit lluitador. Gràcies al teu suport, tot es fa més fàcil. Adrià, la teva manera de veure les coses és un gran exercici de relativitat que realment funciona molt bé en moments com aquest. Al meu pare, que m'ha transmès el bon humor i el caràcter ambiciós, necessari per donar sempre un pas endavant. Al Jordi i a la Mireia, amb qui des que ha arribat la Mariona a les nostres vides, hem aconseguit veure'ns més sovint, com ha de ser. No puc acabar sense agrair als meus tiets, i de nou a la meva mare, haver-me obert les portes de casa seva quan més ho necessitava. I precisament per això, als avis, que els últims mesos han estat molt presents. Qui m'anava a dir que escriuria aquesta tesi al racó on vau passar tantes hores! Per tot això i molt més, aquesta tesi és vostra.

Anna Mas Vinyals, 7 de Juliol de 2018

This page left blank intentionally

This thesis has been made thanks to the fellowship grant of personal novice investigator (FI) SUR funded by the DEC of the Government of Catalonia and the European Social Fund.

Credentials:

[2016FI_B 00255]

[2017FI_B1_00114]

[2018FI_B2_00137]

Generalitat de Catalunya
Departament d'Empresa i Coneixement

Unió Europea
Fons social europeu
L'FSE inverteix en el teu futur

This thesis has also been made thanks to the fellowship grant for the doctorate degree of IQS School of Engineering (2015).

IQS
PERSONA CIENCIA EMPRESA
UNIVERSITAT RAMON LLULL

This page left blank intentionally

Abstract

New design proposal to mimic the joint structure between bone and hyaline cartilage

In medical device engineering, there are several cases where there is an imperative need of obtaining bioresponsive surfaces to achieve an optimal integration of a certain biomaterial with the surrounding tissue. Surface engineering has provided different approaches, however for certain applications obtaining an intimate bonding between the tissue and the implant remains a clinical challenge. In this work, we present a newly developed technique that allows the obtention of biomimetic surfaces onto any substrate that can be subject to plasma modification.

As a proof of concept, we have applied the technology to obtain a heterogeneous scaffold for osteochondral repair, which has a great potential to be used as regenerative therapy. One of the great challenges in osteochondral repair is achieving a high degree of mimicry of the whole joint structure, from the subchondral bone to the surface of hyaline cartilage. Our methodology allows the immobilization of a cartilage-like hydrogel onto a bone-like bioceramic platform by means of a polymeric coating. The bioceramic acts not only as mechanical support and anchoring point to the subchondral bone, but also it acts as a reservoir of calcium and phosphate ions, which through diffusion help in the creation of the stiffness gradient present in joints.

Thus, in the present thesis, we have worked on the design of the different parts that will form the osteochondral heterogeneous scaffold. First, to gain insight into the stiffness gradient creation, we have studied the bioactivity of different commercially available bioceramic bone substitutes, which are potential candidates to be used as bone-like platform. Next, we have validated the viability of the polymeric coating obtained through PECVD in this type of biomaterials and shown how it does not compromise their bioactive properties. Moreover, we have demonstrated how the designed surface modification allows the obtention of a stable interface, which is not disrupted by physiological changes, that enables the subsequent self-assembly of a cartilage-like hydrogel. *In vitro* studies show how our immobilizing technology preserves cell viability, and that our hydrogel formulation enables cell migration as well as it provides a suitable environment for both chondrogenic and osteogenic differentiation of mesenchymal stem cells.

This page left blank intentionally

Resumen

New design proposal to mimic the joint structure between bone and hyaline cartilage

En el diseño de dispositivos médicos existen numerosos casos en los que es necesaria la utilización de superficies bioactivas para lograr la integración óptima de un implante con el tejido que le rodea. La ingeniería de superficies propone diferentes soluciones, sin embargo, en determinadas aplicaciones, la obtención de una unión íntima entre el tejido y el implante aún es un reto clínico. En el presente trabajo, presentamos una técnica que permite la obtención de superficies biomiméticas en cualquier sustrato que pueda ser sometido a modificación por plasma.

Como prueba de concepto, hemos aplicado la tecnología desarrollada en la obtención de un *scaffold* heterogéneo para la regeneración del tejido osteocondral, con un gran potencial para ser usado como terapia regenerativa. Uno de los grandes retos en la regeneración osteocondral, es lograr un grado elevado de semejanza con la estructura articular, desde el hueso subcondral hasta la superficie articular. Nuestra metodología permite la inmovilización de un hidrogel que imita el tejido cartilaginoso en la superficie de una plataforma bioceràmica, la cual reproduce el hueso. Ésta última, actuará como soporte mecánico y punto de anclaje al hueso subcondral, a la vez que proporcionará un reservorio de iones de calcio y fosfato que ayudarán en la creación del gradiente de dureza presente en las articulaciones.

Así pues, en esta tesis hemos trabajado en el diseño de las diferentes partes que conformaran el *scaffold*. En primer lugar, para profundizar en la creación del gradiente de dureza, hemos estudiado la bioactividad de diferentes sustitutos óseos biocerámicos comerciales, los cuales son candidatos potenciales para ser utilizados en la construcción del scaffold. A continuación, hemos validado la viabilidad del recubrimiento polimérico obtenido por PECVD en sustratos biocerámicos y hemos demostrado como no compromete su bioactividad. Además, hemos demostrado como la modificación superficial permite la obtención de una interfaz estable, que no se altera por cambios fisiológicos, la cual permite el autoensamblaje del hidrogel. Los estudios *in vitro* realizados demuestran que la tecnología de inmovilización preserva la viabilidad celular, y que la formulación permite la migración celular además de proporcionar un entorno adecuado para la diferenciación condrogénica y osteogénica de células madre mesenquimales.

This page left blank intentionally

Resum

New design proposal to mimic the joint structure between bone and hyaline cartilage

En el disseny de dispositius mèdics existeixen diversos casos en els quals és necessària la utilització de superfícies bioactives per aconseguir la integració òptima d'un implant amb el teixit que l'envolta. L'enginyeria de superfícies planteja diferents solucions, tot i així, per algunes aplicacions, l'obtenció d'una unió íntima entre el teixit i l'implant encara és un repte clínic. En aquest treball, presentem una tècnica que permet obtenir superfícies biomimètiques en qualsevol substrat que pugui ser sotmès a modificació per plasma.

Com a proba de concepte, hem aplicat la tecnologia desenvolupada en l'obtenció d'un *scaffold* heterogeni per la regeneració del teixit osteocondral, amb un gran potencial per ser utilitzat com a teràpia regenerativa. Un dels grans reptes en la regeneració osteocondral, és assolir un grau elevat de semblança amb l'estructura articular, des de l'òs subcondral fins a la superfície articular. La nostra metodologia permet la immobilització d'un hidrogel que imita el teixit cartilaginós a la superfície d'una plataforma bioceràmica, la qual reprodueix el teixit ossi. Aquesta última, actuarà com a suport mecànic i punt d'ancoratge a l'òs subcondral, a la vegada que proporcionarà un reservori de ions de calci i de fosfat que ajudaran a la creació del gradient de duresa present en les articulacions.

Així doncs, en aquesta tesi hem treballat en el disseny de les diferents parts que conformaran el *scaffold*. En primer lloc, per tal d'aprofundir en la creació del gradient de duresa, hem estudiat la bioactivitat de diferents substituts ossis bioceràmics comercials, els quals son candidats potencials per ser utilitzats en la construcció del scaffold. A continuació, hem validat la viabilitat del recobriment polimèric obtingut per PECVD en substrats bioceràmics i hem demostrat que no compromet la seva bioactivitat. A més, hem demostrat que la modificació superficial permet l'obtenció d'una interfície estable, que no es veu alterada per canvis fisiològics i permet l'autoensamblatge de l'hidrogel. Els estudis *in vitro* realitzats demostren que la tecnologia d'immobilització preserva la viabilitat cel·lular, i que la formulació permet la migració cel·lular a més de proporcionar un entorn adequat per la diferenciació condrogènica i osteogènica de cèl·lules mare mesenquimals.

This page left blank intentionally

Table of Contents

Index of Figures

Index of Tables

This page left blank intentionally

List of Abbreviations

AAS	Atomic adsorption spectroscopy
ACI	Autologous chondrocyte implantation
ADMSCs	Adipose-derived mesenchymal stem cells
AFM	Atomic force microscopy
BCP	Biphasic calcium phosphate
BSA	Bovine serum albumin
cDNA	complementary deoxyribonucleic acid
DAPI	4’,6 – Diamino-2-phenylindole dihydrochloride
DC	Duty Cycle
DMEM	Dulbecco’s Modified Eagle Medium
ECM	Extracellular matrix
FBS	Fetal bovine serum
FGF	Fibroblast growth factor
G’	Storage modulus
GAG	Glycosaminoglycan
HA	Hydroxyapatite
hBMMSCs	Human Bone marrow mesenchymal stem cells
hNDFs	Human Normal dermal fibroblasts
MACI	Matrix-induced autologous chondrocyte implantation
MP	Multiphoton
mRNA	messenger Ribonucleic acid
MSCs	Mesenchymal stem cells
OA	Osteoarthritis
PBS	Phosphate Buffered Saline
PCL	poly(e-caprolactone)
PECVD	Plasma enhanced chemical vapor deposition
PEG	Polyethylene glycol
PFM	Pentafluorophenyl methacrylate
PGA	Polyglycolic acid
PLGA	poly(lactic-co-glycolic acid)
PLLA	poly(l-lactic acid)
PTFE	Polytetrafluoroethylene
PU	Polyurethane
QCM-D	Quartz crystal microbalance with dissipation
RF	Radiofrequency
RMS	Surface roughness
RNA	Ribonucleic acid
RT-PCR	Real Time - Polymerase Chain Reaction
RUNX2	Runt-related transcription factor 2
SBF	Simulated body fluid
SEM	Scanning electron microscopy
SHG	Second harmonic generation
TC	Tropocollagen
TGF-β1	Transforming growth factor β1
XRD	X-ray diffraction

α-MEM	Minimum essential medium eagle – alpha modification
β-TCP	β tricalcium phosphate

Chapter I. Introduction: Osteochondral repair

This page left blank intentionally

Introduction: Osteochondral repair

The present chapter summarizes the current strategies for osteochondral repair, which due to the complex structure of articular cartilage, lead to non-optimal result. The imperative need to improve the outcomes of the existing cartilage repair techniques has motivated the orthopedic research community to seek for new methods. This thesis will focus on the development of a biomimetic scaffold that reproduces the heterogenicity of the osteochondral unit, from the subchondral bone to the articular cartilage.

1.1 Introduction

As life expectancy has increased over the years, population has become more susceptible to non-communicable or chronic diseases, mainly musculoskeletal diseases[1]. Their burden increase is caused to a large extent by aging, and unfortunately, it is expected to keep increasing with the aging of the global population[2].

Musculoskeletal conditions encompass a wide spectrum of disorders, from those of short duration to lifelong disorders, which include osteoarthritis, rheumatoid arthritis, osteoporosis and low back pain[3]. Joint pain constitutes the major cause of disability and pain in middle-aged and older people, more specifically, it has been estimated that half the world's population over 65 years old suffers from osteoarthritis, which is the disorder of articulating joints in humans with a higher prevalence[4]. Osteoarthritis involves the degradation of articular cartilage, thickening of the subchondral bone, osteophyte formation and variable degrees of synovium inflammation[5]. It is characterized by the loss of extracellular matrix (ECM) components, such as collagen and proteoglycans, which perturbs the ECM and flaws tissue's biomechanical properties[6].

Due to its avascular nature, cartilage shows a low tendency for self-repair as it is difficult for progenitor cells to access the damaged site. Thus, even minor injuries may be maintained for years and can eventually lead to progressive damage and osteoarthritic joint degeneration[7].

Back in 1743, the anatomist William Hunter wrote: "Cartilage injury is a troublesome problem […] that, once destroyed it is not recovered"[8]. Since then, different approaches to heal the damaged tissue have been proposed, however, the complete repair of articular cartilage defects still represents a clinical challenge.

The first studies to assess the regenerative potential of autologous chondrocytes were performed back in 1970s by William Green. Using a rabbit model, he tested the potential of autologous and homologous chondrocyte transplantation for articular cartilage repair[9]. His studies marked the beginning of a new era in what was to become the field of cartilage tissue engineering.

Despite the efforts on developing cell-based therapies, by 1980s, procedures such as chondroplasty, microfracture surgery and abrasion arthroplasty and were the most common treatments for the repair of cartilage defects. Chondroplasty is a palliative procedure that consists on trimming and smoothening roughened arthritic joint surfaces to eliminate mechanical sources of pain and dysfunction[10]. Abrasion arthroplasty consists on the superficial abrasion to remove dead osteons and expose viable bone and surface vascularity[11]. Microfracture implies puncturing of the subchondral bone to induce bleeding, which will allow the release of stem cells into the defect site[12]. However, these procedures give poor results as they lead to fibrocartilaginous tissue.

Aiming to overcome the limitations of the before mentioned techniques and following the line of Green, a group of orthopaedic researchers at the Hospital for Joint Diseases in New York City suggested that a cell-based approach could be used for hyaline cartilage repair. Their interest in finding an approach to heal damaged cartilage was motivated by the fact that some of their patients were too young to apply a total joint arthroplasty as it results in joint pain and disability. Using a rabbit model, their strategy consisted of extracting a biopsy of cartilage and extracting the chondrocytes. Then, cells were expanded in vitro and transplanted again using a periosteum flap to minimize cell leakage from the defect[13,14]. This clinical practice is now known as autologous chondrocyte implantation (ACI). As the obtained results at the preclinical stage were promising, the first human trials using the same protocols were performed[15]. Later, randomized clinical trials were performed and ACI showed superior results than those obtained applying microfracture[16].

It must be noticed that ACI implies the implantation of chondrocytes in suspension, which may lead to cell leakage, heterogeneous cellular distribution within the defect[17] and loss of chondrogenic phenotype due to dedifferentiation during monolayer expansion[18]. To surmount such limitations, biodegradable cell-carrier three-dimensional scaffolds have been developed. The first approach was the matrix-induced autologous chondrocyte implantation (MACI) technique. The MACI matrix is built up of a porcine type I/type III bilayer membrane seeded with chondrocytes[19]. The membrane can be fixed directly with fibrin glue and it doesn't require a cover avoiding periosteum harvesting and reducing the time of surgery. No significant differences between ACI and MACI are observed in short term clinical trials[19]. MACI was first developed and marketed in 1999 by Verigen AG (Leverkusen, Germany) and finally acquired by Vericel Corporation (Cambridge, MA) in 2014. It gained EMA's marketing approval, however the license was withdrawn upon the closing of the manufacturing site in Denmark. Figure I-1 shows a schematic diagram of the ACI procedure and a diagram comparing ACI and MACI techniques.

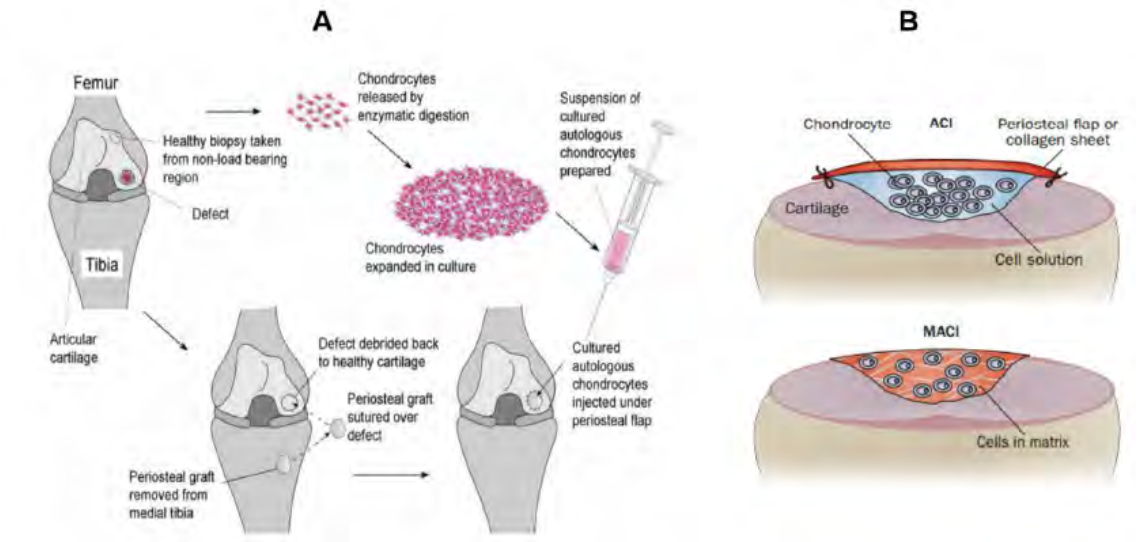

Figure I-1. Cell-based cartilage regeneration techniques. **(A)** Diagram showing the different stages involved in the process of autologous chondrocyte implantation[20]. **(B)** Diagram of both ACI (ACI-P or ACI-C) and MACI (Adapted from Ringe et al.[21])

Still today, the most commonly used surgical procedures to treat damaged articular cartilage in the knee are the before mentioned chondroplasty and microfracture, despite they present several shortcomings[22]. Aiming to overcome the limitations of currently used techniques, different cell-based tissue engineering approaches have emerged, and some of them, such as NOVOCART® 3D and CaReS®, are under clinical trials. These approaches rely on the use of cell-embedded scaffolds to mimic the cartilage tissue.

NOVOCART® 3D (TETEC, Melsungen, Germany) consists of a biphasic type I collagen scaffold seeded with autologous chondrocytes. One layer consists in a dense, cell-impermeable membrane derived from bovine pericardium. The membrane is lyophilized together with a collagen sponge layer, consisting of type I collagen and chondroitin sulphate, allowing the two layers to be firmly connected. At this point, a Phase III trial (n=233) is under development. CaReS® (Arthro Kinetics Biotechnology, Krems, Austria) consists of a type I collagen hydrogel embedded with primary autologous chondrocytes. It has been used in select European Countries and is also approved in Iran, Turkey and China. There is a cell-free version of this product commercially available as CaReS®-1S.

Some of these products are described as second- or third- generation ACI, but they constitute the first generation of tissue engineered cartilage products. However, there is still the need for developing a scaffold that mimics the complete osteochondral junction instead of focusing independently on the cartilage-layer or the bone-layer. To obtain a good reproduction of the osteochondral unit, it is critical to take a closer look into its complex structure, which is responsible of the tissue's functionality.

The articular cartilage hydrated extracellular matrix is the key element of the tissue functionality, and its composition is essential to enable the shock absorbance. It is mainly composed of water (70-80%) embedded into a meshwork of type II collagen fibers that confer tensile support. Proteoglycans, mainly aggrecan, are the other major component of cartilage and are responsible for the compressive strength and the shock absorbing capability of the tissue. Aggrecan, is composed of a core protein with covalently attached sulphated glycosaminoglycans (GAGs), chondroitin sulphate and keratan sulphate. In the cartilage ECM, aggrecan is present in the form of aggregates composed of a hyaluronic acid filament with non-covalently attached aggrecan molecules[23]. In the presence of water, aggrecan swells because of the hydration of GAG chains. This swelling is constrained by the collagen network, and under compression, water molecules are displaced and aggrecan molecules get closer. After unloading, water molecules are drawn back into the tissue[24].

Furthermore, the matrix of articular cartilage presents a highly hierarchical structure as it is arranged in four distinct zones, the superficial or tangential zone, the middle transitional zone, the deep radial zone and the calcified zone[25,26]. As it is illustrated in Figure I-2, each zone is characterized by a specific ECM composition and organization, which leads to different mechanical properties[27]. The superficial zone is the thinnest and can be divided into two layers, an acellular sheet of collagen fibers that covers the joint, and a layer with flattened chondrocytes with their axes parallel to the articular surface. It presents a high collagen concentration and low glycosaminoglycans levels, and its organization gives the superficial zone high tensile strength[28]. In the middle zone, collagen fibers are larger and randomly oriented, chondrocytes present spherical shape and are surrounded by a high concentration of proteoglycans. In the deep zone, spherical chondrocytes are organized in columns as well as collagen fibers, which are oriented perpendicularly to the bone surface. Here, the proteoglycan concentration reaches its maximum while water content reaches its minimum value. Finally, the calcified zone secures the articular cartilage to the underlying subchondral bone with collagen fibers that pass from the deep zone of cartilage to the subchondral bone[29]. It acts as a transition from soft hyaline cartilage to bone. This zone, has to withstand significant shear stress due to the transition from the soft cartilage to the much stiffer bone[30].

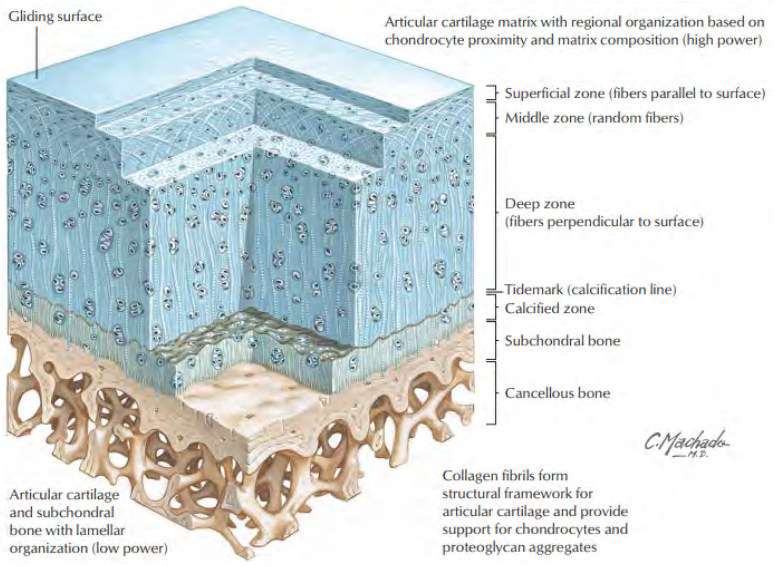

Figure I-2. Illustration of the osteochondral unit[29]. The scheme shows the different zones in which mature cartilage is structured. It reflects phenotypic differences and changes in ECM composition and distribution. Both collagen and glycosaminoglycans content, as well as its orientation and distribution are highly influenced by its location.

As cartilage tissue is anisotropic and presents a heterogeneous structure the use of homogeneous scaffolds for tissue repair leads to non-optimal results. Hence, one of the great challenges of scaffold design for osteochondral repair is to reproduce the gradient structure of the osteochondral unit from the subchondral bone to articular cartilage[31]. Mimicking the mechanical properties of the calcified layer is critical, as it must withstand the high shear stress generated between the stiff bone tissue and the soft cartilage. Thus, interface tissue engineering emerges, from the need of integrating tissue-to-tissue interfaces, as the junction between cartilage and bone. One strategy consists in developing heterogeneous scaffolds, which exhibit phase-specific structural and material properties, with a gradual change in mechanical properties across the scaffold phases, similar to that of the native tissue[32].

The first generation of heterogeneous scaffolds consisted of stratified designs, obtained by fusing together a bone-like and a cartilage-like scaffold[32]. Schaefer et al.[33] reported a biphasic scaffold consisting of a cartilage-like polyglycolic acid (PGA) mesh with chondrocytes and a bone-like poly(lactic-co-glycolic acid) (PLGA)/polyethylene glycol foam seeded with periosteal cells. Gao et al. also proposed a seeded mesenchymal stem cells (MSCs) on a hyaluronan sponge with transforming growth factor β1 (TGF-β1) to induce chondrogenesis joined with an osteogenic porous calcium phosphate scaffold seeded with MSCs using fibrin glue. Chen et al. developed a biphasic scaffold to mimic the osteochondral junction. The cartilage-like layer was made of a collagen sponge, with relatively low mechanical strength, while the bone-like layer was a composite sponge of PLGA with higher mechanical strength[34].These pioneer studies demonstrated the possibility of creating multiphasic scaffolds and engineering different tissues in the same construct. However, these first models do not mimic the interface between the two tissues. Next steps focused on reproducing the osteochondral interface and incorporating it in the

stratified scaffold design. In example, Jiang et al. proposed a continuous multi-phasic osteochondral scaffold consisting of a hydrogel as cartilage-like layer, a polymer-ceramic composite as bone-like layer and an interfacial region between composed of a hybrid between the hydrogel and the polymer-ceramic composite[35]. Kon et al. have conducted a pilot clinical trial to test the use of a multilayer scaffold obtained by freeze drying and composed of type I collagen for the cartilage-like layer, a mixture of collagen type I (60%) and hydroxyapatite (40%) as tidemark layer and collagen type I (30%) and hydroxyapatite (70%) for osteochondral repair[36,37].

However, such stratified designs are susceptible of delamination and present abrupt changes in physical and chemical properties[38] which give poor results as the resulting scaffolds may lead to poor tissue quality and mechanical failure. Gradient approaches may help to overcome the drawbacks of stratified scaffolds, as they present a higher resemblance with biological interfaces with gradual property changes[39]. The need of integrating different tissues with different properties, such as bone and cartilage, to successfully achieve the regeneration of complex orthopedic interfaces, has been the motivation for the development of a new generation of scaffolds in orthopedic tissue engineering.

Hydrogels have attracted a great deal of attention thanks to their intrinsic capacity of mimicking the extracellular matrix and their highly tunable physico-chemical and mechanical properties[40], which make them great candidates for gradient creation. Biomimetic gradient hydrogels present continuous changes in their properties which leads to a high degree of resemblance with tissue interfaces that present zonal organization, such as the osteochondral unit[41].

Regarding their nature, hydrogels can be classified into natural, synthetic, or natural/synthetic biomaterials. Synthetic hydrogels provide a well-defined environment and a high tunability. Moreover, they can be produced under controlled conditions, and present predictable and reproducible mechanical and physical properties[42]. The most used synthetic polymers are poly(L-lactic acid) (PLLA), poly(glycolic acid) (PGA), poly(ε-caprolactone) (PCL), poly(ethylene glycol) (PEG), poly(urethane) (PU) and poly(vinyl alcohol)[43]. Hydrogels made of natural polymers present a high biocompatibility, are inherently biodegradable and bioactive moieties, such as Arg-Gly-Asp (RGD), can be found in their structures. Natural polymers such as alginate[44], hyaluronic acid[45,46], fibrin[47] and collagen[48] have been widely studied for cartilage tissue engineering. The present work is focused on natural polymers, as they are specifically attractive for cartilage tissue engineering, as they can induce *per se* cell adhesion, migration, proliferation and matrix production. Specifically, we have chosen type I atelocollagen as the main constituent of the scaffold. There are reluctances of using collagen as scaffolding material, motivated by the generation of immunologic response after implantation. However, the fact that antigenic determinants on the peptide chains of type I collagen reside mainly on telopeptide regions has motivated the use of atelocollagen as scaffold material[49].

Following the approach of biomimetic gradient hydrogels, Zhu et al.[41] proposed that a stiffness gradient could induce a zone-dependent response of cells embedded in a hydrogel. To demonstrate their hypothesis, they worked with a PEG and chondroitin sulphate methacrylate hydrogel, and through photopolymerization they achieved different degrees of crosslinking, which lead to a stiffness gradient creation from the much stiffer cartilage deep zone to the softer superficial zone. They observed differences in cell morphology and extracellular matrix components, mainly collagen type II and glycosaminoglycans, production through the hydrogel structure.

Despite the several attempts to reproduce the osteochondral junction, the recreation of a stable interface between articular cartilage and subchondral bone still remains a challenge[50]. In this work, focusing on the principles of gradient hydrogels but aiming to go one step further, we introduce in the scaffold design a bioceramic platform which enables subchondral bone mimicry. The latter, together with a collagen-based hydrogel will allow the tissue interface creation when in contact with physiological fluids.

Thus, the main objective of this thesis is the development of a biomimetic scaffold for osteochondral repair based on a cartilage-like self-assembled collagen-based hydrogel, containing hyaluronic acid and chondroitin sulphate, attached to a bone-like bioceramic platform. The bioceramic platform will not only act as a mechanical support by promoting the integration of the implant with the subchondral bone but will also provide means for a stiffness gradient creation acting as a reservoir of calcium and phosphate ions, which in contact with physiological fluids will be able to diffuse through the hydrogel structure and nucleate on collagen fibers.

To achieve the main goal of this work, this thesis has been structured in the following work plan:

- Evaluation of different commercial bone substitute bioceramics as potential candidates to obtain a bone-like platform which mimics the subchondral bone and validation of the polymeric coating as linking interface **(Chapter II).**

- Development and characterization of a self-assembling cartilage-like hydrogel formulation. Evaluation of its interaction with the bone-like platform **(Chapter III).**

- *In vitro* testing of cell-homing capacity, chondrogenic and osteogenic potential of the developed formulation **(Chapter IV).**

1.2 Content of this Dissertation

The use of heterogeneous scaffolds for osteochondral tissue engineering has been considered, as it is critical to mimic the calcified zone that constitutes the interface between bone and hyaline cartilage to ensure the joint regeneration. In this work, we propose the use of a self-assembled cartilage-like collagen-based hydrogel attached to a bone-like bioceramic to reproduce the joint structure from the subchondral bone to the articular cartilage.

First, in **Chapter II**, different commercially available bone substitutes are evaluated, as potential candidates to be used as bone-like platform. Their bioactivity is studied in terms of ionic exchange using a biomimetic method. Next, the polymeric coating that we intend to use as linking interface between the different parts of the construct is presented. Its effect over mineralization is assessed as well as its ability to react with collagen molecules, which will form a monolayer that will serve as anchoring point for the subsequent cartilage-like collagen-based hydrogel self-assembly.

The development of the collagen-based hydrogel formulation and its self-assembling process constitutes the central axis of **Chapter III**. To achieve the maximum degree of similarity with the cartilage ECM, hyaluronic acid and chondroitin sulfate are incorporated in the formulation. Hence, it is critical that the addition of glycosaminoglycans does not block the collagen self-assembling process, allowing hydrogel formation. Moreover, the *in vitro* viability of the polymeric coating as linking interface will be studied.

Once the hydrogel formulation has been obtained and characterized, its potential to induce both osteogenic and chondrogenic differentiation is discussed in **Chapter IV**. To do so, the expression of both chondrogenic and osteogenic markers is evaluated at protein and mRNA levels. Moreover, the mineralization of the hydrogel formulation has been evaluated, as well as the evolution of the mechanical properties of the construct at different times of culture.

1.3 References

(1) Beaudart, C.; Biver, E.; Bruyère, O.; Cooper, C.; Al-Daghri, N.; Reginster, J. Y.; Rizzoli, R. Quality of life assessment in musculo-skeletal health. *Aging Clin. Exp. Res.* **2017**, *0* (0), 1–6 DOI: 10.1007/s40520-017-0794-8.

(2) Chatterji, S.; Byles, J.; Cutler, D.; Seeman, T.; Verdes, E. Health, functioning, and disability in older adults - Present status and future implications. *Lancet* **2015**, *385* (9967), 563–575 DOI: 10.1016/S0140-6736(14)61462-8.

(3) Ellis, B.; Silman, A. Epidemiology: measurement matters--making musculoskeletal disease count. *Nat. Rev. Rheumatol.* **2014**, *10* (8), 449–450 DOI: 10.1038/nrrheum.2014.90.

(4) Xing, D.; Xu, Y.; Liu, Q.; Ke, Y.; Wang, B.; Li, Z.; Lin, J. Osteoarthritis and all-cause mortality in worldwide populations: grading the evidence from a meta-analysis. *Sci. Rep.* **2016**, *6* (1), 24393 DOI: 10.1038/srep24393.

(5) Vinatier, C.; Guicheux, J. Cartilage tissue engineering: From biomaterials and stem cells to osteoarthritis treatments. *Ann. Phys. Rehabil. Med.* **2016**, *59* (3), 139–144 DOI: 10.1016/j.rehab.2016.03.002.

(6) Zhang, W.; Ouyang, H.; Dass, C. R.; Xu, J. Current research on pharmacologic and regenerative therapies for osteoarthritis. *Bone Res.* **2016**, *4*, 15040 DOI: 10.1038/boneres.2015.40.

(7) Im, G.-I. Regeneration of articular cartilage using adipose stem cells. *J. Biomed. Mater. Res. Part A* **2016**, *104* (7), 1830–1844 DOI: 10.1002/jbm.a.35705.

(8) Hunter, W. Of the Structure and Diseases of Articulating Cartilages. *Phil Trans R. Soc* **1743**, *42*, 514–521.

(9) Green, W. T. Articular cartilage repair: Behavior of rabbit chondrocytes during tissue culture and subsequent allografting. *Clin. Orthop. Relat. Res.* **1977**, No. 124, 237–250.

(10) Miller, M. D.; Browne, J. A.; Cole, B. J.; Cosgarea, A. J.; Owens, B. D. *Operative Techniques: Sports Knee Surgery*, Second Edi.; Elsevier: Philadelphia, 2018.

(11) Johnson, L. L. Arthroscopic abrasion arthroplasty: a review. *Clin. Orthop. Relat. Res.* **2001**, No. 391S, S306-17.

(12) Gill, T. J.; Asnis, P. D.; Berkson, E. M. The Treatment of Articular Cartilage Defects Using the Microfracture Technique. *J. Orthop. Sport. Phys. Ther.* **2006**, *36* (10), 728–738 DOI:

10.2519/jospt.2006.2444.

(13) Grande, D. A.; Pitman, M. I.; Peterson, L.; Menche, D.; Klein, M. The repair of experimentally produced defects in rabbit articular cartilage by autologous chondrocyte transplantation. *J Orthop Res* **1989**, *7* (2), 208–218 DOI: 10.1002/jor.1100070208.

(14) Grande, D. A.; Singh, I. J.; Pugh, J.; York, N.; Ny, D. A. G. Healing of Experimentally Produced Lesions in Articular Cartilage Following Chondrocyte Transplantation. *Anat. Rec.* **1987**, *218*, 142–148.

(15) Brittberg, M.; Lindahl, A.; Nilsson, A.; Ohlsson, C.; Isaksson, O.; Peterson, L. Treatment of deep cartilage defects in the knee with autologous chondrocyte transplantation: a review of 28 cases. *N. Engl. J. Med.* **1994**, *331* (14), 889–895.

(16) van Assche, D.; Staes, F.; van Caspel, D.; Vanlauwe, J.; Bellemans, J.; Saris, D. B.; Luyten, F. P. Autologous chondrocyte implantation versus microfracture for knee cartilage injury: A prospective randomized trial, with 2-year follow-up. *Knee Surgery, Sport. Traumatol. Arthrosc.* **2010**, *18* (4), 486–495 DOI: 10.1007/s00167-009-0955-1.

(17) Sohn, D.; Lottman, L.; Lum, L.; Kim, S.; Pedowitz, R.; Coutts, R.; Sah, R. Effect of gravity on localization of chondrocytes implanted in cartilage defects. *Clin Orthop Relat Res.* **2002**, *394*, 254–262.

(18) Caron, M. M. J.; Emans, P. J.; Coolsen, M. M. E.; Voss, L.; Surtel, D. A. M.; Cremers, A.; van Rhijn, L. W.; Welting, T. J. M. Redifferentiation of dedifferentiated human articular chondrocytes: Comparison of 2D and 3D cultures. *Osteoarthr. Cartil.* **2012**, *20* (10), 1170–1178 DOI: 10.1016/j.joca.2012.06.016.

(19) Bartlett, W.; Skinner, J. a; Gooding, C. R.; Carrington, R. W. J.; Flanagan, a M.; Briggs, T. W. R.; Bentley, G. Autologous chondrocyte implantation versus matrix-induced autologous chondrocyte implantation for osteochondral defects of the knee: a prospective, randomised study. *J. Bone Joint Surg. Br.* **2005**, *87* (5), 640–645 DOI: 10.1302/0301-620X.87B5.15905.

(20) Redman, S. N.; Oldfield, S. F.; Archer, C. W. Current strategies for articular cartilage repair. *Eur. Cell. Mater.* **2005**, *9* (0), 23–32.

(21) Ringe, J.; Burmester, G. R.; Sittinger, M. Regenerative medicine in rheumatic disease: Progress in tissue engineering. *Nat. Rev. Rheumatol.* **2012**, *8* (8), 493–498 DOI: 10.1038/nrrheum.2012.98.

(22) Huang, B. J.; Hu, J. C.; Athanasiou, K. A. Cell-based tissue engineering strategies used in the clinical repair of articular cartilage. *Biomaterials* **2016**, *98*, 1–22 DOI:

10.1016/j.biomaterials.2016.04.018.

(23) Kiani, C. H.; Chen, L. I.; Wu, Y. A. O. J. I.; Yee, A. L. J.; Yang, B. U. B. Structure and function of aggrecan. **2002**, *12*, 19–32.

(24) Roughley, P. J.; Mort, J. S. The role of aggrecan in normal and osteoarthritic cartilage. *J. Exp. Orthop.* **2014**, *1* (1), 8 DOI: 10.1186/s40634-014-0008-7.

(25) Gadjanski, I.; Vunjak-Novakovic, G. Challenges in engineering osteochondral tissue grafts with hierarchical structures. *Expert Opin. Biol. Ther.* **2015**, *15* (11), 1583–1599 DOI: 10.1517/14712598.2015.1070825.

(26) Correia, C. R.; Reis, R. L.; Mano, J. F. Multiphasic, Multistructured and Hierarchical Strategies for Cartilage Regeneration. In *Engineering Mineralized and Load Bearing Tissues*; Bertassoni, L. E., Coelho, P. G., Eds.; Springer, 2015; pp 143–160.

(27) Gottardi, R.; Hansen, U.; Raiteri, R.; Loparic, M.; Düggelin, M.; Mathys, D.; Friederich, N. F.; Bruckner, P.; Stolz, M. Supramolecular organization of collagen fibrils in healthy and osteoarthritic human knee and hip joint cartilage. *PLoS One* **2016**, *11* (10), 1–13 DOI: 10.1371/journal.pone.0163552.

(28) Temenoff, J. S.; Mikos, a G. Review: tissue engineering for regeneration of articular cartilage. *Biomaterials* **2000**, *21* (5), 431–440.

(29) Machado, C. A. G.; Greene, W. B. *Netter's Orthopaedics*; Saunders, 2006.

(30) Cohen, N. P.; Foster, R. J.; Mow, V. C. Composition and dynamics of articular cartilage: structure, function, and maintaining healthy state. *J. Orthop. Sports Phys. Ther.* **1998**, *28* (4), 203–215 DOI: 10.2519/jospt.1998.28.4.203.

(31) Levingstone, T. J.; Matsiko, A.; Dickson, G. R.; O'Brien, F. J.; Gleeson, J. P. A biomimetic multi-layered collagen-based scaffold for osteochondral repair. *Acta Biomater.* **2014**, *10* (5), 1996–2004 DOI: 10.1016/j.actbio.2014.01.005.

(32) Lu, H. H.; Subramony, S. D.; Boushell, M. K.; Zhang, X. Tissue engineering strategies for the regeneration of orthopedic interfaces. *Ann. Biomed. Eng.* **2010**, *38* (6), 2142–2154 DOI: 10.1007/s10439-010-0046-y.

(33) Schaefer, D.; Martin, I.; Shastri, P.; Padera, R. F.; Langer, R.; Freed, L. E.; Vunjak-Novakovic, G. In vitro generation of osteochondral composites. *Biomaterials* **2000**, *21*, 2599–2606 DOI: 10.1016/S0142-9612(00)00127-7.

(34) Chen, G.; Sato, T.; Tanaka, J.; Tateishi, T. Preparation of a biphasic scaffold for osteochondral tissue engineering. *Mater. Sci. Eng. C* **2006**, *26* (1), 118–123 DOI:

10.1016/j.msec.2005.07.024.

(35) Jiang, J.; Tang, A.; Ateshian, G. A.; Edward Guo, X.; Hung, C. T.; Lu, H. H. Bioactive stratified polymer ceramic-hydrogel scaffold for integrative osteochondral repair. *Ann. Biomed. Eng.* **2010**, *38* (6), 2183–2196 DOI: 10.1007/s10439-010-0038-y.

(36) Kon, E.; Delcogliano, M.; Filardo, G.; Pressato, D.; Busacca, M.; Grigolo, B.; Desando, G.; Marcacci, M. A novel nano-composite multi-layered biomaterial for treatment of osteochondral lesions: Technique note and an early stability pilot clinical trial. *Injury* **2010**, *41* (7), 693–701 DOI: 10.1016/j.injury.2009.11.014.

(37) Kon, E.; Filardo, G.; Di Martino, A.; Busacca, M.; Moio, A.; Perdisa, F.; Marcacci, M. Clinical Results and MRI Evolution of a Nano-Composite Multilayered Biomaterial for Osteochondral Regeneration at 5 Years. *Am. J. Sports Med.* **2014**, *42* (1), 158–165 DOI: 10.1177/0363546513505434.

(38) Atesok, K.; Doral, M. N.; Karlsson, J.; Egol, K. A.; Jazrawi, L. M.; Coelho, P. G.; Martinez, A.; Matsumoto, T.; Owens, B. D.; Ochi, M.; et al. Multilayer scaffolds in orthopaedic tissue engineering. *Knee Surgery, Sport. Traumatol. Arthrosc.* **2016**, *24* (7), 2365–2373 DOI: 10.1007/s00167-014-3453-z.

(39) Sant, S.; Hancock, M. J.; Donnelly, J. P.; Iyer, D.; Khademhosseini, A. Biomimetic Gradient Hydrogels for Tissue Engineering. *Can. J. Chem. Eng.* **2010**, *88* (6), 899–911 DOI: 10.1002/cjce.20411.

(40) Vilela, C. A.; Correia, C.; Oliveira, J. M.; Sousa, R. A.; Espregueira-Mendes, J.; Reis, R. L. Cartilage Repair Using Hydrogels: A Critical Review of in Vivo Experimental Designs. *ACS Biomater. Sci. Eng.* **2015**, *1* (9), 726–739 DOI: 10.1021/acsbiomaterials.5b00245.

(41) Zhu, D.; Tong, X.; Trinh, P.; Yang, F. Mimicking Cartilage Tissue Zonal Organization by Engineering Tissue-scale Gradient Hydrogels as 3D Cell Niche. *Tissue Eng. Part A* **2018**, *24* (1–2), 1–10 DOI: 10.1089/ten.TEA.2016.0453.

(42) Dhandayuthapani, B.; Yoshida, Y.; Maekawa, T.; Kumar, D. S. Polymeric scaffolds in tissue engineering application: A review. *Int. J. Polym. Sci.* **2011**, *2011* DOI: 10.1155/2011/290602.

(43) Kyle, S.; Aggeli, A.; Ingham, E.; McPherson, M. J. Recombinant self-assembling peptides as biomaterials for tissue engineering. *Biomaterials* **2010**, *31* (36), 9395–9405 DOI: 10.1016/j.biomaterials.2010.08.051.

(44) Park, H.; Lee, H. J.; An, H.; Lee, K. Y. Alginate hydrogels modified with low molecular weight hyaluronate for cartilage regeneration. *Carbohydr. Polym.* **2017**, *162*, 100–107

DOI: 10.1016/j.carbpol.2017.01.045.

(45) Zhu, M.; Feng, Q.; Sun, Y.; Li, G.; Bian, L. Effect of cartilaginous matrix components on the chondrogenesis and hypertrophy of mesenchymal stem cells in hyaluronic acid hydrogels. *J. Biomed. Mater. Res. - Part B Appl. Biomater.* **2017**, *105* (8), 2292–2300 DOI: 10.1002/jbm.b.33760.

(46) Cavallo, C.; Desando, G.; Columbaro, M.; Ferrari, A.; Zini, N.; Facchini, A.; Grigolo, B. Chondrogenic differentiation of bone marrow concentrate grown onto a hylauronan scaffold: Rationale for its use in the treatment of cartilage lesions. *J. Biomed. Mater. Res. - Part A* **2013**, *101 A* (6), 1559–1570 DOI: 10.1002/jbm.a.34460.

(47) Almeida, H. V.; Eswaramoorthy, R.; Cunniffe, G. M.; Buckley, C. T.; O'Brien, F. J.; Kelly, D. J. Fibrin hydrogels functionalized with cartilage extracellular matrix and incorporating freshly isolated stromal cells as an injectable for cartilage regeneration. *Acta Biomater.* **2016**, *36*, 55–62 DOI: 10.1016/j.actbio.2016.03.008.

(48) Yuan, T.; Zhang, L.; Li, K.; Fan, H.; Fan, Y.; Liang, J.; Zhang, X. Collagen hydrogel as an immunomodulatory scaffold in cartilage tissue engineering. *J. Biomed. Mater. Res. - Part B Appl. Biomater.* **2014**, *102* (2), 337–344 DOI: 10.1002/jbm.b.33011.

(49) Efe, T.; Theisen, C.; Fuchs-Winkelmann, S.; Stein, T.; Getgood, A.; Rominger, M. B.; Paletta, J. R. J.; Schofer, M. D. Cell-free collagen type I matrix for repair of cartilage defects-clinical and magnetic resonance imaging results. *Knee Surg. Sports Traumatol. Arthrosc.* **2012**, *20* (10), 1915–1922 DOI: 10.1007/s00167-011-1777-5.

(50) Yousefi, A. M.; Hoque, M. E.; Prasad, R. G. S. V.; Uth, N. Current strategies in multiphasic scaffold design for osteochondral tissue engineering: A review. *J. Biomed. Mater. Res. - Part A* **2015**, *103* (7), 2460–2481 DOI: 10.1002/jbm.a.35356.

This page left blank intentionally

Chapter II. Designing the interface between bone and cartilage

Originally published as:

A. Mas, S. Borrós, “Bioactivity evaluation of commercial calcium phosphate-based bioceramics for bone regeneration”., **Afinidad LXXII**. Vol. 73, No. 575, pp. 170-174, June – September 2016

Patent pending

This page left blank intentionally

Designing the interface between bone and cartilage

In this chapter, the bioactivity evaluation of different commercially available bone substitutes is presented. The analyzed samples are potential candidates to be used as bone-like platform in our design proposal for an osteochondral scaffold. It is shown how the bioactivity of a bioceramic can be tailored by changing its β-TCP/HA ratio, as both chemical composition and degree of crystallinity are critical to define the interaction of a bioceramic with the surrounding media. Moreover, the viability of a PFM coating to be used as part of the linking interface between the bone-like platform and the cartilage-like collagen-based hydrogel, together with a collagen monolayer is studied.

2.1 Introduction

As previously described in Chapter I, mimicking the gradient structure of the osteochondral junction still constitutes a great challenge. Thus, it is critical to reproduce the calcified layer between subchondral bone and articular cartilage. This calcified layer is the responsible of withstanding the high shear stress generated between the stiff bone tissue and the soft cartilage.

As mentioned previously, in the present work we propose the creation of a calcified layer thanks to the intimate contact between a bone-like bioceramic and a cartilage-like hydrogel. The bioceramic will act as mechanical support, promoting the integration of the scaffold with the subchondral bone, and it will also provide means for a stiffness gradient and a mineralized layer creation. Moreover, it will act as a reservoir of calcium and phosphate ions, which in contact with the physiologic fluid will be able to diffuse through the hydrogel structure and precipitate in form of calcium phosphates. Among all synthetic biomaterials for bone regeneration, calcium-phosphate bioceramics are those which chemically resemble more to mammalian bone and teeth[1], which makes them good candidates to be used as bone-like platform.

From the foregoing, the need to bring together bone and cartilage tissue engineering approaches arises. In the present chapter, we will focus on the bone-like platform design which has to meet the requirements of bone graft materials. Moreover, we will introduce the proposed linking interface between the two layers of our osteochondral graft. Using the PECVD technique we will obtain a polymeric coating with great affinity towards amines, which, together with a collagen monolayer will serve as anchoring point for the subsequent hydrogel self-assembly.

Bone grafting is the most commonly used approach in clinics to enhance bone healing process. A bone graft can be defined as any implanted material that alone or in combination with other materials promotes a bone healing response thanks to its osteogenic, osteoinductive or osteoconductive properties[2]. An osteogenic material stimulates osteoblast activity, enhancing

bone formation[3]. Osteoinduction can be defined as the process by which primitive, undifferentiated and pluripotent cells are stimulated to commit to the bone-forming cell lineage[4], or, as proposed by Wilson-Hench the process by which osteogenesis is induced[5]. Finally, a material with osteoconductive properties allows bone growth on its surface or down into pores, channels or pipes[4]. Moreover, to ensure the good performance and integration of the graft it must lead to osseointegration, which implies the direct anchorage of an implant by the formation of bony tissue around the implant without the growth of fibrous tissue at the bone-implant interface[4].

Synthetic bone-grafts, such as calcium phosphate bioceramics, lack of osteogenic and osteoinductive properties themselves, hence they are normally used mixed with autologous bone grafts, growth factors or cells[6]. However, they are osteoconductive, as they provide a scaffold for new bone formation while provide support for osteoblast adhesion and proliferation[7]. When designing calcium phosphate-based bioceramics for bone regeneration, another property that must be considered is bioactivity, which can be defined as the ability of the material to induce apatite formation upon its surface after coming in contact with bone in the body[8]. Hydroxyapatite, constitutes the most important example of a bioactive calcium phosphate ceramic, as it has the ability to stimulate bone tissue formation and thus directly bond with bone and form a uniquely strong biomaterial-bone interface[9], namely osseointegration[10]. It integrates into living tissues by the same process active in remodeling of healthy bone[11]. On the contrary, bioinert materials do not stimulate bone formation, but instead stimulate formation of fibrous tissue and therefore do not directly bond to bone, forming a weak bone-biomaterial interface.

Thus, thanks to its ability to mimic bone tissue, its osteoconductivity, bioactivity and biocompatibility a calcium phosphate-based bioceramic platform is considered as material for the design of the bone-like platform for our heterogeneous scaffold. In order to control stiffness gradient creation through calcium and phosphate ions diffusion through the hydrogel structure and precipitation in form of calcium phosphates, it will be of great importance to control the bioactivity of the bone-like platform.

As for cartilage mimics, we have chosen collagen, which, as it will be described with further detail in the following chapters, thanks to its properties, is one of the natural polymers most commonly used for tissue engineering applications. It has an intrinsic capacity to self-assemble into higher order structures, which in the appropriate conditions lead to hydrogel formation.

As mentioned previously, to obtain an intimate contact between the bone-like bioceramic platform and the cartilage-like collagen-based hydrogel, we have developed a methodology that allows the immobilization of collagen-based hydrogels onto PECVD-modified substrates. The procedure is based on the ability of collagen to self-assemble into higher order structures like hydrogels, and its critical point is the obtention of a collagen monolayer onto a PFM-coated substrate. In previous work[12], it has been reported how the immobilization of peptides onto a substrate by PECVD directs the self-assembling of additional soluble peptides, which assemble forming a thin hydrogel layer. Thus, following the same idea, we will immobilize a collagen

monolayer onto the bioceramic platform by means of a PFM coating obtained by PECVD. The immobilized collagen molecules will serve as anchoring point for the self-assembly of a collagen-based hydrogel, which will consequently remain attached to the substrate.

Plasma polymerization, also called PECVD (Plasma Enhanced Chemical Vapor Deposition) is referred to a deposition of polymeric thin films on the surface of the substrate, without changing the bulk properties of the material[13]. PECVD has been described as an excellent technique to obtain biocompatible polymeric thin films[14,15]. Pentafluorophenyl methacrylate (PFM) is a monomer that offers a highly reactive ester group, which reacts efficiently with amino groups, and a vinyl structure that can be easily polymerized by PECVD techniques[16]. Its highly reactive ester group can be used to attach biomolecules through nucleophilic substitution[16]. PFM has been used as surface-modifying agent in the field of gene therapy[17], developing antibacterial surfaces[18] and to obtain thin film platforms for cell studies[19],[12]. Thus, based on previous research[12] and taking advantage of its high reactivity towards amines, we will use a PFM coating in combination with a collagen monolayer to build our heterogeneous scaffold. We hypothesize that a collagen monolayer can act as an anchoring point for the subsequent collagen fibrillation and hydrogel formation. For all these reasons, we believe that this methodology has great potential to allow the immobilization of a collagen-based hydrogel onto a calcium-phosphate bioceramic bone-like platform.

In order to achieve a high degree of mimicry of the bone-cartilage interface, it is critical to ensure a stable linkage between the two parts of the proposed osteochondral scaffold. Thus, to study the nature and stability of the interaction between collagen molecules and the bone-like bioceramic platform we have chosen quartz crystal microbalance with dissipation (QCM-D).

Our group has experience on using QCM-D technique in surface engineering applications. We have used QCM-D technology for different applications such as evaluation of potential mucoadhesive drug delivery systems[20,21], characterization of thermosensitive thin films[22] and to study the interaction of bovine serum albumin (BSA) with plasma polymerized PFM films and to get a better understanding of the viscoelastic properties of the resulting protein layer[23]. Thus, we propose the use of QCM-D technique to evaluate the interaction between collagen and a bioceramic platform, with and without the presence of a PFM coating.

2.2 Materials and Methods

2.2.1 Physical characterization of commercial bone substitutes

Five commercial calcium phosphate based-bone substitutes and commercial hydroxyapatite powder have been analyzed. Table II-1 summarizes their properties, the main difference being the composition, shape and particle size.

Table II-1. Main specifications of the studied bone substitutes

Sample	Shape	Particle size	Composition
Cerasorb®	Spherical	1000 – 2000 μm 150 – 500 μm 50 – 150 μm	β-TCP
BONIT matrix ® sterile	Cylindrical	0,6x0x4	HA/β-TCP (60:40) in a silica xerogel matrix
BONIT matrix ® unsterile	Cylindrical	0,6x0x4	HA/β-TCP (60:40) in a silica xerogel matrix
Bio-Oss ®	Spherical	0,25-1 mm	Bovine HA
Straumann® BoneCeramic®	Spherical	500 - 1000	HA/β-TCP (60:40)
Hydroxyapatite	Powder	2-6 μm	HA

2.2.1.1 X-ray diffraction (XRD)

Prior to XRD analysis the five samples were grinded into powder. The phase analysis of the HA powders was carried out employing an X-Ray diffractometer (Bruker D-5005) using a Cu Ka radiation generated at 40kV and 100 mA.

2.2.1.2 Scanning electron microscopy (SEM)

Morphological information of the analyzed samples is provided by the suppliers, however, in order to corroborate the information a SEM (JEOL JSM-5310) of two samples with different composition was performed. Prior to observation, samples were placed in a vacuum drier to

remove moisture and covered by a thin gold layer using a sputter coater (SC 7620, Quorum Technologies) to guarantee the conductivity.

2.2.2 Soaking the bioceramic bone substitutes in physiologic media

The interaction of hydroxyapatite – based bone substitutes with physiologic media was determined by soaking the samples in the interest solutions. The analyzed samples were in form of granules or powder. Using a hydraulic press (10 tons), they were compacted into discs of about 13 mm of diameter and 1,5 mm of height.

Bone substitute discs were immersed at 37ºC into simulated body fluid, which was prepared by dissolving the following compounds into 500 ml of Milli-Q water and adjusting the pH with 3.029 g of tris-hydroxymethylaminomethane and HCl to 7.4: 3.273 g of NaCl, 1.134 g of $NaHCO_3$, 0.186 g KCl, 0.0339 g of $Na_2HPO_4 \cdot 12\ H_2O$, 0.152 g of $MgCl_2 \cdot 6H_2O$, 0.184 g of $CaCl_2 \cdot 2H_2O$ and 0.036 g of Na_2SO_4.

Calcium concentration and pH changes at different time points were determined to assess the ionic exchange ability of the samples.

2.2.2.1 Atomic absorption spectroscopy (AAS)

Calcium concentration was determined using a 2280 Atomic Absorption Spectrophotometer (Perkin – Elmer). Calibration of the instrument was performed using 0.5, 1, 2.5 and 5 ppm calcium carbonate standard solutions. To avoid interferences, both the standards and the samples were mixed with lanthanum oxide (La_2O_3). The La_2O_3 stock solution was prepared by mixing 5.865g of the oxide, 50 ml of Milli-Q water and 25 ml of HCl(c) and posterior dilution up to 100 ml in a volumetric flask. The samples and standards were mixed with La_2O_3 maintaining a ratio of 1:2 respectively.

2.2.3 Surface modification by PECVD

2.2.3.1 Plasma reactor

All the surface modifications were carried out using a stainless steel bell jar plasma reactor[18]. Briefly, this reactor consists of a stainless-steel chamber (diameter, 25.5 cm; length, 41.6 cm) vertical plate reactor, Figure II-1. The ground electrode is the reactor chamber, and the radio frequency (RF) electrode is an aluminum plate, which is used to hold the samples for polymerization. Additionally, the RF electrode is connected to a RF pulse generator (13.56 MHz) via a matching box. Gases and monomers are supplied via a standard manifold where gas fluxes can be adjusted with a tree of needle valves. The system pressure is monitored using a vacuum gauge controller (MKS PDR900, Andover, MA, USA) which is connected to a cold cathode/micropirani vacuum transducer (MKS 972 DualMag) positioned at the center of the reactor. The system is equipped with a nitrogen cold trap and a chemical trap filled with active

carbon to prevent non-reacted monomer from reaching the pump (Trivac D 16BCS/PFPE Leybold, Cologne, Germany).

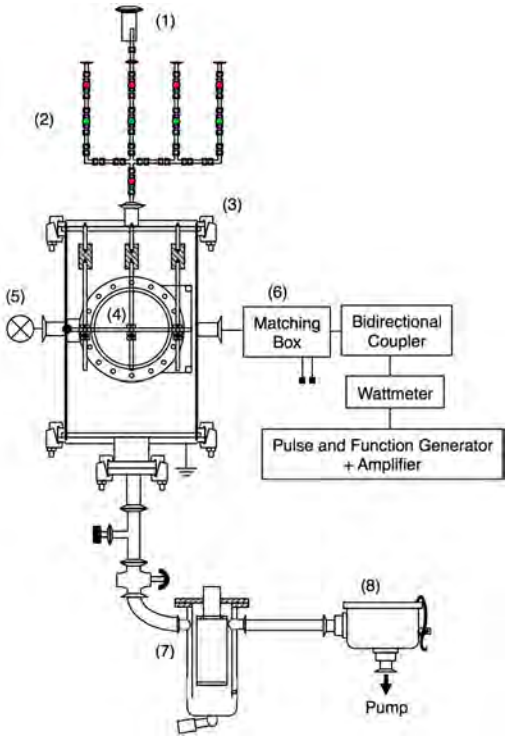

Figure II-1. Schematic diagram of stainless steel vertical plasma reactor and its electrical components[18] **(1)** monomer feed, **(2)** gases feed, **(3)** cylindrical chamber, **(4)** holder sample, **(5)** pirani gauge, **(6)** matching box and electrical system, **(7)** cold trap and **(8)** chemical trap.

2.2.3.2 PECVD modification on hydroxyapatite discs

Hydroxyapatite surface was modified with a coating of pentafluorophenyl methacrylate (PFM) (Apollo Scientific Ltd., Stockport, U.K.) as described below.

Briefly, hydroxyapatite discs were placed on the aluminum plate placed in the middle of the reactor chamber. The monomer, PFM, is introduced inside the reactor at nearly constant pressure around 0,02-0,04 mbar. Once pressure is stable the continuous radio frequency power is fixed at 15W and a pulsed plasma polymerization duty cycle (DC) of 10/20 [$DC=t_{on} / (t_{on}+t_{off})$][24] is carried out during 5 minutes. Next, plasma discharge is turned off and PFM vapor flow is kept running for an additional 3 minutes, to ensure that all active points have reacted. Once the polymerization process is finished samples are removed from the reactor chamber and stored until further use protected from light and under argon atmosphere.

2.2.4 Quartz crystal microbalance (QCM-D) studies

QCM-D technology (Q-Sense E1) was used to characterize the collagen type I (Gibco®, Life Technologies) adsorption onto different surfaces. Stainless steel and hydroxyapatite sensors

were used, both from Q-Sense. The sensors have optically polished gold electrodes, with a surface roughness less than 3 nm (RMS), a diameter of 14 mm and a thickness of 0.3 mm.

The basis of the QCM technique relies on quartz's inherent property of piezoelectricity[25]. Its working principle is explained with further detail elsewhere[26]. A frequency change of the oscillating crystal can be related with the mass adsorbed on its surface according to the Sauerbrey relation (Equation II-1), where the adsorbed mass (∆m) is proportional to the frequency shift (∆f). The constant C represents the mass sensitivity (17.7 ng/cm·Hz for a 5 MHz sensor) and n (1, 3, 5…) the overtone number.

$$\Delta m = -\frac{C}{n}\Delta f$$

Equation II-1

Thus, according to the Sauerbrey relation a decrease in frequency implies an increase of adsorbed mass over the sensor.

The dissipation parameter can be defined as the ratio between the energy dissipated and the energy stored by the oscillating sensor. It is given by the following equation (Equation II-2):

$$D = \frac{E_{Dissipated}}{2\pi E_{Stored}}$$

Equation II-2

The Sauerbrey equation arises from treating the deposited mass as an extension of the quartz crystal sensor. Thus, it can only be applied to uniform, rigid and fully coupled layers. There are many situations in which the Sauerbrey model does not hold, such as not rigid layers, slippery or heterogeneous layers[27]. In these situations, viscoelastic models which take into account the viscoelastic properties of the adsorbed layer such as Voigt or Maxwell should be applied[28].

2.2.4.1 Collagen adsorption onto different substrates

A 10 μg/ml collagen type I (Collagen I Bovine Protein, Gibco®) solution in phosphate-buffered saline (PBS; Phosphate Buffered Saline Tablets; Amresco®) was used for QCM-D assays. Collagen adsorption was evaluated using stainless steel (QSX 304, Q-Sense, Biolin Scientific) and hydroxyapatite (QSX 327, Q-Sense, Biolin Scientific) sensors. A pp-PFM-coated stainless-steel sensor was used to evaluate the effect of the polymeric coating over collagen adsorption. The coating procedure of the QCM-D sensors is the same as the one described for hydroxyapatite disks (detailed previously in point 2.2.3).

Once the sensor was placed in the QCM-D chamber (standard flow module), a baseline with PBS was obtained by flowing the solution until both frequency and dissipation signals stabilization.

Then, the protein solution was recirculated through the chamber allowing the frequency signal to reach a *plateau*, indicating that saturation has been achieved. Finally, a PBS wash was performed, to eliminate the excess of unbound protein.

2.3 Results and discussion

2.3.1 Previous characterization of bioceramic commercial bone substitutes

XDR of all the studied samples were performed in order to analyze both differences in composition and crystallinity can be appreciated. Cerasorb® samples (Figure II-2A-C) show the highest degree of crystallinity while BioOss® (Figure II-4B) and Hydro (Figure II-4C) are the less crystalline ones. The former consists in pure β-TCP and the latter are made of bovine and synthetic hydroxyapatite respectively. Both Straumann® (Figure II-4A) and Bonitmatrix® (Figure II-3A,B) samples consist in a mixture of hydroxyapatite and β-TCP in a ratio of 60:40, however, there are significant differences in their degree of crystallinity. The latter is attributed to the presence of a silica xerogel matrix in Bonitmatrix® sample as mentioned previously in Table II-1. As it will be further discussed in the following lines, there is a connection between the degree of crystallinity and the ionic exchange ability of the sample.

As for the Bonitmatrix® samples, there is no difference in composition between them, thus the following analysis will be performed only for the Bonitmatrix® sterile sample. For the Cerasorb® samples, we will work with the results obtained for the sample with a particle size of 150 – 500 μm. It has to be taken into account that as the samples are compacted into disks, particle size has no effect on the ionic exchange ability of the samples.

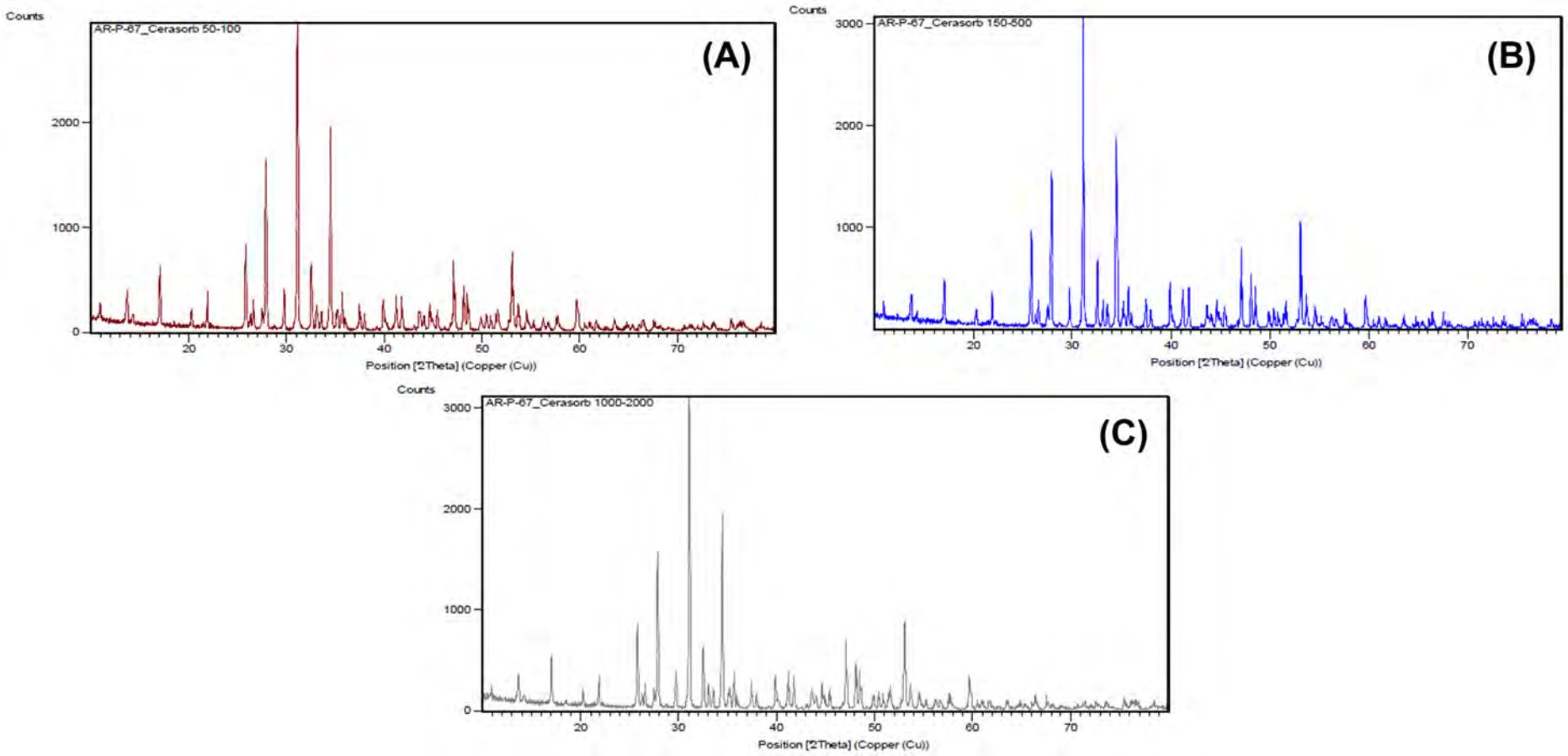

Figure II-2. XRD Spectra of Cerasorb® samples.**(A)** Cerasorb® 50-150 μm **(B)** Cerasorb 150-500 μm **(C)** Cerasorb 1000-2000 μm.

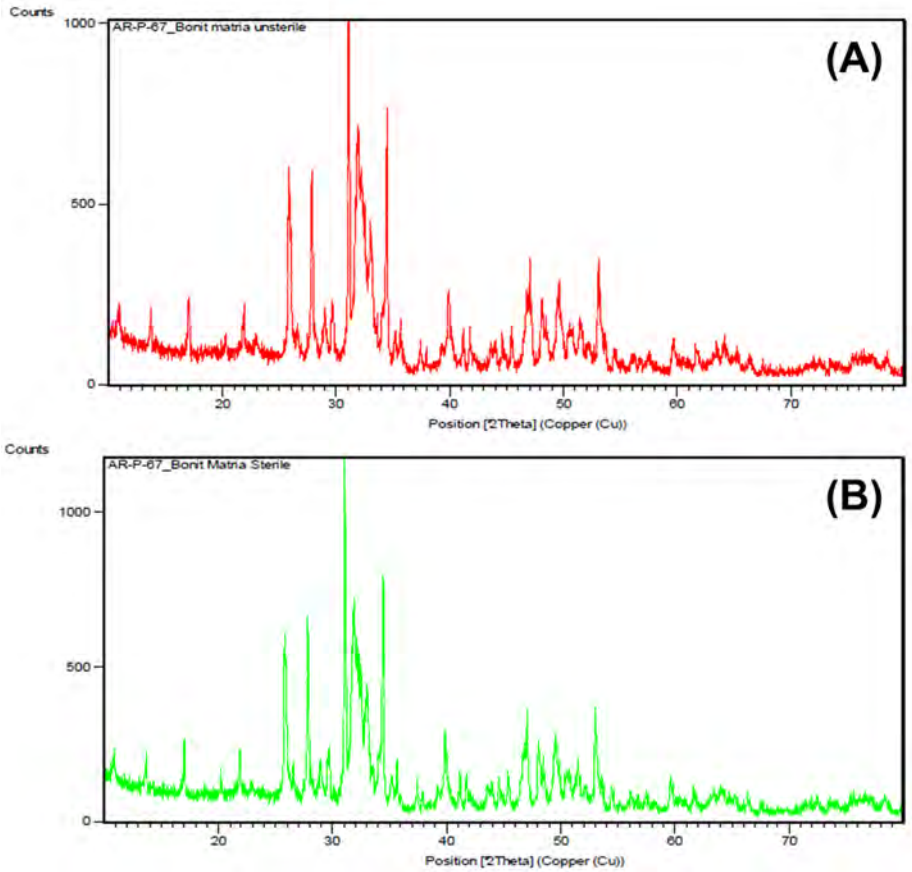

Figure II-3. XRD Spectra of Bonitmatrix® samples.**(A)** Bonitmatrix® Unsterile **(B)** Bonitmatrix® sterile.

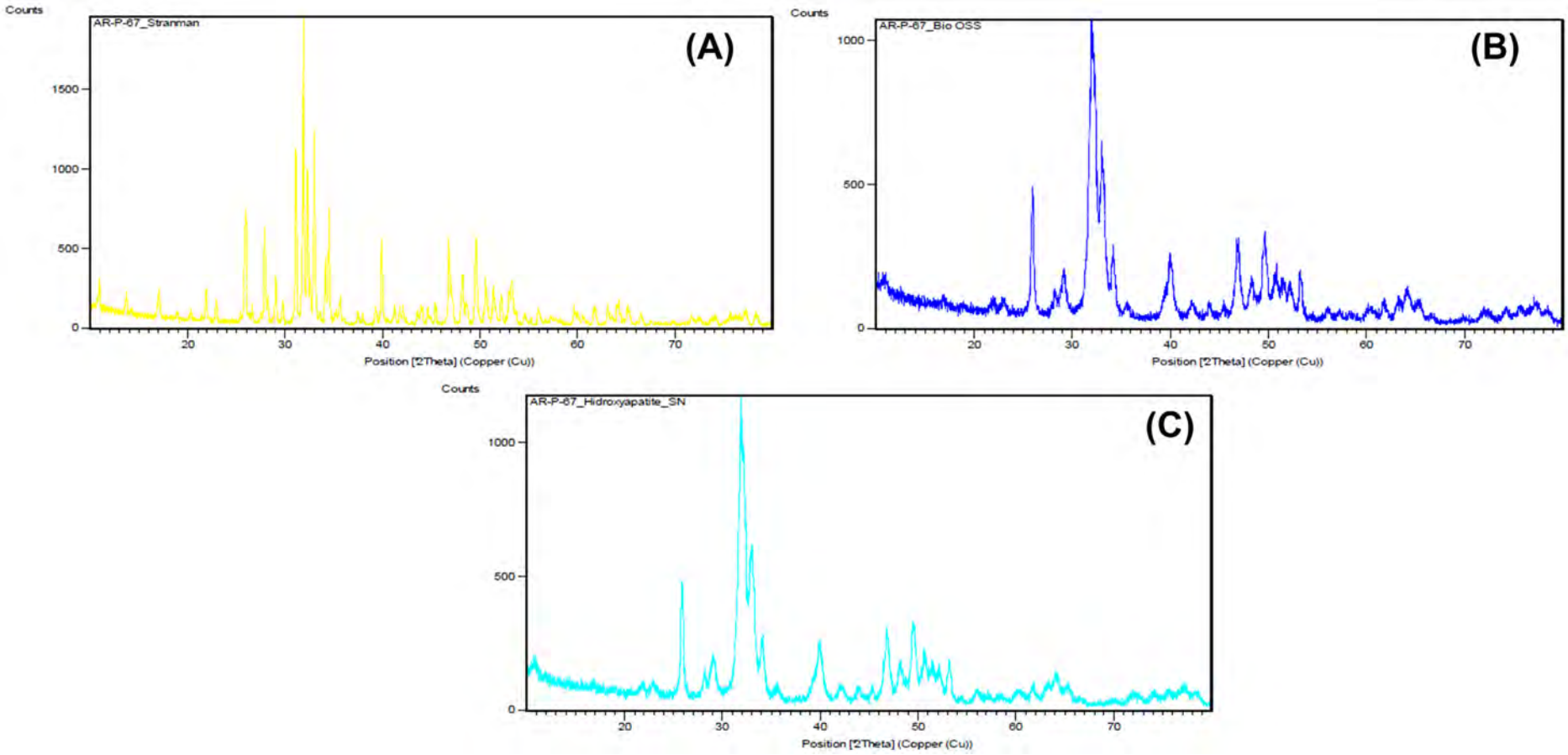

Figure II-4. XRD Spectra of **(A)** Straumann® samples **(B)** Biooss® samples and **(C)** Hydroxyapatite sample.

The morphology of both Cerasorb® (Figure II-5A-C) and Bonitmatrix® (Figure II-5D-F) samples was analyzed by SEM. Samples were chosen on the basis of their composition, as it the property which arouse more interest. Yet, the pore morphology and size differ notably from one sample to another. It can be seen how Bonitmatrix® presents a higher compactness showing smaller pore size, moreover the particles that conform the cylinder show a flattened morphology. On the contrary, Cerasorb® presents a higher pore size and it is formed by round-shaped particles. As they have different composition, one should expect differences in morphology.

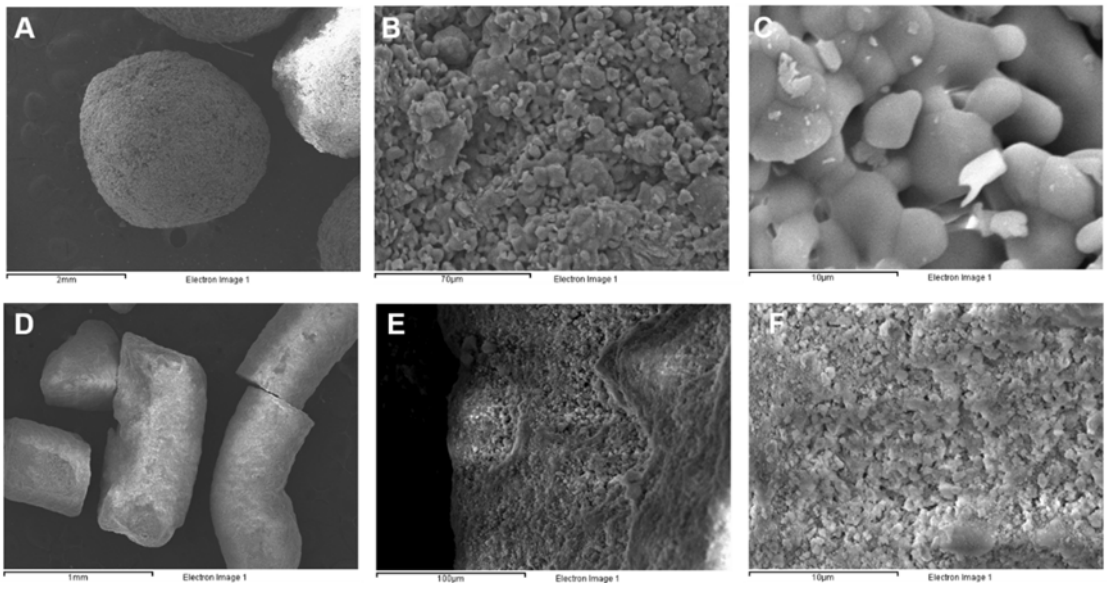

Figure II-5. SEM images of the commercial bone substitutes. **(A-C)** Cerasorb® samples and **(D-F)** Bonitmatrix® samples.

2.3.2 Soaking the bioceramic bone substitutes with physiologic media

Back in 1990 Kokubo et al. reported for the first time the use of SBF in order to assess the bone-like apatite formation onto a bioactive glass ceramic[29]. Based on their results, in 1991, they proposed that the essential requirement for a material to bond to living bone is the formation of bone-like apatite on its surface when implanted in the living body and that this in vivo apatite formation can be reproduced in SBF[30]. Since then, numerous studies have been published which use SBF to evaluate bioactivity[31,32].

Among all the SBF that have been formulated, we use the one described by Takadama et al. in 2004[33]. Table II-2 shows a comparison between the ionic concentrations of blood plasma and SBF.

Table II-2. Comparison of ions concentration between blood plasma and SBF

Ion concentration / mM	Na^+	K^+	Ca^{2+}	Mg^{2+}	HCO_3^-	Cl^-	HPO_4^{2-}	SO_4^{2-}
Blood Plasma	142.0	5.0	2.5	1.5	27.0	147.8	1.0	0.5
SBF	142.0	5.0	2.5	1.5	4.2	103.0	1.0	0.5

In the following lines, we will discuss the ionic exchange ability of the studied samples based on their previous characterization. As its further explained below, features such as chemical composition and degree of crystallinity will be critical for understanding the interaction of the samples with the surrounding physiologic medium.

When the samples were soaked into SBF, all solutions underwent changes in pH and calcium concentration. As it can be seen both pH and [Ca^{2+}] evolution profiles are very similar for all the samples (Figure II-6). It must be noticed how every change of pH occurs simultaneously with a change of [Ca^{2+}], thus, we can be certain that the measured pH changes are due to the interaction between the immersed calcium phosphate disk and the surrounding medium. In order to make comparisons between the studied samples, we will use the pH evolution profile, as it reflects all the events that are taking place during the ionic exchange.

Table II-3 presents the main properties of those calcium orthophosphates most commonly used in biomedical applications, among others. It is important to mention that only those compounds which present a Ca/P molar ratio higher than 1 are suitable for biomedical applications, since a Ca/P ratio less than 1 implies a high solubility and acidity when implanted into the body[34]. The majority of available bioceramics are based on HA, β-TCP, α-TCP and/or biphasic calcium phosphate (BCP) which is an intimate mixture of β-TCP+HA or α-TCP+HA. Hydroxyapatite, compared to α-TCP and β-TCP, presents a higher stability under physiological conditions and it has a lower solubility and a lower resorption rate. Therefore, BCP formulations aim to present the optimum balance between a more stable HA phase and a more soluble TCP for a specific application. It must be noticed that an increase of TCP/HA ratio increases BCP reactivity, thus its *in vivo* bioresorbability can be controlled through the phase composition[35].

Table II-3. Calcium orthophosphates main features[36]

Ca/P molar ratio	Compound	Formula	-log (K_{sp}) at 25ºC	-log (K_{sp}) at 37ºC
0,5	Monocalcium phosphate monohydrate (MCPM)	$Ca(H_2PO_4)_2 \cdot H_2O$	1,14	-
0,5	Monocalcium phosphate anhydrous (MCPA)	$Ca(H_2PO_4)_2$	1,14	-
1	Dicalcium phosphate dihydrate (DCPD)	$CaHPO_4 \cdot 2H_2O$	6,59	6,63
1	Dicalcium phosphate (DCP)	$CaHPO_4$	6,9	7,02
1,33	Octacalcium phosphate (OCP)	$Ca_8H_2(PO_4)_6 \cdot 5H_2O$	96,6	95,9
1,5	α-tricalcium phosphate (α-TCP)	α-$Ca_3(PO_4)_2$	25,5	25,5
1,5	β-tricalcium phosphate (β-TCP)	β-$Ca_3(PO_4)_3(OH)$	28,9	29,5
1,67	Hydroxyapatite (HA)	$Ca_5(PO_4)_3(OH)$	58,4	58,6
2	Tetracalcium phosphate (TTCP)	$Ca_4(PO_4)_2O$	38-44	42,4

The initial dissolution of β-TCP and HA causes an increase in both calcium concentration and pH. In agreement with previous studies[32,37], we hypothesize that due to the dissolution of β-TCP and HA, there is an initial release of calcium ions to the SBF solution, reflected by an increase of pH caused by the absorption of H_3O^+ from the solution. Following the initial increase, SBF pH value seems to stabilize, however, a third phase in which the pH decreases, can be distinguished. We hypothesize that the latter is caused by the surface recrystallization of HA or β-TCP, which leads to an absorption of both OH- and HPO^{3-} ions from the solution to the sample disk. As it is shown in Table II-3, β-TCP presents a higher solubility than HA at 37ºC, so one may think that the initial dissolution would take place faster for Cerasorb® samples, which are composed of pure β-TCP. However, as said before, the degree of crystallinity has a strong relation with the ionic exchange ability of the sample. Higher degrees of crystallinity can be associated with lower dissolution kinetics, so the most crystalline samples tend to present lower solubilities than those less crystalline. Thus, samples such as Straumann (less crystalline than Cerasorb®) which consist in a mixture of HA and β-TCP (60:40), show faster initial dissolution rates, achieving the higher pH value and calcium concentration within the first 24 hours of immersion.

For all bone substitutes, the increase of the pH value that takes place within the first 24 hours represents more than a 30% of the total pH increase, reflecting that the dissolution of the disk surface occurs almost completely during this period.

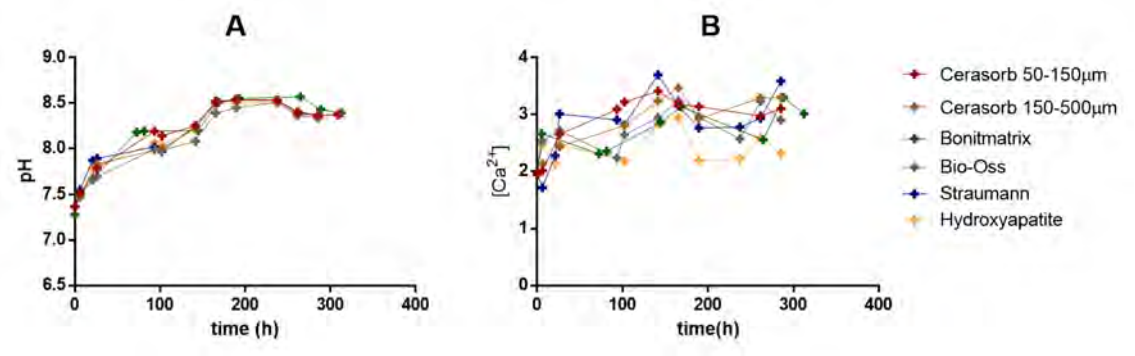

Figure II-6. Bioactivity evaluation.**(A)** pH evolution of SBF solution during sample's immersion period **(B)** Calcium concentration at SBF solution evolution during sample's immersion period.

2.3.3 pp-PFM coating effect over hydroxyapatite bioactivity

Next, the effect of a PFM coating on the bioactivity of a commercial hydroxyapatite (Plasma Biotal Ltd.) disk is analyzed when soaked into both SBF and Minimum essential medium eagle – alpha modification (α-MEM, Sigma-aldrich). The latter is a cell culture medium which incorporates aminoacids and vitamins and thus it allows the study of bioactivity in a more realistic scenario. Hydroxyapatite (HA) was chosen in order to be able to relate the results with those obtained with the quartz crystal microbalance with dissipation (QCM-D) with available hydroxyapatite sensors, that will be discussed later.

To do so, the HA disks were immersed in the interest solutions during 28 days at 37ºC. To avoid calcite ($CaCO_3$) formation, the medium was changed every two days.

The interest in coating the hydroxyapatite disk with PFM arises from the need of designing a suitable linking interface between the bone-like platform and the softer cartilage-like hydrogel. PFM coatings contain a highly reactive ester group, which could be used to bind biomolecules (Figure II-7), such as collagen, promoting cell adhesion and proliferation, thus they have been considered as active coatings for different biomaterials[38].

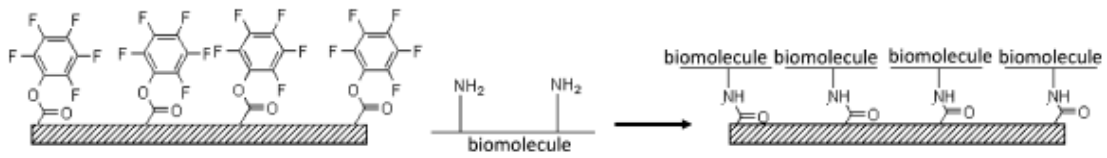

Figure II-7. Biomolecules attachment onto PFM coatings[39].

As it can be seen in Figure II-8, both SBF and α-MEM allow for precipitate formation on the HA surface. The precipitate distribution lacks of homogeneity in all samples, as crystal growth seems to be localized at some points. The latter gives evidence of a mechanism of heterogeneous nucleation, which was expected, as the beginning of apatite formation on calcium phosphate ceramics from SBF solution is usually considered as a process of heterogeneous nucleation[40,41].

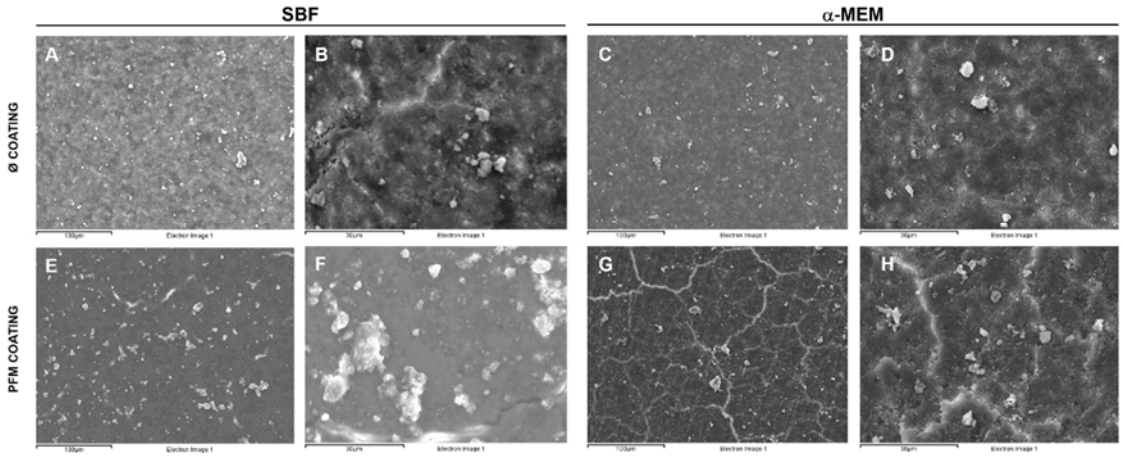

Figure II-8. SEM images of hydroxyapatite discs after 28 days soaked both in α-MEM and SBF.

Moreover, it can be seen how the PFM coating does not block the precipitation events, but instead it seems to provide nucleation points which help the precipitate formation. By comparing Figure II-8B and Figure II-8F, it can be clearly appreciated that for the PFM-coated disk crystals are bigger and their presence is more extended throughout the hydroxyapatite surface. As for the influence of the soaking solution, differences are more evident for the PFM coated samples. It can be seen how when the sample is soaked into SBF, more crystals are formed over the entire surface. This may suggest that the amino acids present in the α-MEM, attach covalently to the PFM coating through their amino groups and thus, block the nucleation sites which help the precipitation of calcium phosphate salts. It seems that amino acids play an important role in hydroxyapatite precipitation, and different studies reveal how they can play both inhibitory and enhancing effect[42,43]. However, with this assay we have proved the ability of a PFM coating to interact with physiologic medium and to improve salt deposition.

Up to now, it has been demonstrated how both chemical composition and the degree of crystallinity are of great importance for the bioactivity of calcium phosphate based bioceramics. Tailoring the bioactivity of a certain bioceramic, for instance by using mixtures of two calcium phosphates could be interesting to achieve the desired effect for a certain application. In those cases where a higher biodegradability is required, a bioceramic with a higher resorption rate shall be used. On the contrary, if we aim to obtain a graft with a longer lifetime its rapid dissolution is not desired and thus, a bioceramic with a lower solubility may be used. Moreover, the effect of the presence of a PFM coating over hydroxyapatite bioactivity has been evaluated, demonstrating how it enhances the interaction with the bioceramic and the physiologic media. Thus, the next step is to study the interaction of the PFM coating with collagen, as the polymeric coating will act as linking interface between the bone-like platform and a cartilage-like collagen-based hydrogel. The PFM coating must allow the immobilization of collagen molecules which will act as anchoring point for the subsequent collagen fibrillation and hydrogel self-assembly. Through its high reactivity towards amines thanks to its active ester groups, PFM coating is expected to allow the covalent immobilization of collagen molecules, avoiding the hydrogel detachment from the bone-

like platform. Thus, in the following lines, a quartz crystal microbalance with dissipation (QCM-D) study of the interaction between collagen and PFM is presented.

2.3.4 Collagen adsorption onto different substrates

One of the major applications of the QCM-D technology is the study of protein adsorption onto different surfaces in order to evaluate the ability of a determinate material to promote protein adsorption[25]. Thus, we have used this technique to evaluate the collagen adsorption onto different substrates, and the influence of different parameters over the adsorption process. As said before, with QCM-D technique, changes in frequency (f) and dissipation (D) of an oscillating sensor are measured. As mass adsorbs onto the sensor, a frequency shift can be appreciated, besides, the dissipation parameter gives information about the viscoelastic properties of the adsorbed layer. Softer coatings lead to an increase of the oscillation damping, which is traduced as an increase of dissipation. Figure II-9 illustrates the behavioral differences between a rigid and a soft layer.

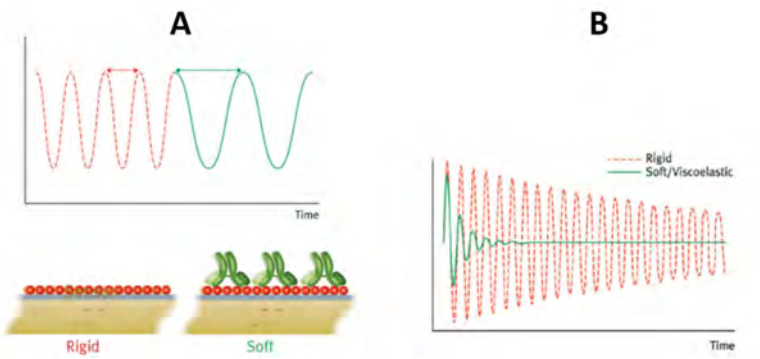

Figure II-9. Differences in behavior between soft and rigid adsorbed layers[44]. **(A)** Frequency change due to an increase of the adsorbed mass by the addition of a molecular layer. This example shows the addition of an antibody (green) to a protein layer (red). **(B)** Difference in the dissipation signal generated by a rigid (red) and a soft (green) adsorbed layer.

Simultaneous measurement of multiple overtones is required to model viscoelastic properties and extract film thickness. The different overtones give information about the homogeneity of the applied layers, as the detection range out from the crystal surface decreases with increasing overtone number. Thus, differences in frequency behavior of the different overtones suggests vertical variations in film properties[45]. Qualitative information about the thickness of the adsorbed layer can be extracted from the separation between the signals of the different overtones: the higher the separation is the thicker is the adsorbed protein layer. To avoid excessive fluctuations due to environmental factors all the calculations shown in this work are performed using the seventh overtone.

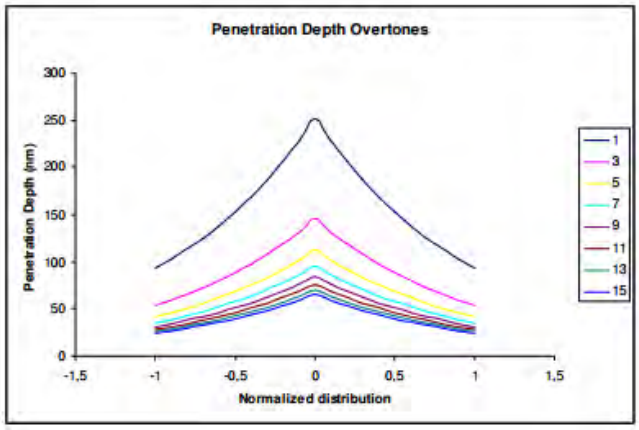

Figure II-10. Viscous penetration depth as function of overtone (Q-Sense reported data).

The immobilization of collagen molecules onto both pp-PFM-coated and non-coated stainless steel and hydroxyapatite was monitored using the QCM-D technology. To evaluate and compare the collagen adsorption under different conditions and onto different surfaces we have established a basic protocol which is illustrated in Figure II-11. First, a baseline is acquired by flowing through the chamber a PBS solution (A), then, once both the frequency and dissipation remain constant the collagen solution is entered to the chamber and a decrease in frequency can be appreciated as the protein starts to interact with the sensor surface (B). As it can be seen, the interaction also leads to an increase of dissipation, as the adsorbed protein layer is softer than the sensor surface. We keep recirculating the protein solution until saturation is reached, which can be associated with the frequency and dissipation reaching a *plateau*. Then, a wash with PBS to eliminate the remaining unbound protein molecules is performed until the signal stabilizes again (C). Finally, a wash with water is carried out (not shown in Figure II-11). The latter is expected to cause the detachment of those molecules not covalently bound to the substrate, reflected by an increase in frequency and a decrease in dissipation signal, as electrostatic interactions are subject to the medium ionic strength.

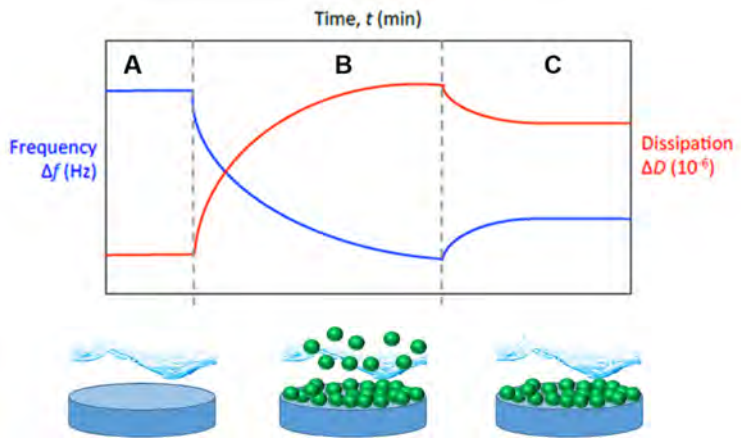

Figure II-11. Frequency and dissipation profiles observed for the standard protocol used in this study[46].

A non-treated stainless-steel sensor (Figure II-12A) has been taken as reference to evaluate the collagen adsorption that takes place onto modified substrates. Adsorption takes place once the protein solution is flown through the QCM-D chamber, as a decrease in sensor's oscillation frequency can be appreciated. The subsequent PBS wash leads to the detachment of a little amount of protein, corresponding to those molecules that are not interacting with the substrate. However, the final water wash causes an increase of frequency which almost reaches the baseline value. The flow of water through the QCM-D chamber causes a change in ionic strength and the detachment of a great amount of protein molecules, as their interaction with stainless steel is purely electrostatic[45].

Next, to gain insight into the interaction that would take place in the interface between the bone-like bioceramic platform and the softer cartilage-like hydrogel, the collagen adsorption onto hydroxyapatite sensor (Figure II-12B) is studied. The adsorption profile follows the same pattern that for the stainless-steel sensor. However, what points out is that the amount of protein molecules adsorbed onto hydroxyapatite is slightly higher than the obtained for the stainless-steel substrate. It can be hypothesized that a higher mass adsorbs onto hydroxyapatite thanks to its higher porosity, which favors the entrapment of collagen molecules. Furthermore, the mineral surface of the sensor could lead to ionic interactions with the collagen molecules, which will also enhance the whole adsorption process. Hence, a hydroxyapatite substrate, compared to stainless steel, would promote collagen adsorption under the studied conditions. The PBS wash does not alter the amount of adsorbed molecules, reflecting the existence of specific electrostatic interactions between the protein molecules themselves and with the substrate. However, as it happened with the stainless-steel sensor, the final water wash results in a significant increase of the frequency signal due to the detachment of a fraction of protein molecules. Thus, it must be considered that the interface between the bone-like platform and the collagen hydrogel could be disrupted in response to ionic strength fluctuations in the surrounding medium. Then, there is the risk of hydrogel leakage from calcium phosphate platform once placed into the body. As such, a superficial modification which provides means for covalent bonding between the two parts is suggested.

As mentioned before, thanks to its ability to bind biomolecules through its highly reactive esters and promote cell adhesion and proliferation, PFM coatings have been considered as active coatings for different biomaterials[38]. Thus, in this thesis we intend to take advantage of the high reactivity of PFM to attach a collagen-based hydrogel via covalent bonding onto both the bone-like platform and the collagen membrane cover.

We have used the QCM-D technique to evaluate collagen adsorption onto a PFM-coated stainless-steel sensor (Figure II-12C). As PFM contains active sites, a high mass adsorption per surface unit is expected. Besides, protein adsorption should be more homogeneous, as the active points of the polymeric coating throughout the sensor surface will act as nucleation points. Moreover, as collagen will be covalently bound to the sensor surface, the ionic strength change

caused by the final water wash shouldn't cause protein detachment. As it can be seen, the amount of adsorbed mass is significantly higher than the observed for both the HA sensor and the non-treated stainless sensor according to the Sauerbrey relation. The PFM coating causes a frequency shift around 400 Hz which represents more than twice the value obtained for the hydroxyapatite sensor. As occurred with the non-treated stainless-steel sensor and the hydroxyapatite sensor, the PBS wash does not alter the amount of adsorbed molecules for the PFM coated sensor, as specific electrostatic interactions between the protein molecules themselves and the substrate take place. Moreover, the hypothesis of a covalent interaction between the PFM coating and the collagen molecules is confirmed, as the final water wash produces a lower frequency shift compared with both the non-treated stainless-steel sensor and the HA sensor. Thus, one can be certain that collagen molecules specifically interact with the PFM coating. The small fraction of detached protein molecules is likely to be electrostatically interacting and removed by the change of ionic strength. If that is so, a plasma polymerized PFM coating would be an appropriate method to anchor the collagen to a desired substrate.

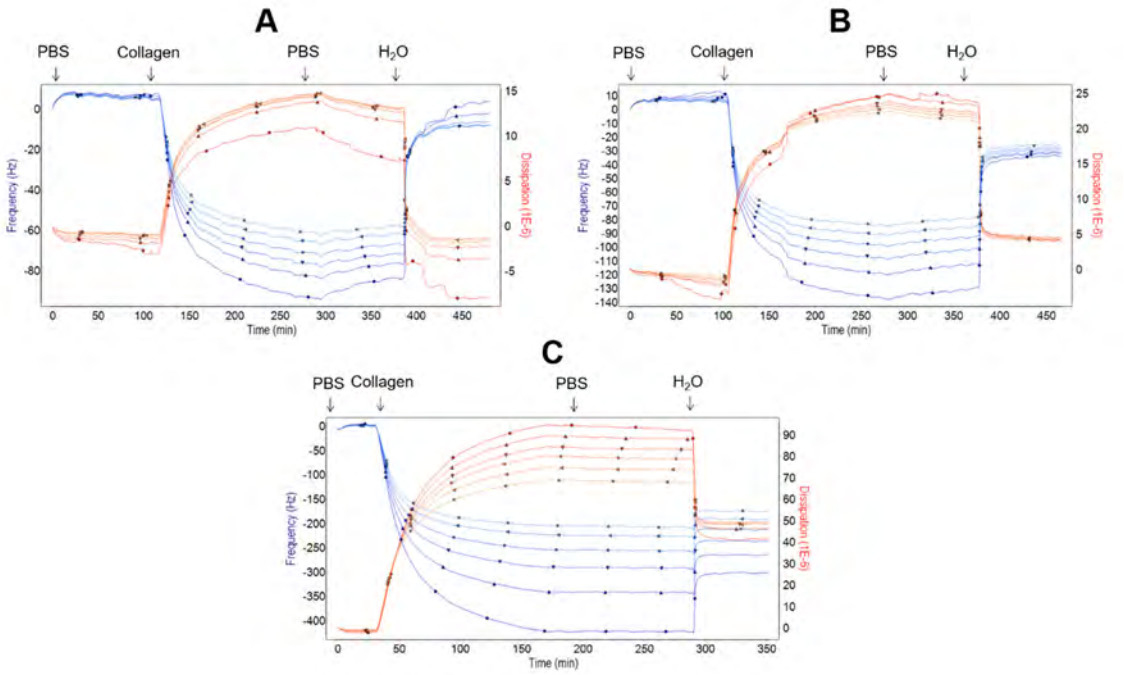

Figure II-12. QCM-D data of collagen adsorption.onto **(A)** stainless steel **(B)** hydroxyapatite and **(C)** PFM-coated stainless-steel sensor. The 3rd (•), 5th (▲), 7th (▼), 9th (♦), 11th (◄), and 13th (✕) overtones are shown.

The obtained frequency data was analyzed using the Sauerbrey model and areal mass values ($\mu g/cm^2$) were obtained (Figure II-13). Sauerbrey only stands for fairly rigid films as it underestimates the amount of adsorbed mass when the adsorbed films are viscoelastic. However, as the viscoelasticity of all films is similar, Sauerbrey is used only for qualitative and comparative purposes.

It can be seen how the PFM-coating allows the immobilization of a greater amount of collagen molecules than both stainless-steel and hydroxyapatite sensors. No statistically significant

differences between mass adsorption onto non-coated stainless-steel and hydroxyapatite sensors can be appreciated.

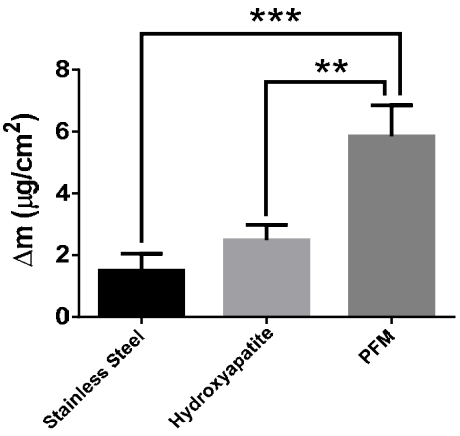

Figure II-13. Mass adsorption of collagen onto different substrates obtained using Sauerbrey model. (Statistical differences are indicated as * for p<0.05, ** for p<0.01, and *** for p<0.001, Two-way ANOVA, n=3).

A method to evaluate the viscoelastic properties of an adsorbed protein layer consists in plotting the variation of the dissipation versus the frequency shift. Thus, time is eliminated as an explicit parameter, and a direct comparison between the energy dissipation (ΔD) per unit mass attached to the surface (Δf) can be done. Then, the influence of protein adsorption on the viscoelastic damping of the crystals resonance can be appreciated, allowing to infer viscoelastic properties of the adsorbed layer[47].

As it is shown in Figure II-14, there is a linear relation between dissipation and frequency shifts during the experiment, before the final water wash. As the adsorption process takes place, changes in slope may suggest alterations within the individual proteins or within the protein layer[48]. Thus, the fact that no change in slope can be appreciated reveals that no changes either in the adsorbed collagen molecules or in the adsorbed protein layer are taking place once the second fresh new collagen solution is entered to the QCM-D chamber. Therefore, we won't consider the formation of a collagen bilayer as we hypothesize that the adsorption of the second protein layer would take place altering somehow the viscoelastic properties of the first layer of adsorbed protein molecules.

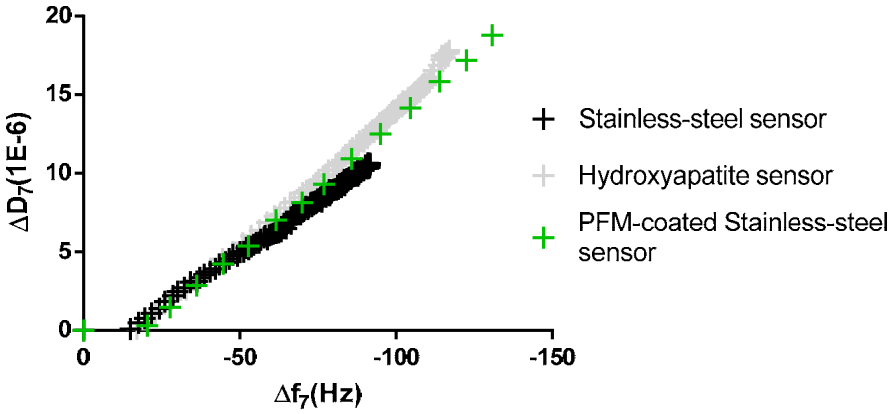

Figure II-14. Viscoelastic properties of the adsorbed collagen layer for the stainless-steel, hydroxyapatite and PFM-coated stainless-steel sensor.

2.4 Concluding remarks

The results presented in this chapter give insights into the design of a bone-like platform, which will be anchored to the subchondral plate, allowing the creation of a mineralized transition zone between bone and the upper cartilage-like collagen-based hydrogel. Then, a PECVD PFM coating is presented as candidate to be used as linking interface between the bone-like platform and the cartilage-like hydrogel. Thanks to its highly reactive ester groups it allows the covalent immobilization of a great amount of collagen molecules, which act as anchoring points for the subsequent collagen hydrogel self-assembly. Moreover, the polymeric coating guarantees the stability of the heterogeneous scaffold holding together its two main differentiated parts.

Thus, the comparative study of the ionic exchange ability of different commercially available bioceramic bone substitutes has been performed using a biomimetic method and it has been demonstrated how both composition and degree of crystallinity have great influence over bioactivity. Moreover, both the presence of a PFM coating over hydroxyapatite bioactivity and its ability to covalently bind collagen molecules to form a protein monolayer have been evaluated.

As for the bioceramic bone substitutes the obtained results show how both the chemical composition and the degree of crystallinity have a great influence over the interaction ability of the samples with the surrounding medium. Despite the higher solubility of the β-TCP with respect to HA, the samples composed by a mixture of β-TCP and HA presented a higher ease of interaction than those composed of pure β-TCP. As the latter presents a higher degree of crystallinity, the initial surface dissolution needed to trigger the ionic exchange events occurs with greater difficulty. Thus, the obtained results reveal that bioceramics bioactivity can be tailored by modifying its β-TCP/HA ratio. Besides, hydroxyapatite has been successfully coated with PFM by PECVD. It has been demonstrated how, the presence of the polymeric coating not only does not block the precipitation of calcium phosphates, but also seems to provide nucleation points that promote precipitate formation.

The adsorption of collagen onto stainless-steel, hydroxyapatite and PFM-coated stainless-steel has been evaluated using QCM-D technique. It has been shown how PFM allows the immobilization of a higher amount of collagen molecules than both stainless-steel and hydroxyapatite. Moreover, it has been demonstrated that thanks to the presence of its highly reactive ester groups and their high reactivity towards amines, collagen molecules remain covalently bound to the PFM polymeric coating, and its interaction is not affected by ionic exchange changes.

In the next chapter, we will study the ability of collagen to self-assemble into a three-dimensional hydrogel structure starting from a collagen monolayer immobilized onto a PFM-coated substrate. Moreover, we will study the interaction of collagen with the glycosaminoglycans hyaluronic acid and chondroitin sulfate, as we intend to introduce them to the cartilage-like hydrogel formulation. Next, we present the proof of concept of how the developed linking

technology allows the immobilization of collagen-based hydrogels onto any substrate which can be subject to PECVD and that it has no toxic effect over cells *in vitro*. Finally, an *in vitro* analysis of the hydrogel formulation and the encapsulation method will be presented.

2.5 References

(1) Dorozhkin, S. V. Calcium Orthophosphates in Nature, Biology and Medicine. *Materials (Basel).* **2009**, *2* (2), 399–498.

(2) Bauer, T.; Muschler, G. Bone Graft Materials. An Overview of the Basic Science. *Clin Orthop Relat Res.* **2000**, *371*, 10–27.

(3) Kini, U.; Nandeesh, B. N. Physiology of Bone Formation, Remodeling, and Metabolism. In *Radionuclide and Hybrid Bone Imaging*; Fogelman, I., Gnanasegaran, G., Wall, H., Eds.; Springer Berlin Heidelberg: Berlin, Heidelberg, 2012.

(4) Albrektsson, T.; Johansson, C. Osteoinduction, Osteoconduction and Osseointegration. *Eur. Spine J.* **2001**, *10*, 96–101.

(5) Wilson-Hench, J. *Definitions in Biomaterials : Proceedings of a Consensus Conference of the European Society for Biomaterials, Chester, England, March 3-5, 1986*; Williams, D. F., Ed.; Elsevier: Amsterdam, 1987.

(6) Giannoudis, P. V; Dinopoulos, H.; Tsiridis, E. Bone Substitutes: An Update. *Injury* **2005**, *36S*, S20-27.

(7) Anselme, K. Osteoblast Adhesion on Biomaterials. *Biomaterials* **2000**, *21* (7), 667–681.

(8) Labres, X.; Camps, A. Graft Materials in Oral Surgery: Revision. *J Biomim Biomater Tissue Eng* **2014**, *19* (1), 1–7.

(9) LeGeros, R. Z. Calcium Phosphate-Based Osteoinductive Materials. *Chem. Rev.* **2008**, *108* (11), 4742–4753.

(10) LeGeros, R. Z.; Craig, R. G. Strategies to Affect Bone Remodeling: Osteointegration. *J. Bone Miner. Res.* **1993**, *8* (2), S583-596.

(11) Best, S. M.; Porter, a. E.; Thian, E. S.; Huang, J. Bioceramics: Past, Present and for the Future. *J. Eur. Ceram. Soc.* **2008**, *28* (7), 1319–1327.

(12) Wu, J.; Marí-Buyé, N.; Muiños, T. F.; Borrós, S.; Favia, P.; Semino, C. E. Nanometric Self-Assembling Peptide Layers Maintain Adult Hepatocyte Phenotype in Sandwich Cultures. *J. Nanobiotechnology* **2010**, *8* (1), 29.

(13) Chu, P. K.; Chen, J. Y.; Wang, L. P.; Huang, N. Plasma-Surface Modification of Biomaterials. *Mater. Sci. Eng. R Reports* **2002**, *36* (5–6), 143–206.

(14) Prasad, G. R.; Daniels, S.; Cameron, D. C.; McNamara, B. P.; Tully, E.; O'Kennedy, R. PECVD of Biocompatible Coatings on 316L Stainless Steel. *Surf. Coatings Technol.* **2005**,

200 (1–4 SPEC. ISS.), 1031–1035.

(15) Nisol, B.; Poleunis, C.; Bertrand, P.; Reniers, F. Poly(Ethylene Glycol) Films Deposited by Atmospheric Pressure Plasma Liquid Deposition and Atmospheric Pressure Plasma-Enhanced Chemical Vapour Deposition: Process, Chemical Composition Analysis and Biocompatibility. *Plasma Process. Polym.* **2010**, *7* (8), 715–725.

(16) Francesch, L.; Borros, S.; Knoll, W.; Förch, R. Surface Reactivity of Pulsed-Plasma Polymerized Pentafluorophenyl Methacrylate (PFM) toward Amines and Proteins in Solution. *Langmuir* **2007**, *23* (7), 3927–3931.

(17) Horna, D.; Ramírez, J. C.; Cifuentes, A.; Bernad, A.; Borrós, S.; González, M. a. Efficient Cell Reprogramming Using Bioengineered Surfaces. *Adv. Healthc. Mater.* **2012**, *1* (2), 177–182.

(18) Gilabert-Porres, J.; Marti, S.; Calatayud, L.; Ramos, V.; Rosell, A.; Borros, S. Design of a Nanostructured Active Surface against Gram-Positive and Gram-Negative Bacteria through Plasma Activation and in Situ Silver Reduction. *ACS Appl. Mater. Interfaces* **2016**, *8*, 64–73.

(19) Marí-Buyé, N.; O'Shaughnessy, S.; Colominas, C.; Semino, C. E.; Gleason, K. K.; Borrós, S. Functionalized, Swellable Hydrogel Layers as a Platform for Cell Studies. *Adv. Funct. Mater.* **2009**, *19* (8), 1276–1286.

(20) Oh, S.; Wilcox, M.; Pearson, J. P.; Borrós, S. Optimal Design for Studying Mucoadhesive Polymers Interaction with Gastric Mucin Using a Quartz Crystal Microbalance with Dissipation (QCM-D): Comparison of Two Different Mucin Origins. *Eur. J. Pharm. Biopharm.* **2015**, *96*, 477–483.

(21) Oh, S.; Borrós, S. Mucoadhesion vs Mucus Permeability of Thiolated Chitosan Polymers and Their Resulting Nanoparticles Using a Quartz Crystal Microbalance with Dissipation (QCM-D). *Colloids Surfaces B Biointerfaces* **2016**, *147*, 434–441.

(22) Pena-Francesch, A.; Montero, L.; Borrós, S. Tailoring the LCST of Thermosensitive Hydrogel Thin Films Deposited by ICVD. *Langmuir* **2014**, *30* (24), 7162–7167.

(23) Cifuentes, A.; Borros, S. Comparison of Two Different Plasma Surface-Modification Techniques for the Covalent Immobilization of Protein Monolayers. *Langmuir* **2013**, *29*, 6645–6651.

(24) Förch, R.; Zhang, Z.; Knoll, W. Soft Plasma Treated Surfaces: Tailoring of Structure and Properties for Biomaterial Applications. *Plasma Process. Polym.* **2005**, *2* (5), 351–372.

(25) Dixon, M. C. Quartz Crystal Microbalance with Dissipation Monitoring: Enabling Real-Time

Characterization of Biological Materials and Their Interactions. *J. Biomol. Tech.* **2008**, *19*, 151–158.

(26) Zhang, B.; Wang, Q. Quartz Crystal Microbalance with Dissipation. In *Nanotechnology Research Methods for Foods and Bioproducts*; Padua, G. W., Wang, Q., Eds.; John Wiley & Sons: Oxford, 2012; pp 181–194.

(27) Dunn, K. E.; Trefzer, M. A.; Johnson, S.; Tyrrell, A. M. Investigating the Dynamics of Surface-Immobilized DNA Nanomachines. *Sci. Rep.* **2016**, *6*, 29581.

(28) McNamara, T. P.; Blanford, C. F. A Sensitivity Metric and Software to Guide the Analysis of Soft Films Measured by a Quartz Crystal Microbalance. *Analyst* **2016**, 2911–2919.

(29) Kokubo, T.; Kushitani, H.; Sakka, S.; Kitsugi, T.; Yamamum, T. Solutions Able to Reproduce in Vivo Surface-Structure Changes in Bioactive Glass - Ceramic A-W. *J. Biomed. Mater. Res.* **1990**, *24*, 721–734.

(30) Ohtsuki, C.; Kushitani, H.; Kokubo, T.; Kotani, S.; Yamamuro, T. Apatite Formation on the Surface of Ceravital-Type Glass-Ceramic in the Body. *J. Biomed. Mater. Res.* **1991**, *25* (11), 1363–1370.

(31) Spanos, N.; Misirlis, D. Y.; Kanellopoulou, D. G.; Koutsoukos, P. G. Seeded Growth of Hydroxyapatite in Simulated Body Fluid. *J. Mater. Sci.* **2006**, *41* (6), 1805–1812.

(32) De Aza, a. H.; Velásquez, P.; Alemany, M. I.; Pena, P.; De Aza, P. N. In Situ Bone-Like Apatite Formation From a Bioeutectic(R) Ceramic in SBF Dynamic Flow. *J. Am. Ceram. Soc.* **2007**, *90* (4), 1200–1207.

(33) Takadama, H.; Hashimoto, M.; Mizuno, M.; Kokubo, T. Test of SBF for in Vitro Measurement of Apatite-Forming Ability of Synthetic Materials. *Phosphorous Res. Bull.* **2004**, *17*, 119–125.

(34) Dorozhkin, S. V. Bioceramics of Calcium Orthophosphates. *Biomaterials* **2010**, *31* (7), 1465–1485.

(35) Daculsi, G.; Laboux, O.; Malard, O.; Weiss, P. Current State of the Art of Biphasic Calcium Phosphate Bioceramics. *J. Mater. Sci. Mater. Med.* **2003**, *14* (3), 195–200.

(36) Dorozhkin, S. V. Calcium Orthophosphates. *J. Mater. Sci.* **2007**, *42* (4), 1061–1095.

(37) Liu, X.; Ding, C. Reactivity of Plasma-Sprayed Wollastonite Coating in Simulated Body Fluid. *J. Biomed. Mater. Res.* **2002**, *59* (2), 259–264.

(38) Duque, L.; Queralto, N.; Francesch, L.; Bumbu, G. G.; Borros, S.; Berger, R.; Förch, R.

Reactions of Plasma-Polymerised Pentafluorophenyl Methacrylate with Simple Amines. *Plasma Process. Polym.* **2010**, *7* (11), 915–925.

(39) Duque, L.; Menges, B.; Borros, S.; Förch, R. Immobilization of Biomolecules to Plasma Polymerized Pentafluorophenyl Methacrylate. *Biomacromolecules* **2010**, *11* (10), 2818–2823.

(40) Duan, Y. R.; Zhang, Z. R.; Wang, C. Y.; Chen, J. Y.; Zhang, X. D. Dynamic Study of Calcium Phosphate Formation on Porous HA/TCP Ceramics. *J. Mater. Sci. Mater. Med.* **2005**, *16* (9), 795–801.

(41) Lu, X.; Leng, Y. Theoretical Analysis of Calcium Phosphate Precipitation in Simulated Body Fluid. *Biomaterials* **2005**, *26* (10), 1097–1108.

(42) Jahromi, M.; Yao, G.; Cerruti, M. The Importance of Amino Acid Interactions in the Crystallization of Hydroxyapatite. *J. R. Soc. Interface* **2013**, *10*.

(43) Solonenko, A. P. Features of Calcium Phosphate Crystallization in the Presence of Amino Acids. **2010**, *18*, 69–76.

(44) Biolin Scientific. *Quartz Crystal Microbalance with Dissipation*; 2011.

(45) Neyra, M. P. Interactions between Titanium Surfaces and Biological Components, Universitat Politècnica de Catalunya, 2009.

(46) Cifuentes, A. Tailoring Carbon Nanotubes Properties for Gene Delivery Applications, Universitat Ramon Llull, 2013.

(47) Feiler, A. a; Sahlholm, A.; Sandberg, T.; Caldwell, K. D. Adsorption and Viscoelastic Properties of Fractionated Mucin (BSM) and Bovine Serum Albumin (BSA) Studied with Quartz Crystal Microbalance (QCM-D). *J. Colloid Interface Sci.* **2007**, *315* (2), 475–481.

(48) Höök, F.; Rodahl, M.; Brzezinski, P.; Kasemo, B. Energy Dissipation Kinetics for Protein and Antibody - Antigen Adsorption under Shear Oscillation on a Quartz Crystal Microbalance. *Langmuir* **1998**, *7463* (21), 729–734.

This page left blank intentionally

Chapter III. Guiding collagen self-assembly onto PECVD modified substrates

Prepared for submission [*Patent pending*]:

Anna Mas-Vinyals, Joan Gilabert-Porres, Salvador Borrós, “Improving the linking interface between collagen-based hydrogels and bone-like substrates”. Langmuir.

This page left blank intentionally

Guiding collagen self-assembly onto PECVD modified substrates

In the present chapter, we present an assessment of collagen fibrillation process using the quartz crystal microbalance with dissipation (QCM-D) technique. We validate our hypothesis that a previously immobilized collagen monolayer can act as anchoring point for subsequent collagen self-assembly which, in the proper condition, leads to the formation of higher order structures such hydrogels. Moreover, we present a study of the interaction between collagen and the glycosaminoglycans hyaluronic acid and chondroitin sulfate, two of the main components of the cartilage extracellular matrix. We intend to add both glycosaminoglycans to our hydrogel formulation enhancing its chondrogenic potential. Finally, we present the *in vitro* viability test of our hydrogel-immobilizing methodology.

3.1 Introduction

In the previous chapter, in order to gain insight into the bone-like platform design, we evaluated the bioactivity of different bioceramics, which are available on the market as bone substitutes. Moreover, we introduced the proposed linking interface between the bone-like platform and the cartilage-like collagen-based hydrogel. It has been shown how the pp-PFM polymeric coating does not block the ionic exchange between the bioceramic and the surrounding medium, and that it allows the immobilization of great amount of collagen molecules. Thanks to the covalent nature of the interaction between collagen and PFM we are able to obtain a stable coating, which will not be disrupted by physiologic changes. Thus, after having validated our linking interface at the molecular level, in this chapter we focus on the analysis of the process by which collagen self-assembly takes place. Fibrillation will be studied and monitored *in vitro* in a cell-free environment, using a previously immobilized collagen monolayer as anchoring point.

It is well known that collagen, self-assembled into hierarchical tissue networks, constitutes the main building block of several biological tissues[1]. The use of collagen in biomaterials and tissue engineering for regenerative purposes has been widely explored. Moreover, as hydrogels possess the unique property of sharing biomechanical characteristics with ECM[2] are great candidates for tissue repair. Collagen exemplifies multi-hierarchical self-assembly as individual collagen triple helix, known as tropocollagen (TC), have the ability of assemble in a complex hierarchical way which causes the formation of macroscopic fibers, which continue to self-assembly linearly and laterally and give rise to a hydrogel network[3] (Figure III-1).

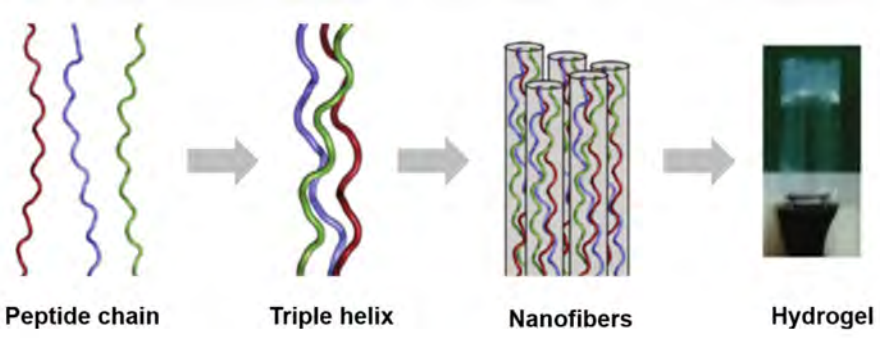

Figure III-1. Collagen self-assembly process: from the peptide chains to a hydrogel structure. Adapted from O'Leary et al[3].

Gross and coworkers[4,5] and Jackson and Fessler[6] reported for the first time the formation of a gel structure by collagen molecules. In their studies, they found that collagen could be extracted from tissues in diluted acids or high-salt buffers, and then reconstituted into fibrils by neutralizing and/or warming the solutions to 37ºC in a buffer containing a neutral salt solution. Under the electron microscope, it was seen how collagen molecules and aggregates of molecules would spontaneously self-assemble forming fibrils that had the characteristic 67 nm repeat distance.

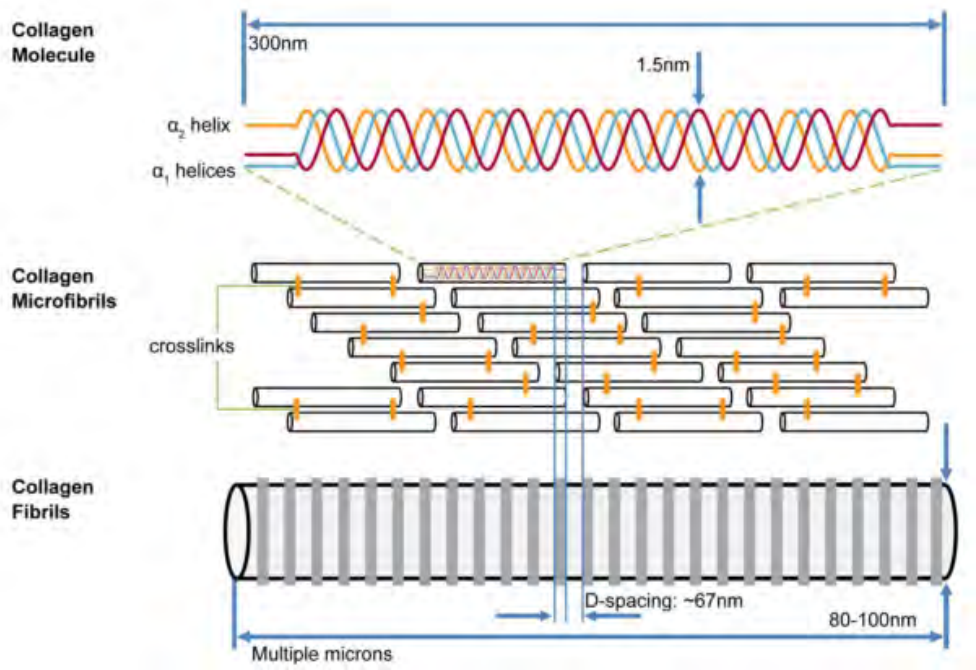

Figure III-2. Scheme of the hierarchical features of collagen, from the amino acid sequence up to collagen fibers[7].

However, the formation of collagen fibrils can be altered by the addition of substances able to modify both electrostatic interactions and hydrophobic bonds[8]. The mechanism of collagen fibril formation has been under debate since 1950s. For instance, thermodynamic studies suggested that native collagen fibril formation was an endothermic process made thermodynamically favorable by the large increase in mobility of water molecules[9]. Other studies indicate that water-mediated hydrogen bonding between polar residues promotes collagen assembly[10]. So far, the collagen fibril formation process can be divided into two stages: nucleation and fiber growth[11]. In the cell, collagen fibrillogenesis begins with the generation of TC monomers by the cleavage of collagen propeptides at each triple helix terminus. TC monomers are flanked by short non-triple helical telopeptides, which are suggested to be important for initiating fibrillogenesis[12]. However, it has been demonstrated how triple helices lacking telopeptides can also assemble into fibrils, which suggests that telopeptides are not essential for collagen fibril formation, but they can accelerate the process[13].

TC monomers have the unique property of being unstable at body temperature, as the random coil is the preferred conformation[14]. Thus, the formation of fibrils must exert a stabilizing effect over the unstable collagen triple helices. This theory is supported by the fact that the assembly of strong macromolecular structures is essential for providing the appropriate mechanical resistance, which enables collagen to withstand stress in one, two and three dimensions[15]. The structure of the collagen microfibril has been determined as a hexagonal unit cell. This model suggests that TC monomers are packed forming super twisted, right-handed microfibrils, which ultimately lead to spiral-like structure of the mature collagen microfibril[16].

By and large, self-assembly processes can be defined as the autonomous organization of components into patterns or structures without human intervention[17]. Molecular self-assembly constitutes an approach for fabricating novel supramolecular architectures. It is mediated by weak, non-covalent bonds, notably hydrogen bonds, ionic bonds (electrostatic interactions), hydrophobic interactions, van der Waals interactions and water-mediated hydrogen bonds. All biomolecules, including peptides and proteins, interact and self-organize to form well-defined structures that are associated with functionality[18].

In contrast to collagen type I fibrillation, the process by which collagen type II, the main constituent of cartilage matrix, is arranged into higher order structures is still not well understood[19]. Thus, in the present work we will produce our cartilage-like hydrogel taking advantage of the widely described ability of collagen type I to self-assemble into hydrogel structures at physiologic conditions, is to say, 37ºC and pH 7,4. We will benefit of the intrinsic ability of collagen to organize into higher order structures and avoid the use of crosslinking agents which could compromise the biocompatibility of the scaffold. Moreover, thinking one step further, the simplest our formulation is, easier will be the regulation pathway towards market approval.

After studying the collagen self-assembly process, we also present an analysis of the interaction between collagen molecules and glycosaminoglycans hyaluronic acid and chondroitin sulfate. Both are key components of cartilage extracellular matrix and we intend to incorporate them into our hydrogel formulation in order to confer a higher chondrogenic potential to our scaffold.

Cartilage extracellular matrix is mainly composed of proteoglycans and collagen. Proteoglycans consist in a protein core at which glycosaminoglycans are attached, forming a bottlebrush-like structure. Proteoglycans can bind or aggregate to a backbone of hyaluronic acid, as depicted below in Figure III-3. They account for approximately 30% of cartilage dry weight[20] while collagen fibers represent from 60 to 70% of the dry weight[21] of the tissue.

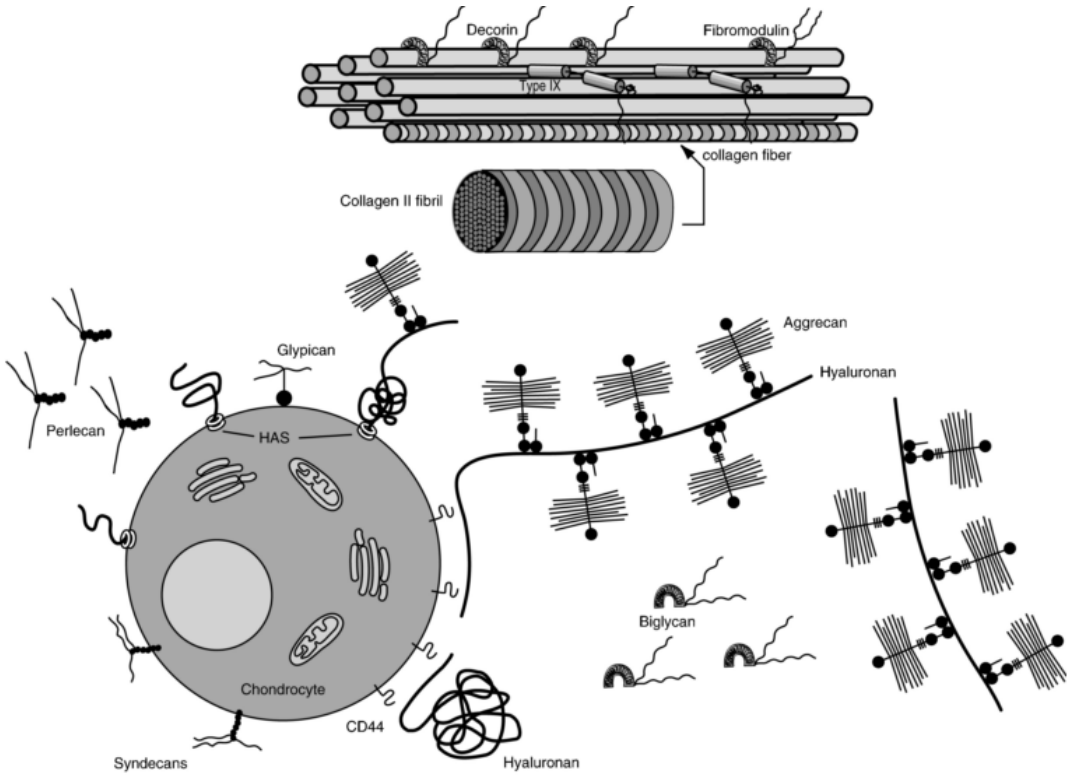

Figure III-3. Proteoglycan presence in cartilage extracellular matrix and its interaction with chondrocytes[22].

The network of collagen fibers provides both tensile strength to cartilage and the capacity to contain the swelling pressure of the embedded proteoglycans. In aqueous media, proteoglycans are polyanionic, as the molecule has negatively charged sites that arise from its sulfate and carboxyl groups. In solution, the mutual repulsion of the negative charges causes the spreading of the aggregated proteoglycan molecules which occupy a large volume, limited by the collagen network. This swelling of the proteoglycans against collagen fibers is critical for the mechanical response of the tissue. When cartilage is under compression, the negative charges of aggrecan

are pushed close together, increasing the repulsive force and conferring the compressive stiffness of the tissue[23].

Besides conferring such mechanical properties, both glycosaminoglycans also play a special role in cell signalling. As for hyaluronic acid, it has been reported that its interaction with the surface antigen CD44, hyaluronan main receptor, is crucial for maintaining cartilage homeostasis[24,25,22]. Besides, previous studies[26] have shown that HA-enriched environments initiates and enhances chondrogenesis of human adipose-derived mesenchymal stem cells. Chondroitin Sulfate induces the synthesis of cartilage-specific markers, collagen, and proteoglycan by stimulating the chondrocyte metabolism[27], moreover it has been shown to prevent proteoglycan degradation and to suppress the hypertrophic mineralization of chondrocytes[28].

Finally, after having studied the process by which our scaffold will be assembled and the interactions between its constituents, we present the biocompatibility assessment of our hydrogel formulation and the validation of the developed hydrogel-immobilizing technology. To do so, we have assessed the biocompatibility of the hydrogel and its immobilizing methodology, which is critical to be used for tissue engineering applications. Moreover, we have tested our immobilization procedure onto different materials which are very different in nature. The possibility of applying our technology to a wide range of materials opens the door to other applications besides osteochondral repair.

Due to the high reactivity towards amines, ester polymer precursors, such as PFM have been used in the field of biomedicine[29,30,31]. However, it must be taken into account that pentafluorophenol has a toxic nature and to avoid cytotoxic effects it must be eliminated from the media after being used for biological purposes[32]. Our group has experience on using PFM thin films for different biological applications. For instance, it has been used to develop functional hydrogel films by initiated chemical vapor deposition (iCVD) that could be easily tailored and combined with biomolecules, being a powerful tool to study cell signaling[33]. Moreover, it has been demonstrated how PECVD PFM polymeric films can be used to develop new culture models as the so-called sandwich cultures, which have been successfully applied to maintain adult hepatocyte phenotype[34].

3.2 Materials and Methods

3.2.1 Collagen fibrillation studies using QCM-D

To evaluate the collagen self-assembly process the QCM-D window module (QWM 401, BiolinScientific AB, Frölunda, Sweden) was used, which enables image acquisition during the progress of the experiment. Thus, images were acquired in real-time with an optical microscope (Leica DM 2500M). The QCM-D experimental protocol was designed based on reported results which show that type I collagen fibrillogenesis and gelation *in vitro* is a multistep process which occurs spontaneously at neutral pH and physiologic temperature[35]. Thus, after acquiring a PBS (E404-200TABS, Amresco®) baseline at 25ºC, a 0,5 mg/ml collagen solution (Fibricol®, #5133-20ML, Advanced Biomatrix) in PBS was recirculated through the QCM-D chamber. Once signal has stabilized indicating substrate saturation, temperature was increased up to 37ºC, is to say, to physiologic temperature. At this point, all the environmental conditions should be appropriate for fibril formation. Next, a fresh collagen solution is then introduced and recirculated through the QCM-D chamber, which will provide collagen molecules necessary for fibril formation. Finally, a PBS wash was performed to eliminate the excess of collagen free molecules.

3.2.2 Optical microscopy and atomic force microscopy (AFM) studies of collagen fibril formation

To further evaluate the progression of collagen fibrillation process using both optical (Leica DM2500 M) and non-contact atomic force microscopy (XE 100 Park System; AFM) the same experimental procedure applied for the QCM-D experiment was reproduced using silicon wafers. Briefly, silicon wafers were incubated following the same pattern and conditions than for QCM-D experiment. As it has been detailed for the QCM-D protocol, the experiment can be divided in four stages: (I) collagen recirculation at 25ºC (II) temperature increase from 25ºC to 37ºC (III) fresh collagen solution recirculation at 37ºC (IV) final PBS wash. Four samples (Table III-1) were prepared, each of them corresponding to one of the stages of the fibrillation process. Samples were incubated following the corresponding procedure under agitation using the orbital shaker.

Table III-1. Reproduction of the QCM-D experiment soaking silicon wafers in a 24-well plate

Sample	Soaking solutions (Soaking time)	QCM-D Equivalence
Wafer 1	PBS 1X (90 min)	PBS Baseline
	Collagen 500 μg/ml at 25ºC (7 hours)	Collagen adsorption at 25ªC
Wafer 2	PBS 1X (90 min)	PBS Baseline
	Collagen 500 μg/ml at 25ºC (7 hours)	Collagen adsorption at 25ªC
	Temperature Change to 37ºC (O/N)	Temperature Change
Wafer 3	PBS 1X (90 min)	PBS Baseline
	Collagen 500 μg/ml at 25ºC (7 hours)	Collagen adsorption at 25ªC
	Temperature Change to 37ºC (O/N)	Temperature Change
	Fresh Collagen Solution 500 μg/ml at 37ºC (7 hours)	Collagen adsorption at 37ªC
Wafer 4	PBS 1X (90 min)	PBS Baseline
	Collagen 500 μg/ml at 25ºC (7 hours)	Collagen adsorption at 25ªC
	Temperature Change to 37ºC (O/N)	Temperature Change
	Fresh Collagen Solution 500 μg/ml at 37ºC (7 hours)	Collagen adsorption at 37ªC
	PBS 1X Wash (90 min)	Final PBS Wash

3.2.3 Studying the interaction of collagen with GAGs: a QCM-D study

3.2.3.1 Studying the Interaction of GAGs with a collagen monolayer

First, the interaction between both hyaluronic acid and chondroitin sulfate with a collagen monolayer has been evaluated using the following methodology. QCM-D gold sensors have been coated with PFM by PECVD, following the procedure described below. First, the experiment has been performed at physiological pH, is to say 7,4. A baseline was obtained flowing a PBS solution through the QCM-D chamber. Next, a 10 μg/ml collagen solution has been recirculated until substrate saturation. Next, a PBS wash has been performed to eliminate the collagen molecules that have not reacted with the PFM film. Then, a solution of 2mg/ml of hyaluronic acid or chondroitin sulfate in PBS has been recirculated through the QCM-D chamber until reaching

signal stabilization. A final PBS wash has been performed to eliminate the non-interacting molecules.

Next, in to evaluate the effect of pH over the interaction between collagen and glycosaminoglycans, the following procedure has been used. First, a PBS baseline was obtained followed by a 10 μg/ml collagen solution recirculation, to obtain a collagen monolayer. It must be considered, that collagen molecules must be deprotonated to be able to react with the underlying PFM film, being this the reason for working at pH 7,4. Next a PBS wash was performed to remove the excess of collagen molecules. To induce a pH change, an acetate buffer at pH 4.0 was flown through the QCM-D chamber. Next, a solution of 2mg/ml of hyaluronic acid or chondroitin sulfate in acetate buffer has been recirculated through the QCM-D chamber, until reaching signal stabilization. Finally, an acetate buffer wash was performed to remove the non-interacting molecules, and it was followed by a PBS wash to return the system to its initial pH conditions.

3.2.3.1 Studying the Interaction of GAGs with self-assembled collagen fibers

In order to study the interaction of GAGs with self-assembled collagen fibers, the QCM-D protocol followed and described before was performed. The entire experiment was performed at pH 7,4, as pH changes could disrupt the previously formed collagen fibers. Thus, after collagen fibril formation, a solution of 2 mg/ml of HMW-HA or LMW-HA was recirculated through the QCM-D chamber. Finally, in order to remove the non-interacting molecules, a PBS buffer wash was carried out.

3.2.4 In vitro testing of the hydrogel formulation

3.2.4.1 Culture of human Normal Dermal Fibroblasts

In order to perform the biocompatibility assessment of the hydrogel formulation, the cell encapsulation protocol and the hydrogel immobilization procedure human Normal Dermal Fibroblasts (hNDFs, C-12302 Promocell, Heidelberg, Germany) were used. hNDFs were cultured in P100 petri dishes (20035, SPL Lifesciences) using DMEM (Lonza) supplemented with 10% fetal bovine serum (FBS, 16SV30180.03, Cultek) 100 U/ml Penicillin / 0,1 mg/ml Streptomycin (L0022, Biowest) and 2mM L-Glutamine (X0550-100, Biowest). Cultures were maintained in the incubator in humidified atmosphere at 37ºC and 5% CO_2.

3.2.4.2 Cell harvesting and subculture from tissue flasks

Petri dishes were washed with 4ml of PBS (L0615-500, Biowest) and treated with 2 ml of Trypsin-EDTA 0,05% (25300062, Gibco - Life Technologies) for 3 minutes at 37ºC, or until cells started to detach from the plate. Trypsin was inactivated adding 8 ml of serum containing DMEM, and cells were disrupted mechanically by pipetting until individual cells were observed under

phase microscopy. Next, cells were counted and resuspended as needed for the next passage or for their encapsulation in hydrogels.

3.2.4.3 3D culture technique using collagen/glycosaminoglycans composite hydrogels

The procedure for cell encapsulation into collagen/glycosaminoglycans composite hydrogels is depicted below in Figure III-4. Briefly, an 8 mg/ml collagen type I (Fibricol®, #5133-20ML, Advanced BioMatrix) solution (hydrogel gelling solution) was prepared by mixing 8 parts of Fibricol®, 1 part of PBS 10X (X0515, Biowest), 0,75 parts of a sterile filtered 0,1M NaOH (A3910, Panreac) solution and 0,25 of cell-culture water (BE17-724Q, Lonza). This solution was mixed with an equal volume of cell suspension ($4 \cdot 10^6$ cells/ml) in PBS containing 0,3 mg/ml of hyaluronic acid and or chondroitin sulfate (both glycosaminoglycans were kindly provided by Bioiberica S.A.U), to obtain a final cell concentration in the hydrogel scaffold of $2 \cdot 10^6$ cells/ml. Next, 100 μl of the scaffold solution was placed in a 48-well plate (30048, SPL Lifesciences) and incubated during 45 minutes at 37ºC and 5% CO2 to allow the hydrogel formation. Finally, 400 μl of supplemented DMEM was added. Cell culture medium was changed every two days.

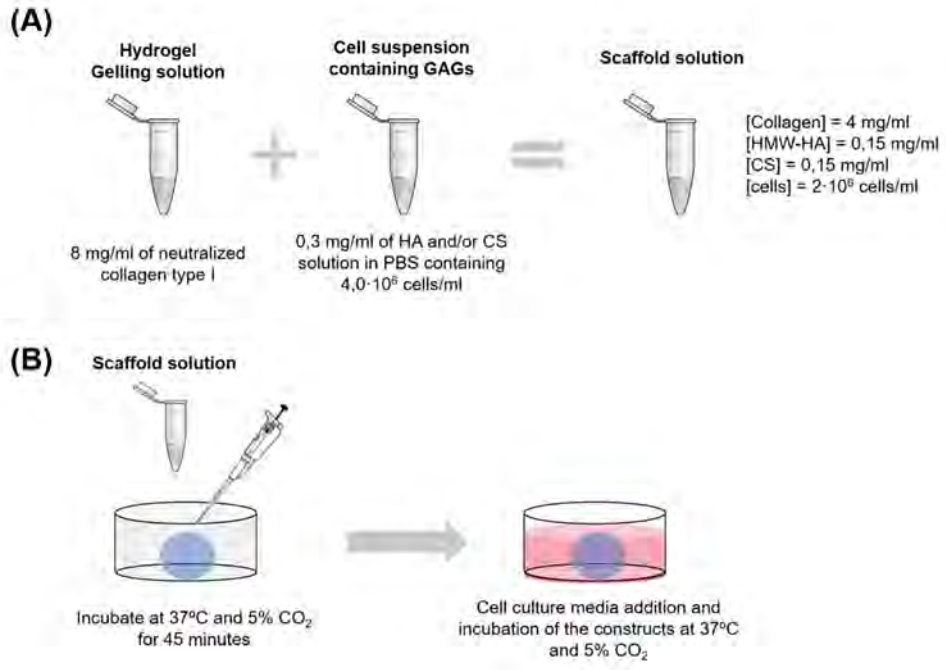

Figure III-4. 3D culture protocol in collagen/glycosaminoglycan composite hydrogel. **(A)** Scaffold solution preparation, **(B)** Hydrogel scaffold self-assembly and further incubation.

3.2.4.4 Collagen layer coating of pp-PFM-coated substrates and cell seeding for in vitro testing

pp-PFM-coated substrates were used to assess the effect of the PFM coating over the cell viability. The materials used for in vitro testing were PTFE membranes (Millipore®), Collagen membranes (Viscofan Bioengineering) and hydroxyapatite disks (Plasma Biotal Ltd.)

Briefly, substrates were coated with PFM by PECVD as it will be described below. After plasma treatment, pp-PFM-coated substrates were incubated overnight at 37ºC with a 0,1 mg/ml collagen solution (Fibricol®, #5133-20ML, Advanced Biomatrix) to obtain a collagen layer onto the polymeric coating. Next, substrates were rinsed with PBS to remove the unbound collagen molecules and the remaining pentafluorophenol groups. Then, collagen-ppPFM-PTFE and the collagen-ppPFM-collagen membranes were sterilized using a 70% ethanol solution[34], while the other substrates were sterilized under UV. Next, a thin collagen hydrogel was self-assembled onto the collagen layer attached to the polymeric coating. To do so, a collagen gelling solution (Fibricol®, #5133-20ML, Advanced Biomatrix) was prepared as follows: 8 parts of a collagen solution 10mg/ml was mixed with 1 part of PBS 10X 0,75 parts of a NaOH solution 0,1M and 0,25 parts of cell culture H_2O. Thus, enough volume of gelling solution to cover the entire surface was placed onto the substrates and incubated during 1 hour at 37ºC to allow the hydrogel formation. Next, cells are seeded on the top of the hydrogel as follows.

To seed the cells onto the coated substrates, the latter were incubated with the corresponding volume of human Normal Dermal Fibroblasts (hNDFs, C-12302, Promocell) cell suspension in DMEM (supplemented with 10% FBS, 1% glutamine and 1% penicillin/streptomycin) at a final concentration of 24000 cells/ml. Following a 48-hour attachment period in the incubator at 37ºC and 5% CO_2, medium was changed to remove dead cells. Cells were left at the incubator and medium was changed every two days.

3.2.4.5 Live/Dead staining

Cell viability was assessed using a two-dye fluorescence assay. Live cells are stained green thanks to intracellular estearase activity, which transforms non-fluorescent fluorescein diacetate into green fluorescent fluorescein. Dead cells appear red as ethidium bromide (EtBr) enters dead cells through damaged membranes and binds nucleic acids. Briefly, culture medium was removed from the wells and the constructs were washed three times with PBS (L0615-500, Biowest). Then, samples were covered with a staining solution of 10 μg/ml fluorescein diacetate (FT378, Sigma-Aldrich) and 40 μg/ml of EtBr (E7637, Sigma-Aldrich) in PBS1X. Samples were analyzed under fluorescence microscope (Zeiss Axiovert 200M).

3.2.4.6 DAPI/Phalloidin staining

To assess cell morphology cells were double stained with DAPI [4',6-diamidino-2-phenylindole] (D9542, Sigma-Aldrich) and phalloidin-tetramethylrhodamine B isothiocyanate (P1951, Sigma-

Aldrich). Shortly, constructs were fixed with 4% paraformaldehyde (PFA) during 30 minutes at 4ºC, followed by three washes with PBS. Next, cell membranes were permeabilized with an incubation in 0,1% (v/v) Triton x-100 in PBS during 30 minutes at room temperature and with soft shaking, followed by three PBS washes. Samples were incubated with phalloidin-TRITC at a final concentration of 1 μg/ml in PBS for 25 minutes. Next, a DAPI solution with a concentration of 1 mg/ml is added onto the previous solution and incubated for 5 minutes. Finally, three washes of 10 minutes each are performed with PBS under agitation.

3.2.4.7 MTT assay

Cell viability was assessed using an MTT [3-(4,5-dimethylthiazol-2-yl)-2,5-diphenyltetrazolium bromide] (M5655, Sigma-Aldrich) assay. Briefly, cell culture medium was aspirated from the wells, and the reagent was added to a final concentration of 0,5 mg/ml in DMEM. Next, samples were incubated during 3 hours at 37ºC in the dark. Subsequently, the reagent solution was aspirated, and the constructs lysed using a 0,04N HCl solution in isopropanol. Finally, the absorbance was read at 550nm.

3.2.5 Surface modifications by plasma techniques

All the surface modifications carried out in the present chapter have been performed using a stainless steel vertical plasma reactor, as described in the previous chapter. Briefly, after obtaining a base pressure of 0.001-0.003 mbar, PFM (K27096, Manchester Organics Ltd.) was heated up to 75ºC and introduced into the reactor chamber achieving a pressure of $3{,}5 \cdot 10^{-2}$ mbar. The continuous radiofrequency power was fixed at 15W and pulsed plasma polymerization with a duty cycle (DC) of 10/20 [DC = $t_{ON}/(t_{ON}+t_{OFF})$][36] was carried out for 5 minutes. Next, plasma discharge was turned off, and PFM vapour flow has been kept constant for 3 additional minutes in order to allow the remaining active sites to react with the monomer.

3.3 Results and discussion

3.3.1 Collagen fibrillation studies using QCM-D

First, the ability to monitor the collagen fibril formation process with the QCM-D technique was evaluated using a non-coated stainless-steel sensor. The experimental procedure was designed based on the capacity of collagen molecules to self-assemble at physiologic conditions, is to say, pH 7,4 and 37ºC[1]. The use of QCM-D to study fibrillation processes has been previously reported[37,38]. Hovgaard et al[37] reported the use of QCM-D in combination with AFM to study glucagon fibrillation, and the obtained results lead us to hypothesize that we could exploit both techniques to study collagen self-assembly process.

Changes in both frequency and dissipation signals recorded by QCM-D are shown in Figure III-6A. As expected, the recirculation of the collagen solution through the QCM-D chamber caused a frequency shift due to the increase of mass adsorbed onto the sensor's surface. Once substrate saturation was reached, is to say, when frequency signal reached a *plateau*, temperature was increased up to 37ºC. At this point, all the environmental conditions should be appropriate for fibril formation. As it can be seen (Figure III-6A), the change of temperature itself entails both a frequency and dissipation shift. In order to determine the magnitude of signal variation inherently tied to the temperature change, the effect of increasing from 25ºC to 37ºC the QCM-D chamber temperature over a PBS buffer solution is measured. As it can be seen in Figure III-5A, a change of temperature has a strong effect over both frequency and dissipation signals. It must be noticed that temperature change does not induce any irreversible change in the flowing solution over the sensor surface, as both signals return to their initial value when temperature is fixed again to 25ºC at the end of the experiment. As temperature changes induce variations in the oscillation of the resonator, variations in the observed viscoelastic behavior of the adsorbed layer are expected. The latter is confirmed by the ΔD versus Δf plot (Figure III-5B), which shows the presence of changes in the viscoelastic properties. I can be seen how the relation between the two parameters is not linear during all the experiment, and changes of slope, which mark the limits between the different processes at which the system has been submitted, can be clearly appreciated. However, the cycle of heating and cooling produces a frequency and dissipation hysteresis, as both signals return to its initial value at the end of the experiment, that is when temperature is returned to its initial value. Thus, one can be certain that changes produces over the resonator by the temperature change itself are reversible. So, if the fibrillation process is related with detectable changes by the QCM-D in viscoelastic properties of the adsorbed layer it will be monitored, and appreciable differences with regard to the blank measurement are expected.

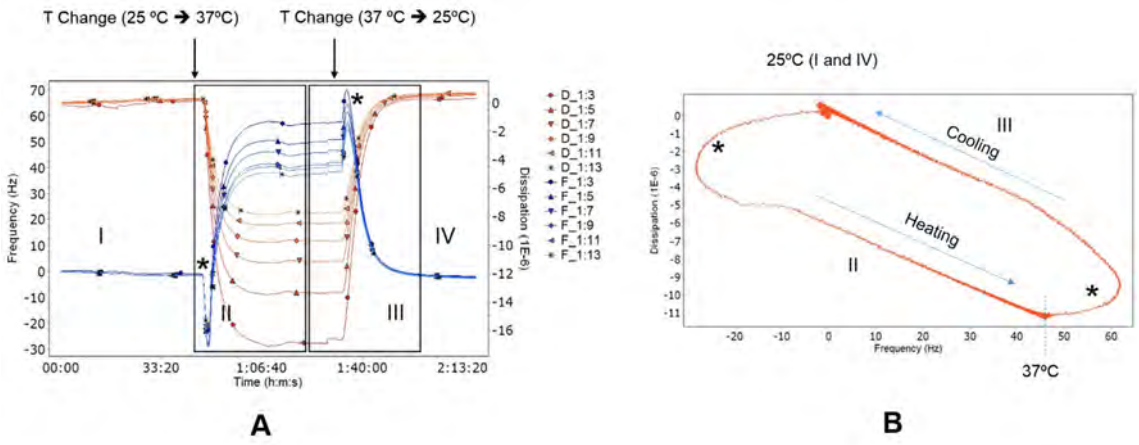

Figure III-5. Effect of temperature change over PBS. **(A)** QCM-D evolution profile. The 3rd (•), 5th (▲), 7th (▼), 9th (♦), 11th (◄), and 13th (✕) overtones are shown. **(B)** ΔD_7 vs Δf_7 (Hz) plot.

Focusing again on Figure III-6A, it can be appreciated how after temperature stabilization, both frequency and dissipation signals reach a *plateau* suggesting that no change in the adsorbed layer is taking place. The collagen solution has been recirculated during several hours, thus, the possibility that free collagen molecules available for fibril formation are exhausted is considered. Thus, a fresh collagen solution is pumped through the QCM-D chamber (Stage III, Figure III-6A) to provide free collagen molecules for fibril formation. The flow of the fresh solution causes an increase in the dissipation signal; however, frequency remains practically constant. The fact that frequency signal remains constant suggests that the system is not reporting a mass increase over the sensor surface. In contrast, the increase in dissipation signal reveals that the adsorbed layer is becoming more dissipative. It could be hypothesized that changes in the system viscoelasticity are due to fibril formation. However, as QCM-D data alone is not enough, further characterization is required to confirm the presence of fibers. Thus, taking advantage of the QCM-D window module potential, which enables real-time sensor optical monitoring of the sensor surface, optical microscopy images are taken as the experiment progresses. Figure III-6C shows the images taken through QCM-D window module at the end of each stage. As it can be seen, after stage I the image gets cloudy, and cloudiness increases with the experiment progression.

To confirm the presence of collagen fibers through higher resolution images, the experiment was reproduced, as detailed before, using silicon wafers as substrate, and following the same protocol than for the QCM-D experiment (Figure III-6D). Collagen fibers can be already seen after the first stage and after the subsequent temperature change, as it is shown in Figure III-6D stages I and II. However, the presence of fibrils is not homogeneous over the entire substrate's surface. Thus, it can be hypothesized that the formation of collagen fibers starts with a heterogeneous nucleation process, by which collagen molecules adsorb at preferential sites onto the substrate surface, for instance superficial defects. After flowing the fresh collagen solution (phase III) and concurring with the dissipation signal shift, the presence of collagen fibers is widespread throughout the substrate, and it is not undermined by the final PBS wash. Therefore, the

introduction of the fresh collagen solution plays an important role in fibril extension, as it provides more protein molecules available for fibril growth. It must be pointed out that the introduction of the fresh collagen solution (phase III) does not trigger fibril formation as it might be thought judging by the QCM-D signal evolution profile alone, instead, the first collagen fibrils can be observed during the initial collagen adsorption at 25ºC. However, no changes in frequency and/or dissipation signal that could be associated with fibrillation occur at stage I. Thus, it is suggested that the detection of the fibrillation process by QCM-D is subject to the extent of fibril formation, as detectable viscoelastic changes in the adsorbed layer may occur when the substrate surface is significantly covered by protein molecules.

Thanks to the combination of QCM-D technique with optical microscopy images, the formation of collagen fibers has been confirmed. It must be pointed out that we have been able to relate the dissipation shift (Figure III-6A) that occurs after the introduction of the fresh collagen solution (stage III) with the extension of fibril presence over the entire sensor's surface. As for the frequency signal, it has been seen that the fact that viscous films are not fully coupled onto the sensor's surface and they do not follow the sensor oscillation[39] could explain that fibril formation does not result in a frequency shift as collagen fibers are highly viscous and they are not fully attached to the sensor surface.

The viscoelastic behavior of the adsorbed layer can be further analyzed by the direct relation between changes in dissipation signal and the frequency shift (Figure III-6B) as alterations in the slope of ΔD-Δf curve can be attributed to configuration changes[37]. The horizontal discontinuous line indicates the change of collagen solution (transition from phase II to phase III), thus, the data above the line corresponds to the recirculation of the fresh new solution. A change in viscoelastic behavior can be appreciated, as two different regions can be clearly distinguished. After the introduction of the fresh collagen solution, the ratio between dissipation changes and frequency shift increases indicating that the adsorbed layer becomes softer and dissipative. Finally, it can be seen how the PBS wash does not alter the slope of ΔD-Δf curve which is in line with both Figure III-6A and Figure III-6D. The former shows no changes in both frequency and dissipation signals after PBS wash, while the latter demonstrates that collagen fibers remain attached to the substrate after the buffer wash. Thus, we can be certain that fibril formation is a superficial phenomenon rather than a change in the bulk solution.

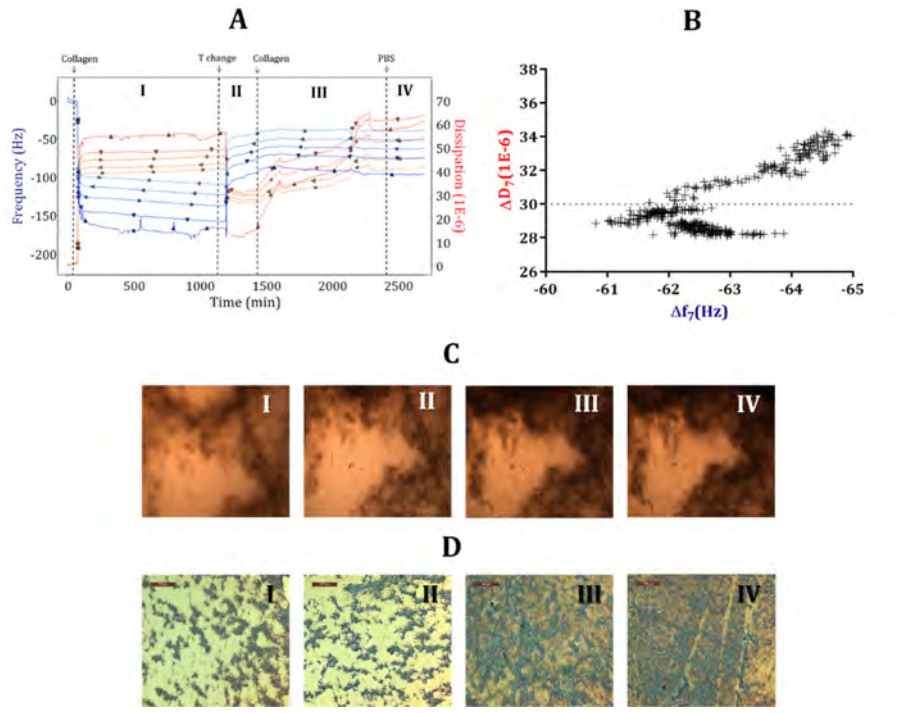

Figure III-6. QCM-D monitoring of collagen fibrillation using the window module. **(A)** frequency (Δf) and dissipation (ΔD) measurements. The 3rd (•), 5th (▲), 7th (▼), 9th (♦), 11th (◄), and 13th (✕) overtones are shown. **(B)** ΔD_7 vs Δf_7 curve **(C)** optical microscopy images taken through the QCM-D window module **(D)** optical microscopy images of the experiment reproduction using silicon wafers.

As it can be seen below in Figure III-7, the presence of collagen fibers at the end of the process was confirmed by AFM.

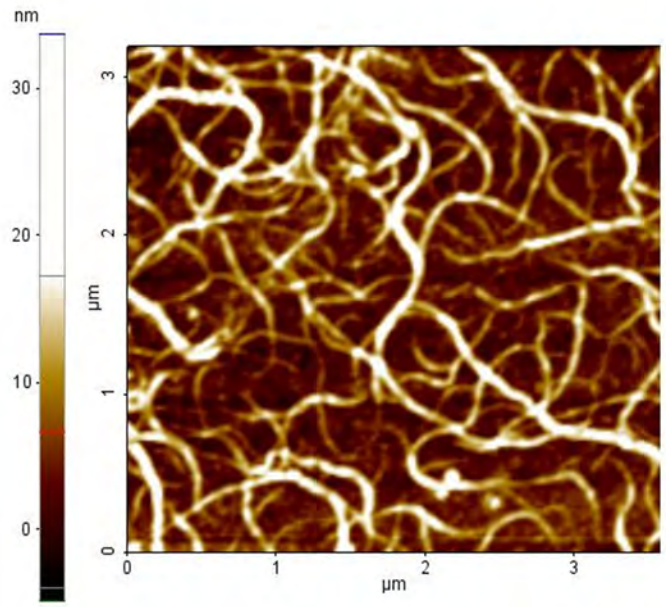

Figure III-7. AFM microscopy performed on a silicon wafer after stage IV.

To get a deeper insight into the viscoelastic changes associated with the dissipation shift which has been related with the fibril formation process, the thickness of the adsorbed layer has been obtained using the Voigt model[40] (Figure III-8). As shown, the thickness follows the same pattern than the dissipation. However, while dissipation signal is affected by the temperature change, the thickness of the adsorbed layer remains nearly unaffected, supporting that the signal variation associated with the temperature change is an artifact of the measurement system. After the addition of the fresh collagen solution there is a sudden increase of thickness which can be attributed to the fibril formation process. Finally, a PBS wash is performed to remove free collagen molecules and stop the fibrillation process. As it can be seen, this washing step causes the stabilization of both dissipation and thickness.

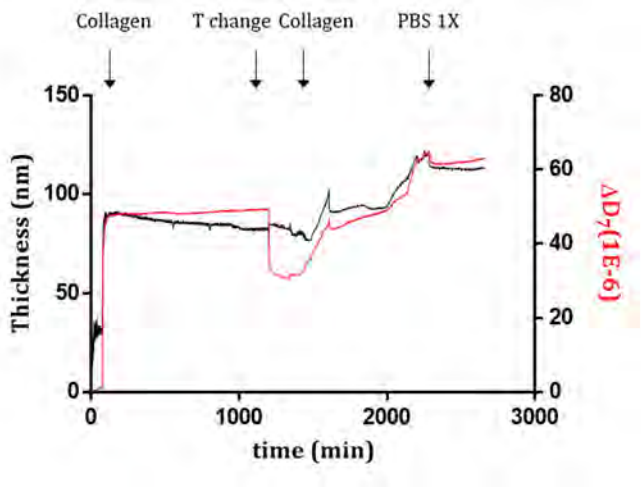

Figure III-8. Progression of thickness obtained with Voigt model together with variation of dissipation (ΔD_7) during the collagen fibril formation process.

To that extent, the ability of the QCM-D technique to monitor collagen self-assembling process has been demonstrated. Next, the previous experiment will be repeated using a PFM-coated sensor, in order to evaluate the effect of the polymeric coating over fibril formation (Figure III-9). To be used as linking interface between a substrate and a collagen-based hydrogel, the PFM coating not only must not disturb the collagen fibrillation process but also should enhance its self-assembly.

As it happened with the non-coated sensor, the recirculation of a collagen solution through the QCM-D chamber caused a frequency shift, as a result of mass adsorption onto the sensor's surface. However, the presence of the PFM coating leads to the absorption of a higher amount of protein, resulting in a higher frequency shift. Next, the temperature change itself caused both a frequency and dissipation shift as it happened with the non-coated sensor. However, in this case the dissipation signal keeps increasing while the frequency signal reaches a plateau after temperature stabilization. The latter can be a caused whether by a change in the pp-PFM coating or by a change in the viscoelasticity of the adsorbed protein layer. To be sure that the polymeric coating is not affected by the temperature change, a control experiment has been performed by

flowing PBS through the QCM-D chamber and changing the temperature from 25 to 37ºC. Again, the temperature change itself caused both a frequency and dissipation shift, however both signals reached a plateau after temperature stabilization (data not shown), demonstrating that the PFM coating remains unaffected by the temperature change. Again, a fresh collagen solution is recirculated through the system after temperature change and stabilization. As it can be seen, after flowing the fresh collagen solution through the chamber, the frequency signal remains constant and dissipation keeps increasing, meaning that the adsorbed layer becomes more dissipative. As PFM provides anchoring points for collagen molecules it is possible that the fibrillation takes place right after the temperature change, as there are sufficient collagen molecules anchored to the sensor's surface to start the process. Moreover, after temperature change, differences between the overtones grow, which may be attributed to a higher surface thickness caused by fibrillation. It should be stressed that for the non-coated sensor the overtone widening was not appreciated.

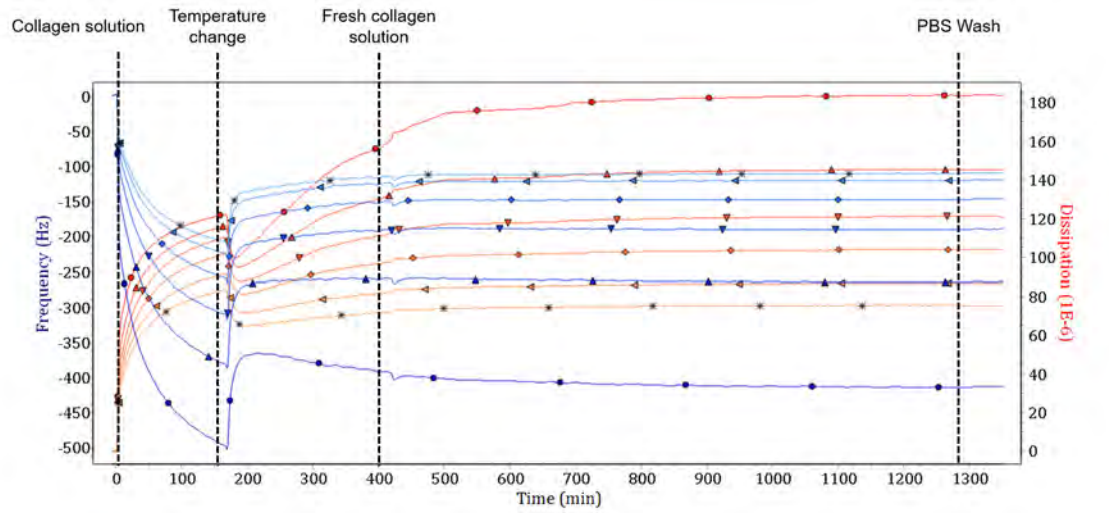

Figure III-9. Frequency and Dissipation changes during collagen fibril formation process for a PFM-coated stainless-steel sensor. The 3rd (●), 5th (▲), 7th (▼), 9th (♦), 11th (◄), and 13th (✕) overtones are shown.

To support the QCM-D results, optical microscopy images obtained after the incubation of both non-coated and PFM-coated silicon wafers are shown in Figure III-10. The most significant difference between the non-coated and the PFM-coated substrate is that the latter is entirely covered by collagen fibers right after temperature change. Thus, it can be hypothesized that the formation of collagen fibers starts with a heterogeneous nucleation process, by which collagen molecules adsorb at preferential sites onto the substrate's surface. For the non-coated substrate, those preferential sites are mainly superficial defects, while for the PFM-coated substrate are the reactive groups of the polymeric coating, which are homogeneously distributed. Moreover, for the non-coated substrate there is a significant difference between the image taken before and the one taken after flushing the fresh collagen solution, which causes the appearance of a great amount of fibers. On the contrary, for the PFM-coated substrate the extent of fiber formation is less affected by the addition of a fresh collagen solution. Thus, it has been demonstrated how the

presence of the polymeric coating promotes the self-assembling process as it provides anchoring points for collagen molecules accelerating the fibril formation process.

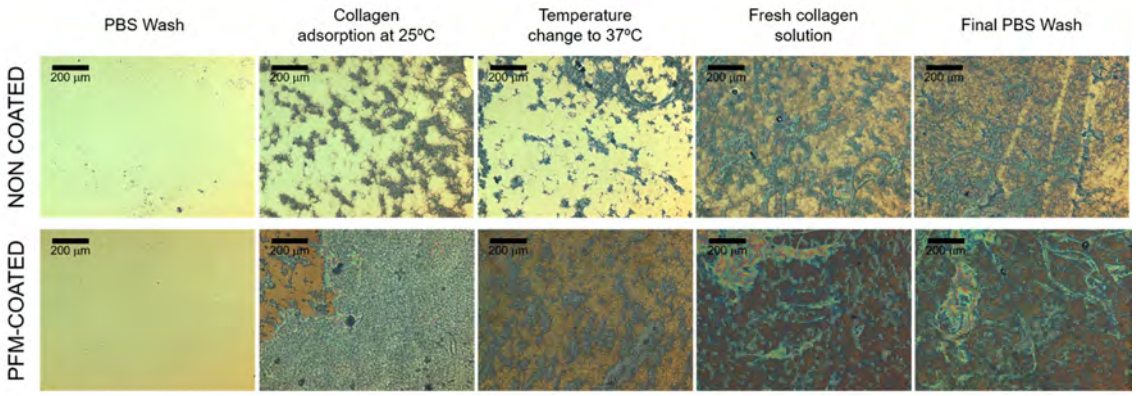

Figure III-10. Stimulation of the QCM-D experiment with silicon wafers for both non-coated and PFM-coated wafers.

3.3.2 Interaction of GAGs with collagen: a QCM-D study

As already mentioned, hyaluronic acid and chondroitin sulphate are key components of the cartilage extracellular matrix. Hence, to obtain a high degree of mimicry with cartilaginous tissue we will incorporate both of them to our hydrogel formulation. Thus, after having studied the collagen fibril formation process and demonstrated the viability to monitor the process through QCM-D technique, we continue our study analyzing the interaction between collagen and both hyaluronic acid and chondroitin sulphate. Again, we used QCM-D technique, as it is well known that it constitutes a powerful technique to understand the interaction between biomolecules and to evaluate the viscoelastic properties of thin films.

To proceed with the study, we have coated QCM-D gold sensors with a PFM coating through PECVD technique. Gold sensors were chosen to perform these experiments in order to simplify the experimental procedure, as they are easy to clean allowing a high reproducibility.

Next, we have immobilized a collagen monolayer, reproducing the linking interface that we intend to use for our osteochondral graft. Following collagen immobilization, solutions of hyaluronic acid, both high and low molecular weight, or chondroitin sulfate have been flown through the QCM-D chamber, allowing them to interact with the previously immobilized collagen molecules.

Figure III-11 shows the obtained results for the immobilization of collagen onto a pp-PFM-coated gold sensor followed by hyaluronic acid (HA), both high molecular weight (HMW) (Figure III-11A) and low molecular weight (LMW) (Figure III-11B), solution recirculation through the QCM-D chamber. All the experiment has been carried out at pH 7,4, is to say, physiological pH. The initial collagen adsorption leads to nearly the same amount of immobilized protein (Δf_7 (▼) =-250Hz) for both experiments, however the obtained results after the recirculation of hyaluronic

acid depend on its molecular weight. As it can be seen, the recirculation HMW-HA causes a slight decrease of frequency (∆f=60Hz), while after the recirculation of the LMW-HA frequency remains nearly constant (Figure III-11B). As for dissipation signal, an increase can be appreciated in both cases, being higher in the case where HMW-HA was used (Figure III-11A). The slight change in frequency signal could lead to hypothesize that no interaction takes place between collagen and hyaluronic acid. However, as it has been shown previously for the collagen fibrillation process, some events can only be detected by changes in dissipation signal. As it occurred with collagen self-assembly, we can hypothesize that the introduction of big molecules of hyaluronic acid to the system increase its viscoelasticity, and as the resulting film is not fully coupled to the sensor's surface it is not able to report frequency changes, as the film does not follow the oscillation of the resonator[39]. Moreover, the fact that hyaluronic acid is a polyanionic molecule must be considered. Negative charges from its carboxylic acid and sulfate groups may cause the swelling of the hydrogel thin film, as to avoid repulsion hyaluronic acid molecules expand occupying a large volume. Precisely, this effect is the main responsible of the high compressive strength of cartilaginous tissue.

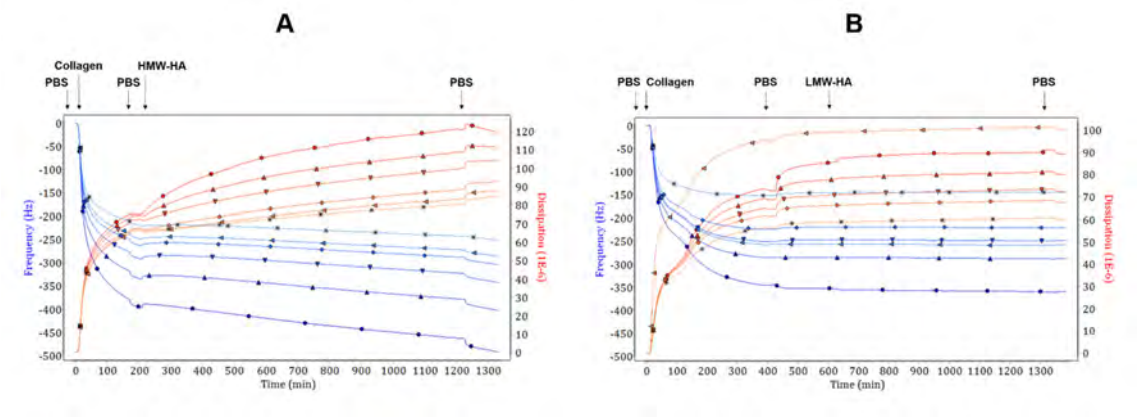

Figure III-11. Frequency (∆f) and dissipation (∆D) changes of collagen and hyaluronic acid absorption onto a pp-PFM-coated sensor. **(A)** HMW-HA **(B)** LMW-HA. The 3rd (•), 5th (▲), 7th (▼), 9th (♦), 11th (◄), and 13th (✕) overtones are shown.

Next, the same procedure as the one followed for hyaluronic acid was used to analyze the interaction between a collagen molecules and chondroitin sulfate. Figure III-12 shows frequency and dissipation changes for the immobilization of collagen followed by chondroitin sulfate recirculation through the QCM-D chamber. Again, the recirculation of chondroitin sulfate causes a slight decrease in frequency signal, however, in this case the increase of dissipation is also nearly negligible. It must be taken into account that chondroitin sulfate is a smaller molecule, and thus, if recirculated at the same concentration than HA the negative charge density in the system is higher, which leads to a high repulsion. This repulsion may avoid the interaction of CS with the underlying collagen monolayer.

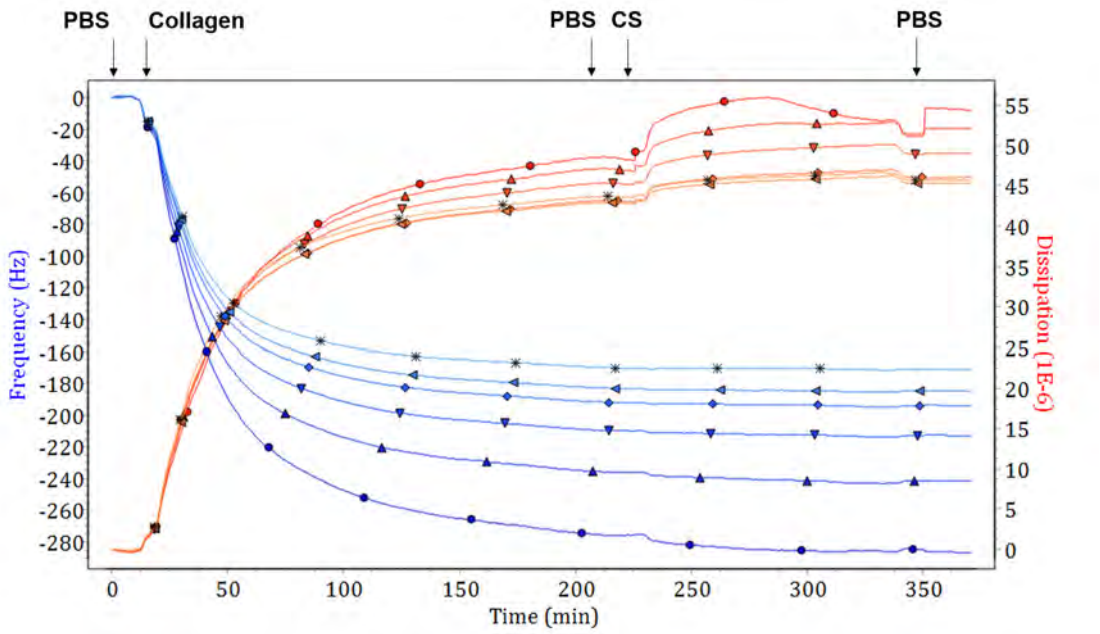

Figure III-12. Frequency (Δf) and dissipation (ΔD) changes of collagen and chondroitin sulfate adsorption onto a pp-PFM coated sensor. The 3rd (•), 5th (▲), 7th (▼), 9th (♦), 11th (◄), and 13th (✕) overtones are shown.

As frequency changes observed for both types of hyaluronic acid and chondroitin sulfate were subtle in physiologic conditions, we considered performing pH changes in order to cause the protonation of collagen molecules. Thus, the interaction between the protonated collagen monolayer and the negatively charged glycosaminoglycans will be analyzed.

According to its isoelectric point and pKa values respectively (Table III-2), both hyaluronic acid and chondroitin sulfate are negatively charged at physiologic pH, however, as the isoelectric point of collagen is between pH 7 and 8 we cannot assure that collagen is protonated at physiologic conditions.

Table III-2. Isoelectric points and pKa of collagen, hyaluronic acid and chondroitin sulfate

Compound	Isoelectric point / pK_a at pH
Collagen type I	7-8 (According to the manufacturer)
Hyaluronic acid[41]	2,5
Chondroitin Sulfate[42]	pKa (carboxyl) 3-5
	pKa (sulfate) 1,5-2

Thus, the experimental procedure shown in Figure III-13 has been developed. Briefly, collagen is immobilized at pH 7,4, as its amino groups need to be deprotonated in order to react with PFM. After protein immobilization, we change the pH by performing and acetate buffer (pH 4.0) wash. Next, we flow a solution of glycosaminoglycans (hyaluronic acid or chondroitin sulfate) in acetate buffer through the QCM-D chamber.

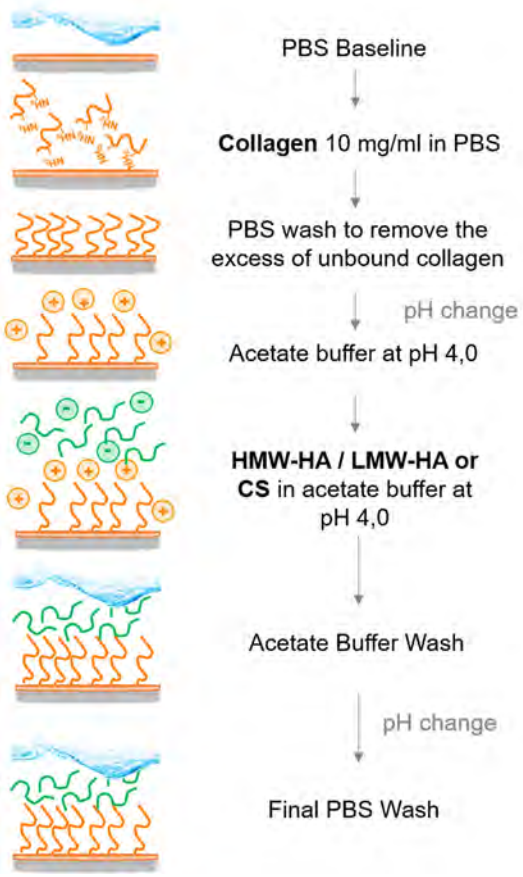

Figure III-13. QCM-D procedure to study the effect of pH change over the interaction between collagen and hyaluronic acid and chondroitin sulfate.

Again, the frequency and dissipation changes observed for hyaluronic acid (Figure III-14) are subtle. However, it can be seen how, in contrast with the results obtained at physiological pH, the recirculation of hyaluronic acid causes an increase in frequency and a decrease in dissipation. It must be noticed that changes are more evident for LMW-HA (Figure III-14B). The fact that dissipation signal decreases means that the adsorbed film becomes more rigid after hyaluronic acid recirculation. The increase of rigidity of the adsorbed layer can be attributed to a collapse, caused by the interaction between the positively charged collagen monolayer and the negatively charged hyaluronic acid chains. Thus, if the adsorbed layer collapses, it is likely that the increase of frequency is related to a loss of water, as it has been previously reported[43].

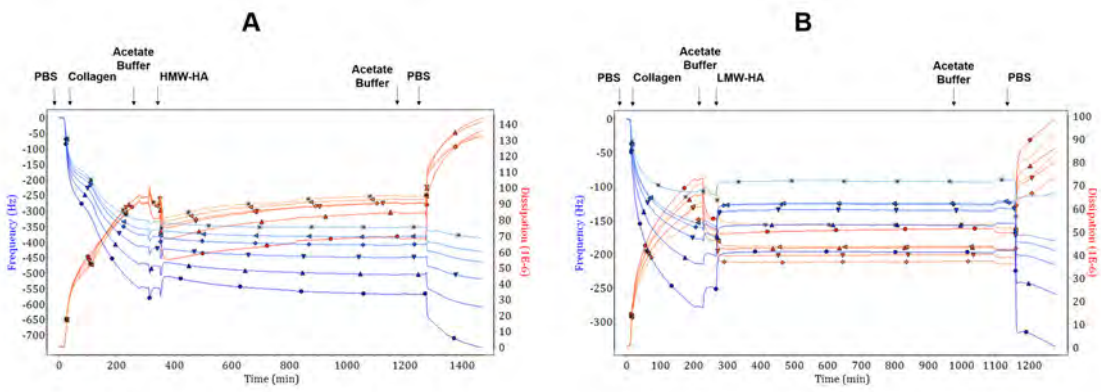

Figure III-14. Frequency (Δf) and dissipation (ΔD) changes of collagen and hyaluronic acid absorption onto a pp-PFM-coated sensor. **(A)** HMW-HA **(B)** LMW-HA. The 3rd (●), 5th (▲), 7th (▼), 9th (♦), 11th (◄), and 13th (✕) overtones are shown.

Next, Figure III-15 shows the evolution of frequency and dissipation signal for the absorption of collagen onto a PFM-coated gold QCM-D sensor followed by chondroitin sulfate recirculation through the QCM-D chamber. The initial flow of the collagen solution causes, as expected, a decrease of frequency and an increase of dissipation, due to protein adsorption onto the sensor's surface. Then, the recirculation of chondroitin sulfate solution after the pH change leads to an increase of the frequency signal and to a decrease of the dissipation signal. Changes are more evident than those observed for hyaluronic acid. Again, it must be considered that chondroitin sulfate is a smaller molecule, and thus, at the same concentration than HA, the density of negative charges in the system will be higher. Dissipation signal increases as the film becomes more rigid due to the ionic interaction between collagen molecules and chondroitin sulfate. Again, this increase in rigidity is caused by the adsorbed layer collapse, which at the same time can be related with the expulsion of water molecules out of the adsorbed layer[43].

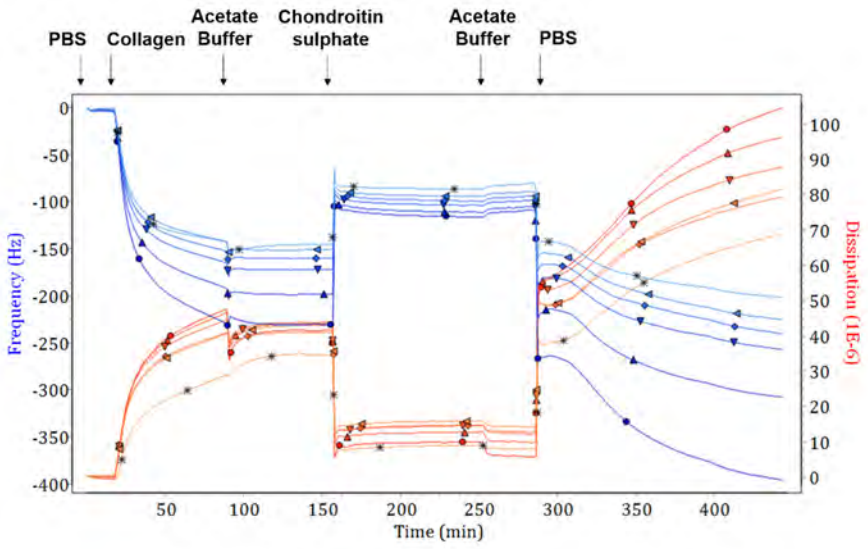

Figure III-15. Frequency (Δf) and dissipation (ΔD) changes of collagen and chondroitin sulfate adsorption onto a pp-PFM coated sensor. The 3rd (•), 5th (▲), 7th (▼), 9th (♦), 11th (◄), and 13th (✕) overtones are shown.

Next, once the interaction between collagen molecules and both hyaluronic acid and chondroitin sulfate, the interaction between the glycosaminoglycans and collagen fibers is evaluated. The entire experiments are performed at physiological pH, as pH changes could disrupt collagen fibers.

Then, the result of flowing an HMW-HA after collagen fibril formation through the QCM-D chamber is presented (Figure III-16). As it can be appreciated, the recirculation of HA causes a decrease in frequency signal for the external overtones (Δf3, Δf5, Δf7 and Δf9). As expected, the adsorbed film becomes more dissipative, as high molecular weight hyaluronic acid is highly viscoelastic. The fact that changes are only sensed by external overtones, support our theory that when working with highly dissipative films, the sensor does not sense completely the adsorbed mass onto its surface, as it is not fully coupled. Finally, it must be noticed how the final PBS wash causes an increase of frequency and a decrease of dissipation, to the levels before hyaluronic acid recirculation. This phenomenon shows that hyaluronic acid is not able to penetrate into the collagen network, and thus remain entrapped after the final buffer wash. Moreover, as hyaluronic acid is such a big molecule, the electrostatic interaction between HA and collagen fibers must be very weak.

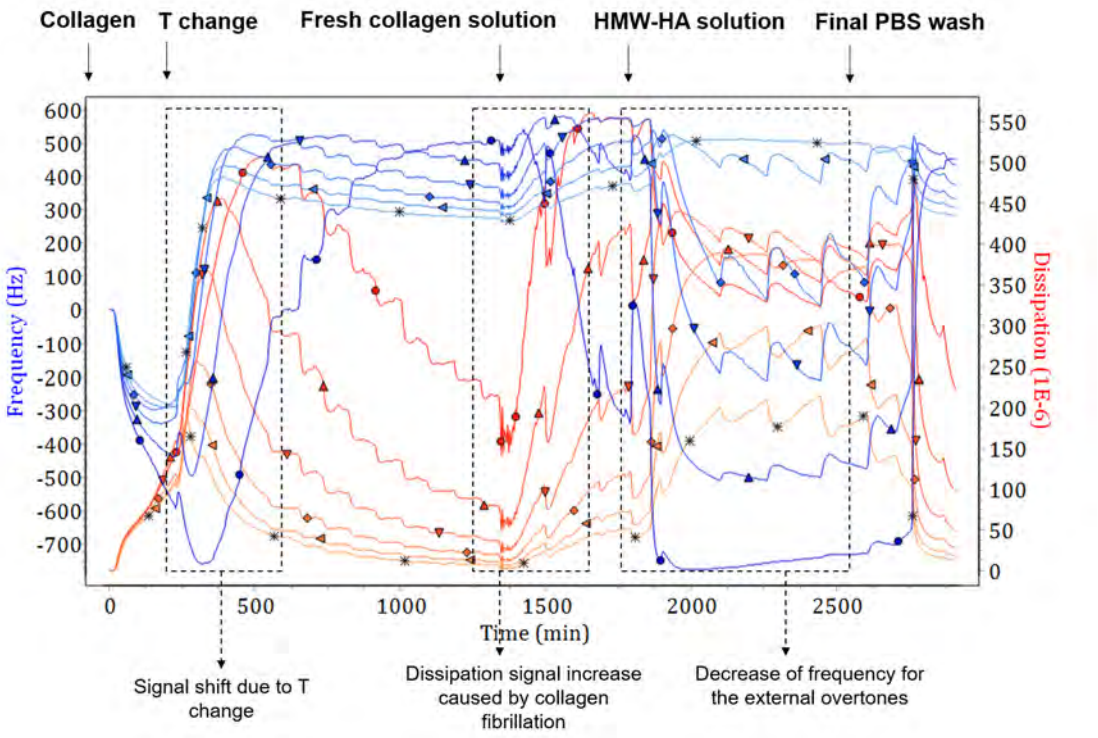

Figure III-16. Frequency (Δf) and dissipation (ΔD) changes of collagen fibrillation and HMW-HA recirculation through the QCM-D chamber. The 3rd (•), 5th (▲), 7th (▼), 9th (♦), 11th (◄), and 13th (✕) overtones are shown.

Next, the previous experiment was reproduced using LMW-HA solution (Figure III-17). As it can be seen, the flow of LMW-HA causes a significant increase of frequency signal for the external overtone (ΔD_3), however in this case frequency remains nearly constant. Again, the fact that a highly viscous film is adsorbed onto the sensor surface, and that LMW-HA molecules are smaller than those of HMW-HA may cause that no changes are appreciated for frequency signal. The increase of dissipation may be related with the interaction of hyaluronic acid molecules with the outer part of collagen mesh layer. It points out, that in contrast with the previous experiment, the final PBS wash does not cause significant changes in both signals. The latter can be attributed that the smaller size of LMW-HA enables its partial entrapment into the collagen mesh, creating a stronger interaction that is not disrupted by the buffer wash.

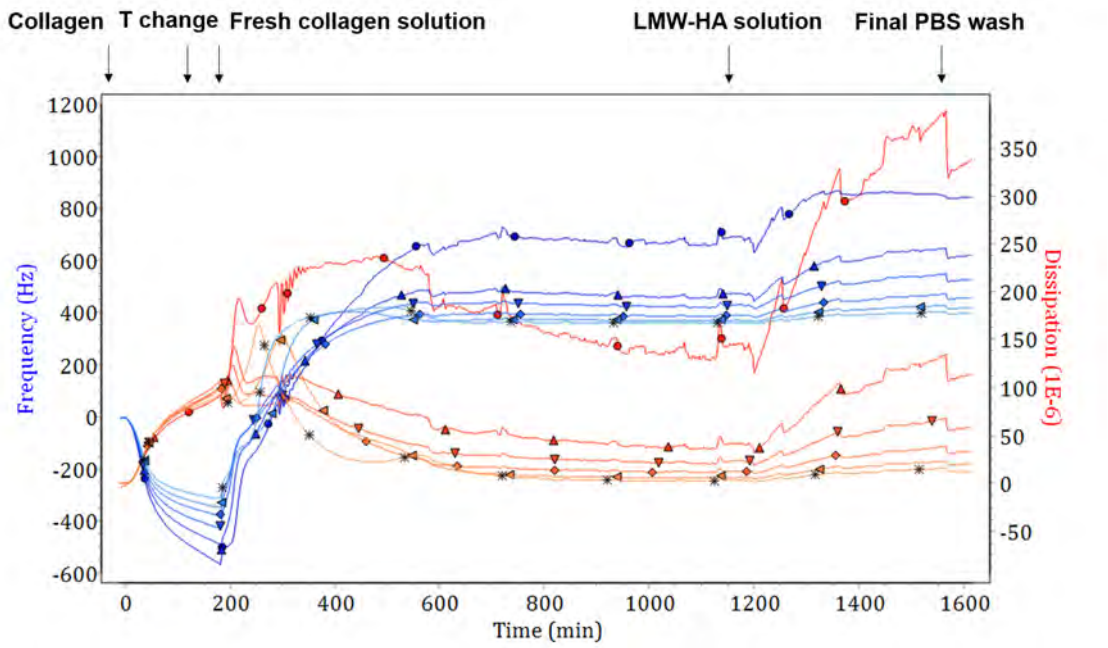

Figure III-17. Frequency (∆f) and dissipation (∆D) changes of collagen fibrillation and LMW-HA recirculation through the QCM-D chamber. The 3rd (•), 5th (▲), 7th (▼), 9th (♦), 11th (◄), and 13th (✕) overtones are shown.

Next, Figure III-18 shows the result of flowing a chondroitin sulfate solution after the formation of collagen fibrils. As it can be seen, once CS is introduced in the QCM-D chamber frequency signal increases as consequence of the interaction between negatively charged chondroitin and positive charges of collagen which causes the expulsion of water molecules embedded in the collagen fiber mesh. As for dissipation signal, it can be seen how the distance between the overtones increases, as chondroitin sulfate interacts with the outer layer of the adsorbed collagen mesh.

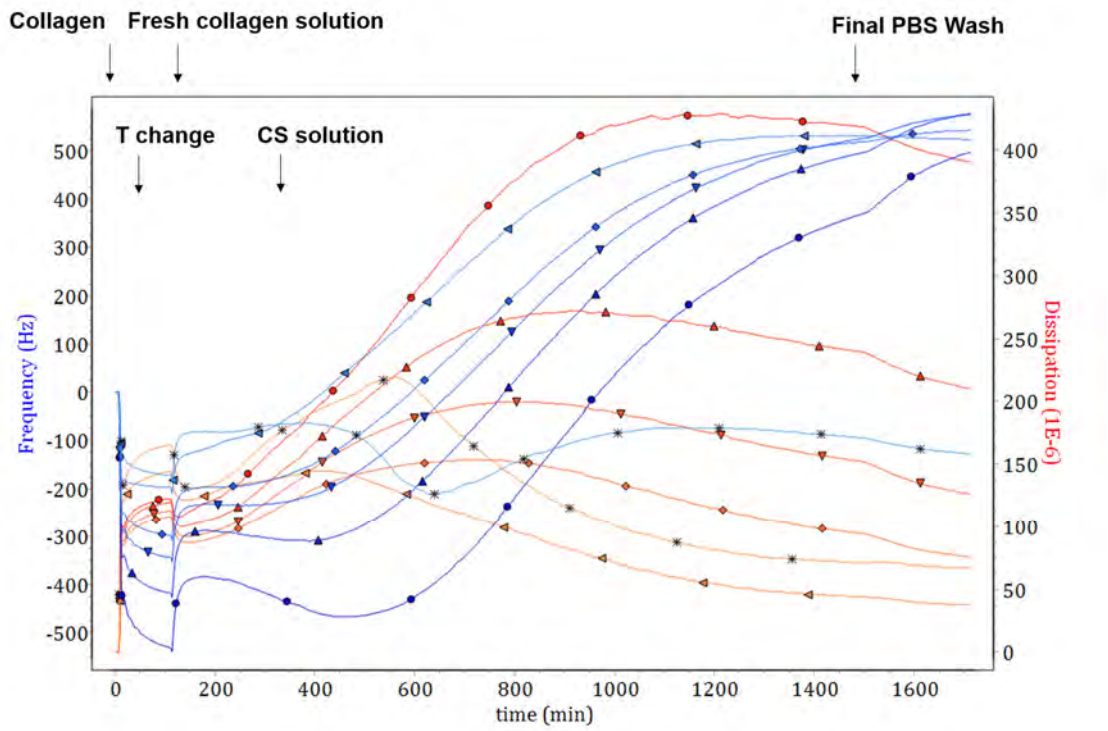

Figure III-18. Frequency (∆f) and dissipation (∆D) changes of collagen fibrillation and CS recirculation through the QCM-D chamber. The 3rd (•), 5th (▲), 7th (▼), 9th (♦), 11th (◄), and 13th (✕) overtones are shown.

Next, once we have studied the mechanisms by which the designed matrix is assembled, we present a biocompatibility assessment of the hydrogel formulation and a proof of concept for the validation of the developed hydrogel immobilization methodology.

3.3.3 In vitro testing of the hydrogel formulation and cell encapsulation methodology

As already mentioned, following the evaluation of the hydrogel matrix formation we proceeded with biocompatibility studies, to evaluate both the matrix composition and the designed cell encapsulation process. To do so, human Normal Dermal Fibroblasts (hNDFs) were encapsulated in both collagen and collagen/GAGs hydrogel formulations and MTT assays were performed at different time points.

¡Error! No se encuentra el origen de la referencia. shows the obtained results for the MTT assays. As it can be seen, cell viability was analyzed at different time points, and it is shown how it remains nearly constant along time and it remains unaffected by the addition of glycosaminoglycans.

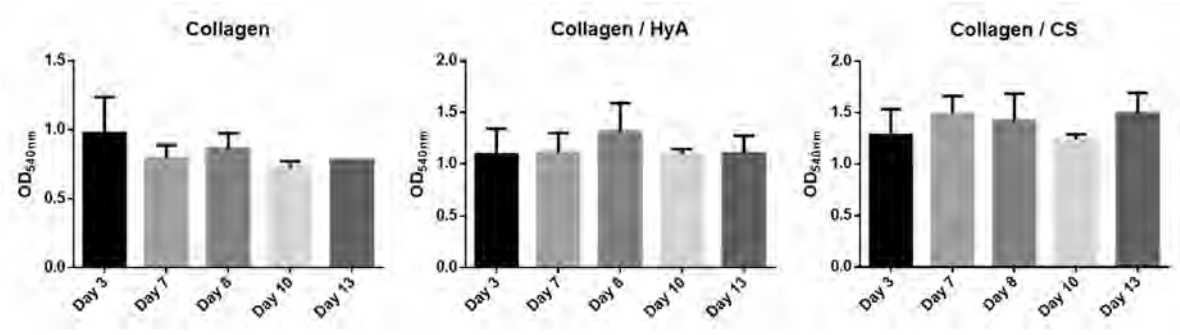

Figure III-19. Viability assessment using the MTT assay of hNDFs embedded in Collagen, Collagen / Hyaluronic acid (HyA) and Collagen / Chondroitin sulfate (CS) hydrogel formulations. (Results presented as average mean with standard deviation represented as error bars. t test was used for statistical analysis, giving no significant differences between the analyzed time points.)

Moreover, a viability staining with fluorescein diacetate (FDA) and ethidium bromide (EtBr) was performed to qualitatively determine the viability of cells embedded in collagen hydrogels (Figure III-20A), collagen/hyaluronic acid hydrogels (Figure III-20B) and collagen/chondroitin sulphate hydrogels (Figure III-20C). It can be seen how the vast majority of cells are alive for the three analyzed formulations, thus we can be certain that the incorporation of the glycosaminoglycans in the collagen-based hydrogel formulation has no negative effect over cell viability. Moreover, by comparing the MTT results obtained for the three studied formulations (Figure III-20D) after 10 days of culture, it can be seen how the addition of both glycosaminoglycans has a significant positive effect over cell viability. The highest value is obtained with the addition of chondroitin sulfate, followed by the hyaluronic acid-containing hydrogel formulation.

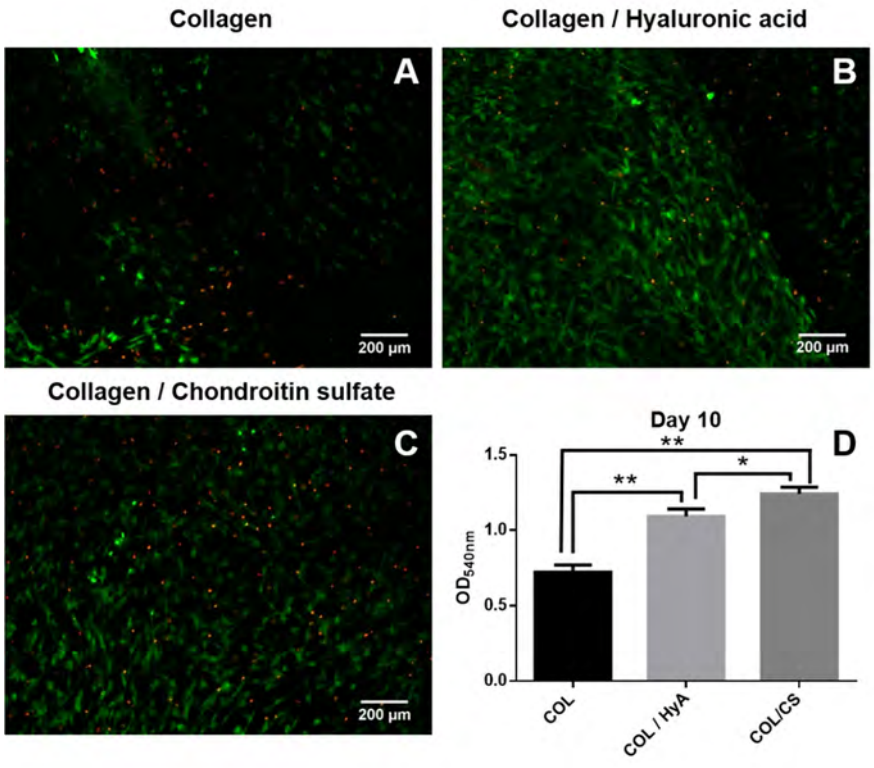

Figure III-20. Viability assessment using human Normal Dermal Fibroblasts (hNDFs) embedded in: **(A)** collagen hydrogel, **(B)** collagen/hyaluronic acid hydrogel **(C)** collagen/chondroitin sulfate after 10 days of culture using fluorescein diacetate and ethidium bromide staining **(D)** comparison of the MTT results obtained for the three tested formulations at day 10 of culture. Living cells appear stained green while dead cells are stained red. (Statistical differences are indicated as. * for $p<0.05$, ** for $p<0.01$, and *** for $p < 0.001$, t test, n=3).

Finally, Figure III-21 shows the viability staining of a hydrogel containing both hyaluronic acid and chondroitin sulphate, and as it occurred with the previous formulations it can be stated that the simultaneous addition of both glycosaminoglycans does not affect cell viability, as the majority of cells appear stained green, meaning that they are alive.

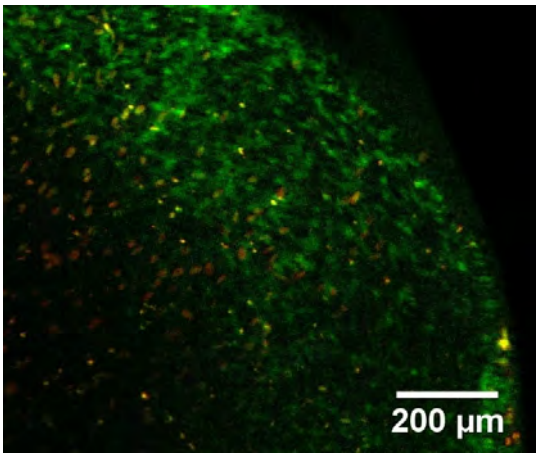

Figure III-21. Viability assessment using human Normal Dermal Fibroblasts (hNDFs) embedded in a collagen / hyaluronic acid / chondroitin sulfate hydrogel. Living cells appear stained green while dead cells are stained red.

Thus, the results of the viability analysis give proof that the composition of the tested hydrogel formulations has no toxic effects as well as they demonstrate that the cell encapsulating process and the hydrogel polymerization are harmless, and lead to high cell viability.

Next, aiming to go one step further, we present a proof of concept for the validation of the developed immobilizing protocol. Both its versatility, which would enable its application in a wide range of materials, and biocompatibility are studied.

3.3.4 Collagen-based hydrogel immobilization onto different substrates: a proof of concept

The results obtained with the QCM-D demonstrate, at a molecular level, how the presence of a PFM-coating allows the immobilization of a greater amount of protein than those not treated, as well as it promotes and accelerates the fibrillation process. Moreover, it has also been proved how the presence of a collagen monolayer is critical for the subsequent fibrillation process.

With the proof of concept shown in Figure III-22, we aim to scale up to a macroscopic level the results obtained previously with QCM-D. We have chosen three substrates very different in nature to demonstrate the versatility of the hydrogel-immobilization technique: a collagen membrane, a PTFE membrane and a hydroxyapatite disk. The use of collagen and PTFE membranes is widespread in dentistry, especially in guided bone regeneration. PTFE membranes, besides of being used with tissue regeneration purposes constitute the worst-case scenario, as they present a high hydrophobicity which makes it highly effective at preventing interactions with biological tissues[44], as it prevents both protein and cell adhesion. The hydroxyapatite disk is used as bone mimics.

Thus, a porous collagen membrane (Figure III-22A), a PTFE membrane (Figure III-22B) and a hydroxyapatite disk (Figure III-22C) have been submitted to our surface treatment. Substrates have been coated with PFM by PECVD and incubated with a collagen solution to obtain a protein monolayer. Next a collagen-based hydrogel has been allowed to polymerize on the top of them and it has been successfully immobilized on their surface. As it can be seen, the polymeric coating allows the attachment of the hydrogel on the substrates which provides easiness of manipulation, as the constructs can be handled using tweezers.

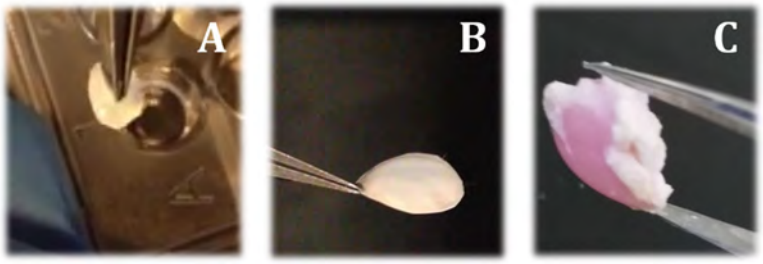

Figure III-22. Collagen-based hydrogel attachment onto different substrates. **(A)** hydrogel attached onto a PFM-coated collagen membrane, **(B)** hydrogel attached onto a non-porous PFM-coated PTFE membrane, **(C)** hydrogel attached onto a PFM-coated hydroxyapatite disk.

The biocompatibility of pp-PFM coating was a critical factor for its use in tissue engineering. As the hydrolysis of PFM leads to the liberation of pentafluorophenol group which has a toxic nature[32], the effect over cell viability of the presence of a PFM coating as linking interface between a collagen thin film and both PTFE membranes and PDMS was evaluated using hNDFs. The followed procedure is summarized in Figure III-23. Briefly, the incubation of plasma-treated substrates (Figure III-23A) with a collagen solution induces the pp-PFM hydrolysis and pentafluorophenol groups are released allowing the reaction of the collagen free amines with the remaining ester groups forming a protein monolayer (Figure III-23B). To eliminate the excess of unbound collagen molecules and to minimize the presence of the toxic pentafluorophenol group a PBS wash was performed. Next, the self-assembling ability of collagen was leveraged and the synthesis of the collagen/hyaluronic acid/chondroitin sulfate thin hydrogel was performed over a collagen monolayer (Figure III-23C) which acts as an anchoring point for the subsequent collagen fibrillation, as previously reported[34] and demonstrated in the present work using the QCM-D technique. After hydrogel thin film synthesis, cells were cultured on the top of the construct.

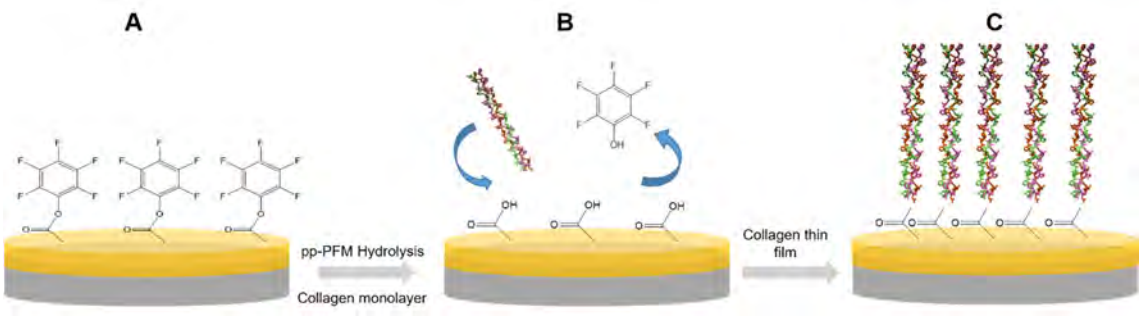

Figure III-23. Hydrogel immobilizing technology. **(A)** Plasma deposition of a PFM coating onto the desired substrate, **(B)** collagen immobilization **(C)** Formation of a collagen thin film by self-assembly using the collagen monolayer as anchoring points.

Cell viability (Figure III-24A) and morphology (Figure III-24B) were assessed using fluorescence microscopy. The vast majority of cells remain alive after 8 days of culture and they present an elongated, normal fibroblastic morphology demonstrating that the use of a pp-PFM coating as linking interface does not compromise cell integrity.

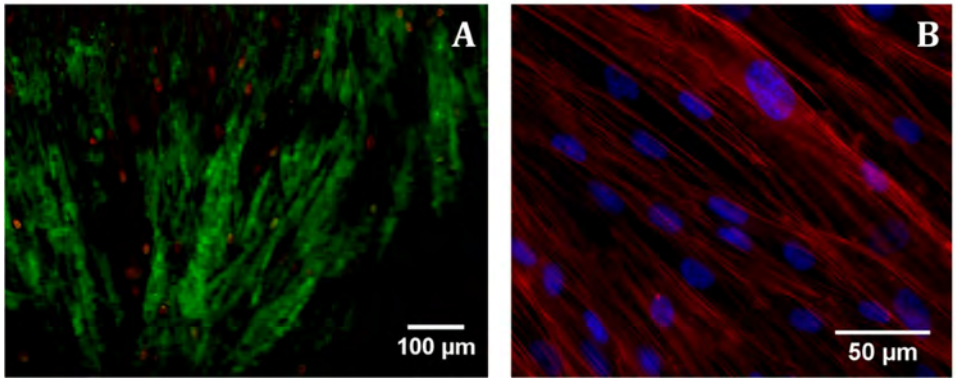

Figure III-24. Human Normal Dermal Fibroblasts (hNDFs) viability and morphology staining. **(A)** Viability staining of cells seeded onto a pp-PFM-coated PTFE membrane at day 8 of culture. Living cells are stained green while dead cells appear red. **(B)** DAPI/Phalloidin staining of cells seeded onto a PFM-coated silicone wafer coated with a collagen thin film. Cell nuclei appear stained blue and actin filament appear stained red.

3.4 Concluding remarks

In the present chapter, we have demonstrated how QCM-D technique enables the monitorization of collagen fibrillation process. It has been seen how, fiber formation is reflected in dissipation changes, while frequency signal remains nearly unaffected. This phenomenon may be caused by the highly viscoelastic nature of the collagen mesh adsorbed onto the sensor's surface. As the adsorbed layer is not fully coupled to the sensor, the latter remains unaffected by fibrillation process. When using a PFM-coated sensor to study the fibrillation process, it can be seen how, in contrast with uncoated sensors, fibril formation begins right after temperature change. This can be related with the immobilization of higher amounts of collagen molecules thanks to the presence of the polymeric coating.

Moreover, the interaction between collagen, hyaluronic acid and chondroitin sulfate has been analyzed. It has been observed how there is a strong interaction between positively charged collagen molecules and negatively charged GAGs. The interaction causes the collapse of collagen thin film, as water molecules are expulsed from the adsorbed layer. The interaction between GAGs and collagen fibrils is not that evident, as the big sized hyaluronic acid cannot penetrate into the previously formed collagen mesh.

In vitro studies have shown how the composite hydrogel formulation has no toxic effect over cells, and the encapsulation procedure does not affect cell viability either. Finally, a proof-of-concept of our hydrogel immobilization technology has been performed, using different substrates very different in nature. The viability of the linking interface has also been tested and it has been demonstrated how the designed immobilization protocol enables the elimination of the cytotoxic group pentafluorophenol and it does not affect cell viability.

In the following chapter, we have focused on the evaluation of the cell-homing capacity of the hydrogel formulation as well as of its both chondrogenic and osteogenic potential. As it will be discussed with further detail, in osteochondral repair, scaffolding techniques are often combined with subchondral bone stimulation, which causes the migration of mesenchymal stem cells towards the defect site. Thus, we will assess the capacity of our hydrogel matrix to allow cell migration and colonization. Moreover, an assessment of both the chondrogenic and osteogenic potential is presented, as being able to provide a suitable environment for cell differentiation is critical to ensure the obtention of a functional osteochondral tissue.

3.5 References

(1) Fang, M.; Goldstein, E. L.; Matich, E. K.; Orr, B. G.; Holl, M. M. B. Type I collagen self-assembly: the roles of substrate and concentration. *Langmuir* **2013**, *29* (7), 2330–2338 DOI: 10.1021/la3048104.

(2) Geckil, H.; Xu, F.; Zhang, X.; Moon, S.; Demirci, U. Engineering hydrogels as extracellular matrix mimics. *Nanomedicine* **2010**, *5* (3), 469–484 DOI: 10.2217/nnm.10.12.Engineering.

(3) O'Leary, L. E. R.; Fallas, J. a; Bakota, E. L.; Kang, M. K.; Hartgerink, J. D. Multi-hierarchical self-assembly of a collagen mimetic peptide from triple helix to nanofibre and hydrogel. *Nat. Chem.* **2011**, *3* (10), 821–828 DOI: 10.1038/nchem.1123.

(4) Gross, J.; Hichberber, J.; Schmitt, F. Some factors involved in the fibrogenesis of collagen in vitro. *Proc Soc Exp Biol Med* **1952**, *80* (3), 462–465.

(5) Factors, R.; Gross, J.; Kirk, D. The Heat Precipitation of Collagen from Neutral Salt Solutions : SomeRate-Regulating Factors. *J. Biol. Chem* **1958**, *233* (2), 355-.

(6) Jackson, D.; Fessler, J. Isolation and properties of a collagen soluble in salt solution at neutral pH. *Nature* **1955**, *176*, 69–70.

(7) Canelón, S. P.; Wallace, J. M. β-Aminopropionitrile-induced reduction in enzymatic crosslinking causes in vitro changes in collagen morphology and molecular composition. *PLoS One* **2016**, *11* (11), 1–13 DOI: 10.1371/journal.pone.0166392.

(8) Silver, F. H.; Freeman, J. W.; Seehra, G. P. Collagen self-assembly and the development of tendon mechanical properties. *J. Biomech.* **2003**, *36* (10), 1529–1553 DOI: 10.1016/S0021-9290(03)00135-0.

(9) Cooper, a. Thermodynamic studies of the assembly in vitro of native collagen fibrils. *Biochem. J.* **1970**, *118* (3), 355–365.

(10) Leikin, S.; Rau, D.; Parsegian, V. Temperature-favoured assembly of collagen is driven by hydrophilic not hydrophobic interactions. *Nat. Struct. Biol.* **1995**, *2* (3), 205–210.

(11) Shoulders, Matthew D., Raines, R. T. Collagen Structure and Stability. *Annu Rev Riochem.* **2009**, *78*, 929–958 DOI: 10.1146/annurev.biochem.77.032207.120833.COLLAGEN.

(12) Prockop, D. J. Inhibition of the Self-assembly of Collagen I into Fibrils with Synthetic Peptides. DEMONSTRATION THAT ASSEMBLY IS DRIVEN BY SPECIFIC BINDING SITES ON THE MONOMERS. *J. Biol. Chem.* **1998**, *273* (25), 15598–15604 DOI: 10.1074/jbc.273.25.15598.

(13) Kuznetsova, N.; Leikin, S. Does the Triple Helical Domain of Type I Collagen Encode Molecular Recognition and Fiber Assembly while Telopeptides Serve as Catalytic Domains?: EFFECT OF PROTEOLYTIC CLEAVAGE ON FIBRILLOGENESIS AND ON COLLAGEN-COLLAGEN INTERACTION IN FIBERS. *J. Biol. Chem.* **1999**, *274* (51), 36083–36088 DOI: 10.1074/jbc.274.51.36083.

(14) Leikina, E.; Mertts, M. V; Kuznetsova, N.; Leikin, S. Type I collagen is thermally unstable at body temperature. *Proc. Natl. Acad. Sci. U. S. A.* **2002**, *99* (3), 1314–1318 DOI: 10.1073/pnas.032307099.

(15) Buehler, M. J. Nature designs tough collagen: explaining the nanostructure of collagen fibrils. *Proc. Natl. Acad. Sci. U. S. A.* **2006**, *103* (33), 12285–12290 DOI: 10.1073/pnas.0603216103.

(16) Orgel, J. P. R. O.; Miller, A.; Irving, T. C.; Fischetti, R. F.; Hammersley, A. P.; Wess, T. J.; Fk, S. The In Situ Supermolecular Structure of Type I Collagen. *Structure* **2001**, *9* (01), 1061–1069.

(17) Whitesides, G. M.; Grzybowski, B. Self-assembly at all scales. *Science* **2002**, *295* (5564), 2418–2421 DOI: 10.1126/science.1070821.

(18) Zhang, S. Fabrication of novel biomaterials through molecular self-assembly. *Nat. Biotechnol.* **2003**, *21* (10), 1171–1178 DOI: 10.1038/nbt874.

(19) Dong, M.; Xu, S.; Bünger, M. H.; Birkedal, H.; Besenbacher, F. Temporal Assembly of Collagen Type II Studied by Atomic Force Microscopy. *Adv. Eng. Mater.* **2007**, *9* (12), 1129–1133 DOI: 10.1002/adem.200700220.

(20) Han, L.; Grodzinsky, A.; Ortiz, C. Nanomechanics of the cartilage extracellular matrix. *Annu. Rev. Mater. Res.* **2011**, 133–168 DOI: 10.1146/annurev-matsci-062910-100431.Nanomechanics.

(21) Gentili, C.; Cancedda, R. Cartilage and Bone Extracellular Matrix. *Curr. Pharm. Des.* **2009**, *15*, 1334–1348 DOI: 10.2174/138161209787846739.

(22) Aspberg, A. Cartilage proteoglycans. *Cartil. Vol. 1 Physiol. Dev.* **2001**, *12*, 69–78 DOI: 10.1007/978-3-319-29568-8_1.

(23) Mansour, J. M. Biomechanics of Cartilage. In *Kinesiology: the mechanics and pathomechanics of human movement*; Wolters Kluwer Health, 2013; pp 69–83.

(24) Knudson, C. B. Hyaluronan and CD44: Strategic players for cell-matrix interactions during chondrogenesis and matrix assembly. *Birth Defects Res. Part C - Embryo Today Rev.* **2003**, *69* (2), 174–196 DOI: 10.1002/bdrc.10013.

(25) Betre, H.; Ong, S. R.; Guilak, F.; Chilkoti, A.; Fermor, B.; Setton, L. A. Chondrocytic differentiation of human adipose-derived adult stem cells in elastin-like polypeptide. *Biomaterials* **2006**, *27* (1), 91–99 DOI: 10.1016/j.biomaterials.2005.05.071.

(26) Wu, S. C.; Chang, J. K.; Wang, C. K.; Wang, G. J.; Ho, M. L. Enhancement of chondrogenesis of human adipose derived stem cells in a hyaluronan-enriched microenvironment. *Biomaterials* **2010**, *31* (4), 631–640 DOI: 10.1016/j.biomaterials.2009.09.089.

(27) Jerosch, J. Effects of glucosamine and chondroitin sulfate on cartilage metabolism in OA: Outlook on other nutrient partners especially omega-3 fatty acids. *Int. J. Rheumatol.* **2011**, *2011* DOI: 10.1155/2011/969012.

(28) Varghese, S.; Hwang, N. S.; Canver, A. C.; Theprungsirikul, P.; Lin, D. W.; Elisseeff, J. Chondroitin sulfate based niches for chondrogenic differentiation of mesenchymal stem cells. *Matrix Biol.* **2008**, *27* (1), 12–21 DOI: 10.1016/j.matbio.2007.07.002.

(29) Nuhn, L.; Hartmann, S.; Palitzsch, B.; Gerlitzki, B.; Schmitt, E.; Zentel, R.; Kunz, H. Water-soluble polymers coupled with glycopeptide antigens and T-cell epitopes as potential antitumor vaccines. *Angew. Chemie - Int. Ed.* **2013**, *52* (40), 10652–10656 DOI: 10.1002/anie.201304212.

(30) Allmeroth, M.; Moderegger, D.; Biesalski, B.; Koynov, K.; R??sch, F.; Thews, O.; Zentel, R. Modifying the body distribution of HPMA-based copolymers by molecular weight and aggregate formation. *Biomacromolecules* **2011**, *12* (7), 2841–2849 DOI: 10.1021/bm2005774.

(31) Hemmelmann, M.; Knoth, C.; Schmitt, U.; Allmeroth, M.; Moderegger, D.; Barz, M.; Koynov, K.; Hiemke, C.; Rösch, F.; Zentel, R. HPMA based amphiphilic copolymers mediate central nervous effects of domperidone. *Macromol. Rapid Commun.* **2011**, *32* (9–10), 712–717 DOI: 10.1002/marc.201000810.

(32) He, L.; Szameit, K.; Zhao, H.; Hahn, U.; Theato, P. Postpolymerization modification using less cytotoxic activated ester polymers for the synthesis of biological active polymers. *Biomacromolecules* **2014**, *15* (8), 3197–3205 DOI: 10.1021/bm500902t.

(33) Marí-Buyé, N.; O'Shaughnessy, S.; Colominas, C.; Semino, C. E.; Gleason, K. K.; Borrós, S. Functionalized, swellable hydrogel layers as a platform for cell studies. *Adv. Funct. Mater.* **2009**, *19* (8), 1276–1286 DOI: 10.1002/adfm.200801561.

(34) Wu, J.; Marí-Buyé, N.; Muiños, T. F.; Borrós, S.; Favia, P.; Semino, C. E. Nanometric self-assembling peptide layers maintain adult hepatocyte phenotype in sandwich cultures. *J. Nanobiotechnology* **2010**, *8* (1), 29 DOI: 10.1186/1477-3155-8-29.

(35) Silver, F. H. Type I Collagen Fibrillogenesis in Vitro. *J Biol Chem* **1981**, *256*, 4973–4977.

(36) Förch, R.; Zhang, Z.; Knoll, W. Soft plasma treated surfaces: Tailoring of structure and properties for biomaterial applications. *Plasma Process. Polym.* **2005**, *2* (5), 351–372 DOI: 10.1002/ppap.200400083.

(37) Hovgaard, M. B.; Dong, M.; Otzen, D. E.; Besenbacher, F. Quartz crystal microbalance studies of multilayer glucagon fibrillation at the solid-liquid interface. *Biophys. J.* **2007**, *93* (6), 2162–2169 DOI: 10.1529/biophysj.107.109686.

(38) Walters, R. H.; Jacobson, K. H.; Pedersen, J. A.; Murphy, R. M. Elongation Kinetics of Polyglutamine Peptide Fibrils: A Quartz Crystal Microbalance with Dissipation Study. *J Mol Biol* **2012**, *29* (10), 1883–1889 DOI: 10.3174/ajnr.A1256.Functional.

(39) Dixon, M. C. Quartz Crystal Microbalance with Dissipation Monitoring: Enabling Real-Time Characterization of Biological Materials and Their Interactions. *J. Biomol. Tech.* **2008**, *19*, 151–158.

(40) Liu, S. X.; Kim, J. T. Application of Kevin-Voigt Model in Quantifying Whey Protein Adsorption on Polyethersulfone Using QCM-D. *SLAS Technol. Transl. Life Sci. Innov.* **2009**, *14* (4), 213–220 DOI: 10.1016/j.jala.2009.01.003.

(41) Gatej, I.; Popa, M.; Rinaudo, M. Role of the pH on hyaluronan behavior in aqueous solution. *Biomacromolecules* **2005**, *6* (1), 61–67 DOI: 10.1021/bm040050m.

(42) Chandran, P. L.; Horkay, F. Aggrecan, an unusual polyelectrolyte: review of solution behavior and physiological implications. *Acta Biomater.* **2012**, *8* (1), 3–12 DOI: 10.1016/j.actbio.2011.08.011.

(43) Mhanna, R. F.; VörÖs, J.; Zenobi-Wong, M. Layer-by-layer films made from extracellular matrix macromolecules on silicone substrates. *Biomacromolecules* **2011**, *12*, 609–616 DOI: 10.1021/bm1012772.

(44) Puleo, D. A.; Bizios, R. *Biological Interactions on Materials Surfaces: Understanding and Controlling Protein, Cell, and Tissue Responses*; Springer: Lexington, 2009.

Chapter IV. Cell-homing, chondrogenic and osteogenic-inducing potential of the collagen-based hydrogel formulation

Prepared for submission:

A. Mas-Vinyals, Salvador Borrós, “Cell homing, chondrogenic and osteogenic potential of the collagen-based hydrogel formulation”. (Advanced Healthcare Materials)

This page left blank intentionally

Cell-homing, chondrogenic and osteogenic potential of the collagen-based hydrogel formulation

In this chapter we present the evaluation of cell-homing capacity of the designed hydrogel formulation as well as its both chondrogenic and osteogenic potential. As for the cell-homing capacity, we have evaluated the potential of the hydrogel formulation to allow or even attract cell migration thinking in a cell-free version of the proposed scaffold. Thus, we have studied how cells colonize the hydrogel structure using different approaches and setups. Next, to study both chondrogenic and osteogenic potential, the expression of marker genes has been analyzed, and the effect of both hyaluronic acid and chondroitin sulfate glycosaminoglycans has been evaluated. The obtained results show how the hydrogel formulation can induce the expression of the selected marker genes, when cultured in growth media as well as when using both chondrogenic and osteogenic induction media.

4.1 Introduction

Cartilage and the subchondral bone should be treated as one unit when it comes to osteochondral regeneration as there is evidence that without the support of the subchondral bone, treatments of the cartilage layer are likely to fail[1]. As the cartilage layer and the subchondral bone are tightly connected, a lesion in one of the tissues will affect the homeostasis of the whole joint. Keeping this in mind, we have focused on developing a heterogeneous scaffold capable of reproducing the entire joint structure, from the subchondral bone to the cartilage layer. Thus, the designed hydrogel formulation must provide a suitable environment for cell proliferation and differentiation. In the present chapter, we focus on the assessment of both chondrogenic and osteogenic potential of our hydrogel formulation.

Moreover, we have studied the potential of the designed hydrogel formulation to allow or even promote cell migration towards its structure. Migration studies were performed in cell-free scaffolds, to evaluate the cell-homing capacity intrinsic to the hydrogel matrix. The use of cell-free scaffolds allows mimicking the scenario where a hydrogel is implanted cell-free in the defect site. The latter, if applied in combination with a subchondral bone stimulation technique could attract cells from the subchondral plate. Then, cells will colonize the hydrogel structure, and ideally, develop different phenotypes depending on its position through the scaffold. Those cells closer to the bone-like platform, where the degree of mineralization reaches its higher value would adopt a hypertrophic phenotype, characteristic of cartilage calcified layer. On the contrary, we would expect a high degree of expression of cartilaginous ECM components, such as collagen

type II, aggrecan and hyaluronic acid, at the rest of the hydrogel, varying its content according to the distance from the underlying subchondral bone.

Thus, if the hydrogel scaffold enables cell colonization, it could be implanted cell-free, easing the regulatory pathway. It must be considered that those medical devices containing cells, are considered as Class III and are subject to strict and costly clinical trials. Thus, beginning the pathway towards market approval with a cell-free product seems a good strategy.

It must be considered that cartilage is an avascular tissue, with an intrinsic low capacity for self-repair[2]. Without the presence of blood supply, the set of biological processes that take place to repair the damaged tissue are prevented[3]. Moreover, the highly dense extracellular matrix of cartilage tissue hinders chondrocyte migration towards the defect site[4]. However, when defects reach the subchondral bone, the repair process is initiated by undifferentiated mesenchymal stem cells (MSCs) which migrate into the defect site. The migration of endogenous MSCs to injured tissues and their subsequent involvement in immunomodulation and tissue healing, are considered a natural self-repair response[5]. Thus, strategies to stimulate and enhance MSCs mobilization towards damaged site have aroused interest. As for cartilage repair, marrow stimulation is the first line of treatment. Marrow stimulation techniques imply the drilling of the subchondral bone plate, allowing blood and bone marrow containing MSCs to enter the defect site. However, this technique typically leads to fibrocartilage formation[6].

MSCs have the potential to differentiate into chondrocytic cells and produce a cartilaginous matrix, however, as already mentioned, in large defects they lead to fibrocartilage scar tissue[7]. The latter, contains a greater amount of collagen type I than hyaline cartilage, which leads to inferior mechanical properties, and does not allow withstanding the normal physical stresses found in articular joints[6]. Different approaches have been proposed to enhance marrow stimulation and direct the repair process towards hyaline cartilage rather than fibrocartilage. Scaffolding techniques have great potential and as they allow the incorporation of active agents that trigger signaling pathways that induce MSCs differentiation towards the desired cell phenotype, with the subsequent expression of specific cartilage ECM components.

As already discussed in the previous chapter, we have incorporated both hyaluronic acid and chondroitin sulfate into our hydrogel formulation, as both glycosaminoglycans have been shown enhance chondrogenesis of mesenchymal stem cells, promoting the expression of cartilage-specific markers. Thus, we expect that if cells are able to migrate into the hydrogel scaffold, they will develop a chondrocyte-like phenotype which enables the obtention of hyaline cartilage. To gain insight into the cell-homing potential of the hydrogel formulation, as first approach, we have studied cell migration through our hydrogel structure using different experimental configurations, as it will be described with further detail in the present chapter.

Apart from assessing the cell-homing potential of our scaffold, in the present chapter we also present the evaluation of both chondrogenic and osteogenic potential of the hydrogel formulation.

This feature is of great importance when designing both for cell-free and cell-containing biomaterials.

As previously mentioned in this chapter, it is critical to select properly the source of cells used for osteochondral regeneration. It is well known that adult chondrocytes possess limited capacity of regeneration and can undergo dedifferentiation[8]. Moreover, it has been demonstrated how they may fail on forming bone tissue in the subchondral bone region, which limits their application for osteochondral regeneration. Thus, to overcome the limitations of chondrocytes, mesenchymal stem cells have been widely studied for the development of osteochondral regeneration approaches. Mesenchymal stem cells are multipotent mesoderm-derived progenitor cells and can be isolated from different human tissues[9]. They can differentiate into multiple lineages including bone, cartilage, fat, tendon and muscle[10], among others (Figure IV-1).

Although, bone marrow mesenchymal stem cells are the most widely studied cells for both cartilage and bone tissue engineering, adipose-derived mesenchymal stem cells (ADMSCs) constitute a great alternative thanks to their availability, proliferation and easiness of extraction[2].

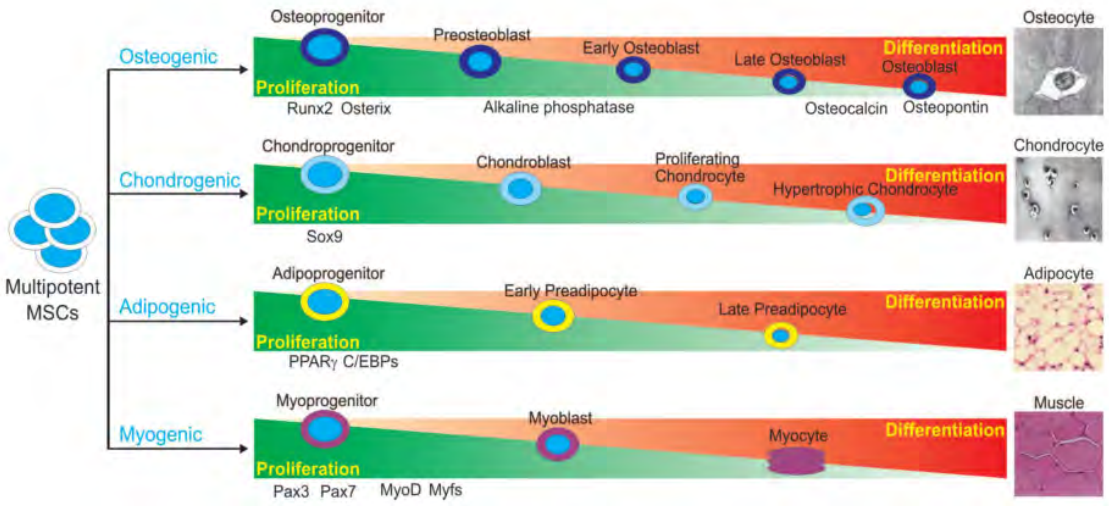

Figure IV-1. Multipotency of mesenchymal stem cells (MSCs).In the appropriate environment, MSCs can differentiate into multiple lineages including osteogenic, chondrogenic, adipogenic or myogenic lineages[11].

ADMSCs have been widely used in both bone and cartilage regeneration. It has been reported how under an osteogenic environment, ADMSCs are observed to express genes and proteins associated with an osteoblastic phenotype, such as alkaline phosphatase, type I collagen, osteopontin, osteonectin, osteocalcin among others[12,13]. Moreover, different studies have demonstrated how ADMSCs can undergo chondrogenesis under the appropriate conditions[14,15]. In addition, and in line with the work presented in this thesis, some studies report the use of ADMSCs for the simultaneous regeneration of hyaline cartilage and the subchondral bone. Zhang et al.[16] reported the use of a heterogeneous scaffold containing a cartilage-like layer composed by a poly(L-glutamic acid) (PLGA) / chitosan (CS) amide bonded hydrogel and a bone-like

PLGA/CS/nHA-g-PLGA polyelectrolyte complex (PEC). Cell seeding in the cartilage-like hydrogel resulted in chondrogenic differentiation, while the bone-like platform allowed subchondral bone regeneration. Thus, *a priori*, ADMSCs seem a good candidate to test the ability of our scaffold to trigger both chondrogenic and osteogenic differentiation.

After analyzing the cell-homing potential of our scaffold, we present a study of its both chondrogenic and osteogenic potential. As already mentioned, it is critical to provide a suitable environment for cell differentiation and the subsequent obtention of a functional tissue. Thus, we have selected different markers, which play different roles in the process of differentiation towards a chondrocytic or osteoblastic phenotypes.

As for chondrogenesis, we will evaluate the expression of type II collagen (COL2), which is the major component of cartilage extracellular matrix[17]. Related with the latter, we have also chosen SOX9, as it is reported to be essential for the expression of type II collagen gene[18]. It has been shown how the expression of SOX9 overlaps largely with that of COL2, suggesting that SOX9 controls COL2 expression[19]. Moreover, the expression of aggrecan (ACAN) will also be evaluated, as a large amount of the proteoglycan is present in the cartilage matrix, in fact, as already mentioned, it is the responsible of the ability of cartilage to withstand high mechanical loads. As for hypertrophic markers we have selected both RUNX2 and collagen type X (COL10). Type X collagen is specific to cartilage and it is synthesized by hypertrophic chondrocytes. It is thought that collagen X facilitates calcification processes and its expression is restricted to hypertrophic chondrocytes matrix[20]. RUNX2 has been found to regulate the expression of collagen type X and matrix calcification. It is the pivotal transcription factor for type X collagen expression and chondrocyte hypertrophy[21].

To study osteogenesis, we have selected alkaline phosphatase (ALP). It is a ubiquitous cellular protein and consequently it cannot be considered bone specific. However, it has been reported how it may act as an early indicator of cellular activity and differentiation. Moreover, ALP levels have also been shown to be upregulated in response to mechanical force application. Collagen type I is an important component of bone extra-cellular matrix, and it forms several connections with cell surface integrin and other ECM proteins. Osteonectin (OSN) or SPARC, which expression is closely aligned with that of fibrillar collagens such as collagen type I. In the osteoid (pre-mineralized bone matrix) it is thought to bin collagen and hydroxyapatite crystals, and release calcium ions perhaps enhancing mineralization of the collagen matrix in bones. It clearly plays a critical role in regulating bone remodeling and maintaining bone mass and quality[22]. Osterix (OSX) is thought to act in the regulation of numerous osteoblast genes including: osteocalcin, osteonectin, osteopontin, bone sialoprotein and collagen type I. Osteocalcin (OCN), known as γ-carboxyglutamic acid-containing protein (BGLAP) preferentially expressed by osteoblasts, is the most abundant non-collagenous bone matrix protein. Thus, it is often used as late marker for bone formation. Osteocalcin modulates the mineral species maturation during osteogenic differentiation of MSCs[23]. The homeodomain protein dlx5 is an activator of RUNX2 and is thought

to be an important regulator of bone formation. DLX5 is a central regulator of bone turnover as it activates bone formation directly and bone resorption[24]. Finally, RUNX2 has a positive effect over osteogenesis at early stages of differentiation. It induces the expression of specific osteoblastic genes and upregulates osteogenic differentiation. However, it is known to inhibit the large stage of osteoblast maturation[25].

As it can be extracted from the description of the selected markers involved in both chondrogenic and osteogenic differentiation, its expression is regulated by complex processes. The latter are intimately bound up to signals provided by the extracellular matrix or, in our case, the provided scaffold. Thus, it is important to analyze the obtained results with a critical view and tailor the matrix design to obtain the desired cell response.

Therefore, the main objectives of the present chapter are the study of the cell-homing capacity and both chondrogenic and osteogenic potential of the developed hydrogel formulation. Thus, we present different experimental setups to study the ability of cells to migrate through hydrogel structure. Moreover, we have used real time PCR to assess both chondrogenic and osteogenic marker expression.

4.2 Materials and Methods

4.2.1 Culture of normal dermal fibroblasts

Human normal dermal fibroblasts (hNDFs, C-12302 Promocell) were used for migration studies and to assess the chondrogenic potential of the hydrogel formulation. They were cultured as detailed in the previous chapter. Briefly, they were cultured in P100 petri dishes (20035, SPL Lifesciences) using DMEM (Lonza) supplemented with 10% fetal bovine serum (FBS, 16SV30180.03, Cultek) 100 U/ml Penicillin / 0,1 mg/ml Streptomycin (L0022, Biowest) and 2mM L-Glutamine (X0550-100, Biowest). Cultures were maintained in the incubator in humidified atmosphere at 37ºC and 5% CO_2.

4.2.2 Culture of adipose-derived mesenchymal stem cells

For cell migration studies and in order to assess the chondrogenic potential of the designed hydrogel formulation, adipose-derived mesenchymal stem cells (ADMSCs, PCS-500-011, ATCC) were used. ADMSCs were cultured in P100 petri dishes (20035, SPL Lifesciences) at a minimum cell density of 5000 cells/cm^2 using DMEM (H3BE12-733F, Lonza) supplemented with 10% fetal bovine serum (FBS, 16SV30180.03, Cultek) 100 U/ml Penicillin / 0,1 mg/ml Streptomycin (L0022, Biowest), 2mM L-Glutamine (X0550-100, Biowest) and 5 ng/ml of fibroblast growth factor (FGF Basic, 100-18A, Peprotech). Cultures were maintained in the incubator in humidified atmosphere at 37ºC an 5% CO_2.

4.2.3 Culture of human bone marrow mesenchymal stem cells

Human bone marrow mesenchymal stem cells (hBMMSCs, HMSC.BM-500, Tebubio) were used to evaluate cell migration using Incucyte® S3 Live-Cell Analysis System (Essen Bioscience).

hBMMSCs were cultured in P100 petri dishes (20035, SPL Lifesciences) at a minimum cell density of 5000 cells/cm^2 using DMEM (H3BE12-733F, Lonza) supplemented with 10% fetal bovine serum (FBS, 16SV30180.03, Cultek) 100 U/ml Penicillin / 0,1 mg/ml Streptomycin (L0022, Biowest), 2mM L-Glutamine (X0550-100, Biowest) and 5 ng/ml of fibroblast growth factor (FGF Basic, 100-18A, Peprotech). Cultures were maintained in the incubator in humidified atmosphere at 37ºC an 5% CO_2.

4.2.4 Cell harvesting and subculture

Petri dishes were washed with 4 ml of PBS (L0615-500, Biowest) and treated with 2 ml of Trypsin-EDTA 0,05% (25300062, Gibco - Life Technologies) for 3 minutes at 37ºC, or until cells started to detach from the plate. Trypsin was inactivated adding 8 ml of serum containing DMEM, and cells were disrupted mechanically by pipetting until individual cells were observed under phase microscopy. Next, cells were counted and resuspended as needed, with a minimum

density of 5000 cells/cm^2 for mesenchymal stem cells cultures, for the next passage or for their encapsulation in hydrogels.

4.2.5 3D culture technique using collagen/glycosaminoglycans composite hydrogel

The procedure for cell encapsulation is the same as described in the previous chapter. Briefly, an 8 mg/ml collagen type I (Fibricol®, #5133-20ML, Advanced BioMatrix) solution (hydrogel gelling solution) was prepared by mixing 8 parts of Fibricol®, 1 part of PBS 10X (X0515, Biowest), 0,75 parts of a sterile filtered 0,1M NaOH (A3910, Panreac) solution and 0,25 of cell-culture water (BE17-724Q, Lonza). This solution was mixed with an equal volume of cell suspension ($4 \cdot 10^6$ cells/ml) in PBS containing 0,3 mg/ml of hyaluronic acid and or chondroitin sulfate (both glycosaminoglycans were kindly provided by Bioiberica S.A.U), to obtain a final cell concentration in the hydrogel scaffold of $2 \cdot 10^6$ cells/ml. Next, 100 μl of the scaffold solution was placed in a 48-well plate (30048, SPL Lifesciences) and incubated during 45 minutes at 37ºC and 5% CO2 to allow the hydrogel formation. Finally, 400 μl of supplemented DMEM was added. Cell culture medium was changed every two days. Cell cultures under chondrogenic differentiation were induced at day 2 of culture with chondrogenic medium: control medium (containing 5% of FBS, 100 U/ml Penicillin / 0,1 mg/ml Streptomycin and 2mM L-Glutamine) supplemented with 10 ng/ml of TGFβ1 (GF111, Millipore), 50 μg/ml of L-ascorbic acid 2-phosphate (A8960, Sigma), 1mM of sodium pyruvate (11360-070, Gibco), 100nM of dexamethasone (D8893, Sigma) and ITS supplement (10 μg/ml insulin, 5,5 μg/ml transferrin and 5 ng/ml of sodium selenite) (I3146, Sigma). Cell cultures under osteogenic differentiation were induced at day 2 of culture with osteogenic medium: control medium (containing 5% of FBS, 100 U/ml Penicillin / 0,1 mg/ml Streptomycin and 2mM L-Glutamine) supplemented with 50 μg/ml of L-ascorbic acid 2-phosphate (A8960, Sigma), 1mM of sodium pyruvate (11360-070, Gibco), 100nM of dexamethasone (D8893, Sigma) and 10mM β-glycerophosphate (G9422, Sigma).

4.2.6 Analyzing the cell homing-capacity of the composite hydrogel formulation

Cell-homing potential of the hydrogel formulation was studied using human Normal Dermal Fibroblasts (hNDFs, C-12302 Promocell), adipose-derived mesenchymal stem cells (ADMSCs, PCS-500-011, ATCC) and human bone marrow mesenchymal stem cells (hBMMSCs, HMSC.BM-500, Tebubio). Different experimental setups were used which are explained in detail below.

4.2.6.1 Vertical migration of human Normal dermal fibroblasts (hNDFs) through a cell-free composite hydrogel

First, the migration capacity of hNDFs through the hydrogel structure was analyzed. To do so, the experimental setup depicted in Figure IV-2 was used. The hydrogel formulation is polymerized at the bottom of a cell culture insert (PICM01250, Millipore) placed in a 24 well-plate. The procedure to obtain the hydrogel has been already described in the previous chapter. Briefly, a collagen gelling solution of 8 mg/ml (Fibricol®, #5133-20ML, Advanced Biomatrix) was prepared as follows: 8 parts of a collagen solution 10mg/ml was mixed with 1 part of PBS 10X 0,75 parts of a NaOH solution 0,1M and 0,25 parts of cell culture H_2O. Next, the gelling solution was mixed with an equal volume of a glycosaminoglycans solution in PBS 1X containing both high molecular weight hyaluronic acid and chondroitin sulfate (both kindly provided by Bioiberica, S.A.U) at a concentration of 0,3 mg/ml. For those hydrogels without GAGs, the gelling solution was mixed with an equal volume of PBS 1X.

After about 40 minutes incubation at 37ºC and 5% CO_2, once gellification has occurred, a cell suspension of $2 \cdot 10^6$ cells/ml in growth media, DMEM (12-733-F, Lonza) supplemented 10% fetal bovine serum (FBS, 16SV30180.03, Cultek) 100 U/ml Penicillin / 0,1 mg/ml Streptomycin (L0022, Biowest) and 2mM L-Glutamine (X0550-100, Biowest) is placed at the top of the hydrogel and incubated at 37ºC and 5% CO_2. Cell culture medium is changed every two days.

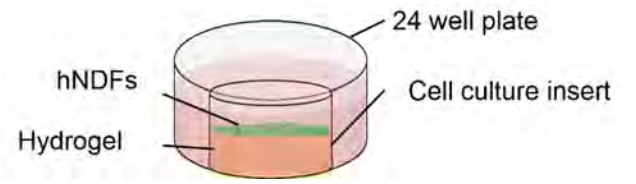

Figure IV-2. Model to study hydrogel recruiting ability and cell migration through the hydrogel structure.

Samples were analyzed under fluorescence microscope (Zeiss Axiovert 200M) and using confocal with multiphoton microscopy (Leica TCS SP5 MP).

4.2.6.2 Horizontal migration of human adipose-derived mesenchymal stem cells (ADMSCs) towards a cell-free composite hydrogel

Migration of ADMSCs will be studied in both growth medium and under chondrogenic induction. Both cell-seeded collagen and cell-free collagen/glycosaminoglycans hydrogels are prepared using a 96-well plate as mold. After an incubation of 40 minutes at 37ºC and 5% CO_2, once hydrogels are polymerized they are placed in a 24-well plate as shown below in Figure IV-3. Briefly, the cell-seeded collagen hydrogel is placed at the right side of the well and the cell-free collagen/glycosaminoglycans hydrogel is placed at the left side of the well. Then, the well is filled with growth medium DMEM (12-733-F, Lonza) supplemented 10% fetal bovine serum (FBS,

16SV30180.03, Cultek) 100 U/ml Penicillin / 0,1 mg/ml Streptomycin (L0022, Biowest), 2mM L-Glutamine (X0550-100, Biowest) and 5 ng/ml of fibroblast growth factor (FGF Basic, 100-18A, Peprotech) and the plate is incubated at 37ºC and 5% CO_2. Medium is changed every two days and triplicates of each type of configuration are performed.

Chondrogenic induction is started after 2 days of culture in growth medium. Growth medium is replaced with chondrogenic medium for the samples that will be submitted to the differentiation process.

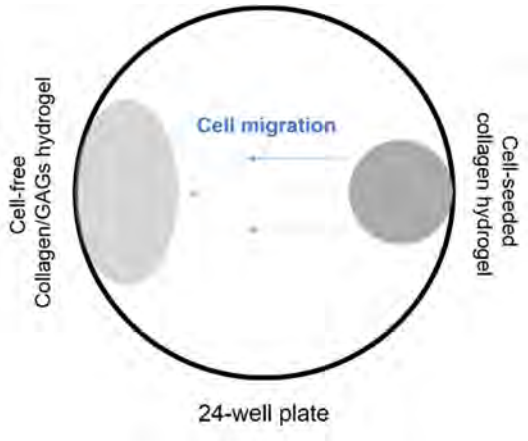

Figure IV-3. Scheme of the horizontal experiment setup.

4.2.6.3 Analyzing cell migration of human Bone Marrow Mesenchymal stem cells using Incucyte® system

Cell migration in different configurations (Figure IV-4) was monitored using Incucyte® S3 Live-Cell Analysis System. Briefly, an automated imaging on the 24-well plate using the whole well imaging feature (4X objective) was scheduled and image acquisition was performed every six hours for nine days.

As shown in Figure IV-4, three different configurations were analyzed. The first configuration (Figure IV-4A) consists of two cell-free hydrogels, one of collagen (left) and the other of collagen/glycosaminoglycans (right), and a monolayer of cells in the center of the well obtained using a polytetrafluoroethylene (PTFE) mold. The other two approaches involve one cell-free and a cell-seeded hydrogel to study the cell migration from one gel to the other. In the configuration shown in Figure IV-4B the migration from a cell-seeded collagen/glycosaminoglycans hydrogel to a cell-free collagen hydrogel was evaluated. Finally, with the setup shown in Figure IV-4C, cell migration from a cell-seeded collagen hydrogel to a collagen/glycosaminoglycans hydrogel was studied.

To mount the different constructs, both cell-free and cell-seeded hydrogels were polymerized using a 96-well plate mold and placed in a 24-well plate (3526, Costar) suitable for Incucyte® S3 Live-Cell Analysis System (Essen Bioscience). Growth medium (DMEM, Lonza) supplemented with 10% FBS, 1% glutamine, 1% penicillin/streptomycin and 5 ng/ml of fibroblast growth factor (FGF Basic, 100-18A, Peprotech) was added and replaced every two days.

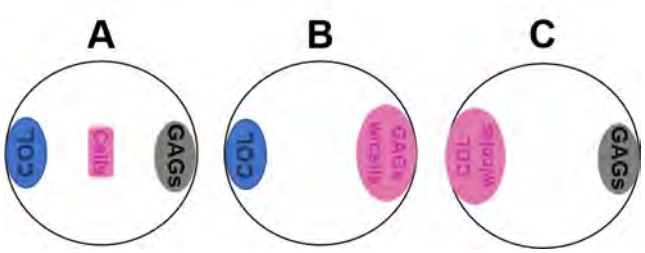

Figure IV-4. Experimental setup for Incucyte® assay in a 24-well plate. **(A)** Cell-free collagen hydrogel and cell-free collagen/glycosaminoglycans hydrogel with a cell monolayer at the center of the well, **(B)** Cell-free collagen hydrogel and cell-seeded collagen/glycosaminoglycans hydrogel **(C)** Cell-seeded collagen hydrogel and cell-free collagen/glycosaminoglycans hydrogel.

4.2.7 Gene expression analysis by real time RT-PCR

4.2.7.1 RNA extraction and purification

The RNA was extracted and quantified using the RNeasy Mini Kit (74104, Qiagen). First both 2D and 3D cultures were washed with PBS and lysed with RNA lysis buffer (Provided with the RNeasy Mini Kit). The constructs were disrupted by pipetting up and down with the micropipette or a pestle and stored -80ºC for further analysis. Next, RNA was extracted following the instructions provided by the manufacturer.

4.2.7.2 cDNA synthesis by reverse transcriptase polymerase chain reaction

cDNA was synthesized using the High Capacity cDNA Reverse Transcription Kit (4368814, Applied Biosystems) following the instructions provided by the manufacturer.

4.2.7.3 Real time PCR

Real-time reverse transcriptase chain reactions were performed using iQ™ SYBR® Green Supermix (170-8882, Bio-Rad) and the primers listed in Table IV-1 and Table IV-2 for the study of chondrogenic and osteogenic differentiation respectively.

Table IV-1. Primers used for the evaluation of chondrogenic markers by qPCR: SOX9, aggrecan (ACAN), collagen type X (COL10), collagen type I (COL1), collagen type II (COL2), RUNX2 and ribosomal protein L22 (RPL22) as housekeeping gene[26].

Gene	F/R	Primer sequence (5' - 3')	Length (bp)	T_m (ºC)
SOX9	F	CAGACGCACATCTCCCCCAA	20	62
	R	GCTTCAGGTCAGCCTTGCC	19	62
ACAN	F	TGGTGATGATCTGGCACGAG	20	64
	R	CGTTTGTAGGTGGTGGCTGT	20	64
COLX	F	CCAATGCCGAGTCAAATGGC	20	60
	R	GGGGGAAGGTTTGTTGGTCT	20	60
COL1	F	AGACGGGAGTTTCTCCTCGG	20	60
	R	CGGAGGTCCACAAAGCTGAA	20	60
COL2	F	ATGACAATCTGGCTCCCAAC	20	55
	R	CTTCAGGGCAGTGTACGTGA	20	55
RUNX2	F	GGTTCAACGATCTGAGATTTGTGGG	25	55
	R	CACTGAGGCGGTCAGAGAACAAACTAG	27	55
RPL22	F	TGACATCCGAGGTGCCTTTC	20	60
	R	GTTAGCAACTACGCGCAACC	20	60

Primers for the study of osteogenesis (Table IV-2) were designed using Primer Blast Software from National Center for Biotechnology Information (NCBI).

Table IV-2. Primers used for the evaluation of osteogenic markers by qPCR:Alkaline phosphatase (ALP), osteonectin (OSN), osterix (OSX), collagen type I (COL1), distal-less homeobox 5 (DLX5), osteocalcin (OCN), RUNX2 and ribosomal protein L22 (RPL22) as housekeeping gene.

Gene	F/R	Primer sequence (5' - 3')	Length (bp)	T_m (ºC)
ALP	F	CCGTGGCAACTCTATCTTTGG	21	60
	R	GCCATACAGGATGGCAGTGA	20	60
OSN	F	ATCTTCCCTGTACACTGGCAGTTC	24	62
	R	CTCGGTGTGGGAGAGGTACC	20	62
OSX	F	TGAGCTGGAGCGTCATGTG	19	60
	R	TCGGGTAAAGCGCTTGGA	18	60
COL1	F	AGACGGGAGTTTCTCCTCGG	20	60
	R	CGGAGGTCCACAAAGCTGAA	20	60
DLX5	F	ACCATCCGTCTCAGGAATCG	20	60
	R	CCCCCGTAGGGCTGTAGTAGT	21	60
OCN	F	CTGTATCAATGGCTGGGAGC	20	52
	R	GCCTGGAGAGGAGCAGAACT	20	52
RUNX2	F	GGTTCAACGATCTGAGATTTGTGGG	25	55
	R	CACTGAGGCGGTCAGAGAACAAACTAG	27	55
RPL22	F	TGACATCCGAGGTGCCTTTC	20	60
	R	GTTAGCAACTACGCGCAACC	20	60

The conditions at which real-time PCR was carried out for the chondrogenic markers are the following: 1 cycle of 10 minutes at 95ºC, followed by 40 cycles of 15 seconds at 94ºC for denaturation of the cDNA, 30 seconds at 55ºC (COL2 and RUNX2) or 60ºC (RPL22, COL1 and COL10) or 62ºC (SOX9) or 64ºC (ACAN) for primer annealing and 30 seconds at 72ºC for extension.

For the osteogenic markers, the real-time PCR was carried out as follows: 1 cycle of 10 minutes at 95ºC, followed by 40 cycles of 15 seconds at 94ºC for denaturation of the cDNA, 30 seconds at 60ºC (ALP, OSX, COL1, DLX5 and RPL22) or 62ºC (OSN) or 55ºC (RUNX2) or 52ºC (OCN).

Finally, for both chondrogenic and osteogenic markers melting curves were obtained from 58ºC to 95ºC. Relative gene-fold variations were obtained using the $\Delta\Delta$Ct method and the RPL22 has housekeeping gene.

For all the real-time PCR analysis 3 biological replicates of each sample and 3 technique replicates of each biological replicate were used.

4.2.8 Western Blot

Western Blot was used to analyze collagen type II expression.

Samples were lysed using RIPA buffer (20-188, Sigma), and total protein content was determined using a BCA Protein Assay kit (23225, Thermo Fisher). Acrylamide gels were

prepared at a concentration of 7,5% (w/v). Cell lysates, containing 5μg of total protein, were run applying 150V for 90 minutes. Once the run was complete, proteins were transferred to a polyvinylidene (PVDF) membrane (Immobilon-P, IPVH00010, Millipore) by applying 40V during 2h at room temperature (RT). Next, the membrane was incubated for 2 hours in blocking buffer (4% (w/v) non-fat powdered milk in PBST). After the blocking step, membranes were incubated with the primary antibodies (Table IV-3) at a final concentration of 1 μg/ml in PBST. Next, membranes were incubated during 1 hour at RT with a secondary antibody IgG-HRP (AP160P, Millipore) (Table IV-4) at a final concentration of 1 mg/ml in PBST. Finally, membranes were revealed for HRP detection using Luminata™ Forte Western HRP (WBLUF0100, Millipore). Chemiluminescent images were taken in ImageQuant™ LAS 4000 mini (GE Healthcare). Images were analyzed using ImageQuant™ Image Analysis Software. Actin was used as internal protein standard.

Table IV-3. Primary antibodies used for Western Blot.

Primary antibodies	Description	Molecular Weight	Reference	Brand
Actin	Mouse monoclonal to Actin C4	43 kDa	MAB1501	Millipore
Collagen 2A1	Mouse monoclonal to Collagen II	140 kDa	Ab3092	Abcam

Table IV-4. Horseradish peroxidase (HRP) conjugated secondary antibody used for Western Blot.

Secondary antibodies	Reference	Brand
Rabbit anti-Mouse	AP160P	Millipore

4.2.9 Mineralization assessment

4.2.9.1 Alizarin red staining

Cell cultures are fixated with 4% p-formaldehyde during 30 minutes at 4ºC. After fixation, cultures are covered with 1mg/ml alizarin red (A5533, Sigma-Aldrich) solution in milliQ water and incubated during 5 minutes at room temperature. After several milliQ water washes and a last ethanol wash, samples are observed under optical microscope (Nikon Eclipse TE2000-U) and under zoom stereomicroscope (Nikon SMZ800).

4.2.9.2 Von Kossa staining

Cell cultures were washed with PBS and fixed with p-formaldehyde 1% during 1 hour at room temperature. Next, cultures were washed several times with milliQ water to remove phosphate ions from PBS and prevent their precipitation with silver nitrate solution. Then, samples were incubated with a freshly prepared 5% (w/v) silver nitrate (209139, Sigma-Aldrich) solution in milliQ H_2O for 1 hour in the dark at room temperature. After incubation, samples are placed under a

strong source of light for 10 minutes to stimulate the reaction. Finally, samples are observed under zoom stereomicroscope (Nikon SMZ800).

4.2.10 Mechanical characterization of cell seeded hydrogels

Constructs were fixed with 4% paraformaldehyde (w/v) in PBS during 1 hour at room temperature. A compression assay using DMA Multi frequency strain mode and a frequency sweep test was carried out with a DMA Q800 (TA Instruments). The thickness and diameter of each construct was determined before each measurement. The conditions of the assay are listed below in Table IV-5.

Table IV-5. DMA analysis conditions

Condition	Value
Amplitude (μm)	10
Preload (N)	0,03
Frequency (Hz)	1

The results were analyzed with TA Universal analysis software.

4.2.11 Statistics

Values are expressed as mean ± SD. For samples prepared in triplicate, statistical differences were analyzed with GraphPad Prism 6. For the comparison of two groups, the student's unpaired t test was used, while for the comparison of three or more groups the statistical analysis was performed by 1-way or 2-way ANOVA.

4.3 Results and discussion

As already mentioned, to achieve tissue regeneration, it is critical to provide an environment that allows cell colonization and that supplies the appropriate signaling to trigger cell differentiation processes. Thus, in the following lines, we present a study of the cell-homing capacity of our hydrogel formulation, as well as an assessment of its both chondrogenic and osteogenic potential.

4.3.1 Cell-homing potential of the hydrogel formulation

First, we have performed a study of the cell-homing potential of the designed hydrogel formulation. To do so, we have designed two experimental setups, which are described and analyzed in detail below. Briefly, we have studied cell migration process using both a vertical and a horizontal setup. With the vertical setup we demonstrate how cells can penetrate trough the hydrogel network, and with the horizontal setup we confirm the obtained results eliminating the gravity effect, which could favor the process.

4.3.1.1 Vertical migration of human normal dermal fibroblasts (hNDFs) through a collagen / glycosaminoglycans hydrogel

First, we have evaluated cell migration through the hydrogel structure using a vertical approach. To do so, cells were seeded on the top of a previously polymerized hydrogel and allowed to proliferate and migrate during 11 days in growth medium. To perform this experiment, we have used human-normal dermal fibroblasts (hNDFs) and as mentioned, cultures have been maintained in growth medium, to avoid the interference of differentiation processes which would add complexity to result analysis. Migration process has been studied in both collagen and collagen/glycosaminoglycans hydrogels. Thus, the effect of the presence of hyaluronic acid and chondroitin sulfate in the hydrogel formulation has been analyzed.

The progress of cell migration was evaluated by dapi/phalloidin staining and observed under fluorescence microscopy analysis (Figure IV-5). Collagen hydrogels were stained after 4 (Figure IV-5A) and after 11 (Figure IV-5C) days of culture, as well as collagen / glycosaminoglycans hydrogels which were also stained after 4 (Figure IV-5B) and 11 (Figure IV-5D) days of culture.

Dapi/phalloidin staining of the hydrogels (Figure IV-5) revealed that the collagen/glycosaminoglycans hydrogel presented a higher number of cells than the collagen hydrogel both at day 1 (Figure IV-5B) and day 11 (Figure IV-5D), being the initial cell density the same for both formulations. Moreover, it can be seen how cells are aligned at day 11 when cultured in the collagen/glycosaminoglycan composite hydrogel. Thus, it can be hypothesized that the addition of glycosaminoglycans into the hydrogel formulation has effect over cell behavior.

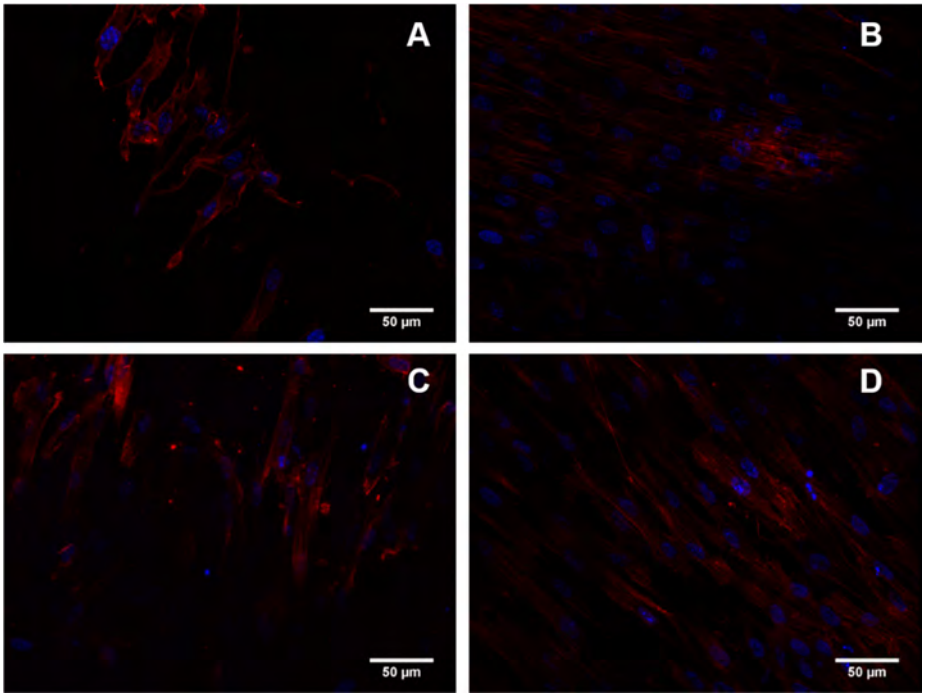

Figure IV-5. Dapi/phalloidin staining of hNDFs cultures. **(A)** Collagen hydrogel after 4 days of culture, **(B)** Collagen / glycosaminoglycans composite hydrogel after 4 days of culture **(C)** Collagen hydrogel after 11 days of culture **(D)** Collagen / glycosaminoglycans composite hydrogel after 11 days of culture. (Cell nuclei appear stained blue while actin filaments appear stained red).

To gain further insight into the migration process, confocal microscopy with multiphoton (MP) was used. Second harmonic generation (SHG) enables the visualization of collagen fibers, which have been green-colored using imaging software. As it will be discussed, SHG signal differs depending on collagen fibers organization. Again, collagen and collagen/glycosaminoglycans composite hydrogels have been analyzed and differences observed between the two formulations have been studied. Following the same procedure than in the previous experiment, hydrogel formulations were stained with dapi/phalloidin at day 1 and day 11 of culture to evaluate the progression of the cell migration process.

Next, in Figure IV-6 the results obtained for collagen hydrogels are shown. The images shown are montages of slices taken at different heights of the hydrogel. Again, as it has been observed in Figure IV-5A, we observe a little number of cells at day 1 (Figure IV-6A) of culture. After 11 days (Figure IV-6B), cell number seems to have increased, and it can be clearly appreciated how collagen fibers have rearranged forming a characteristic defined pattern.

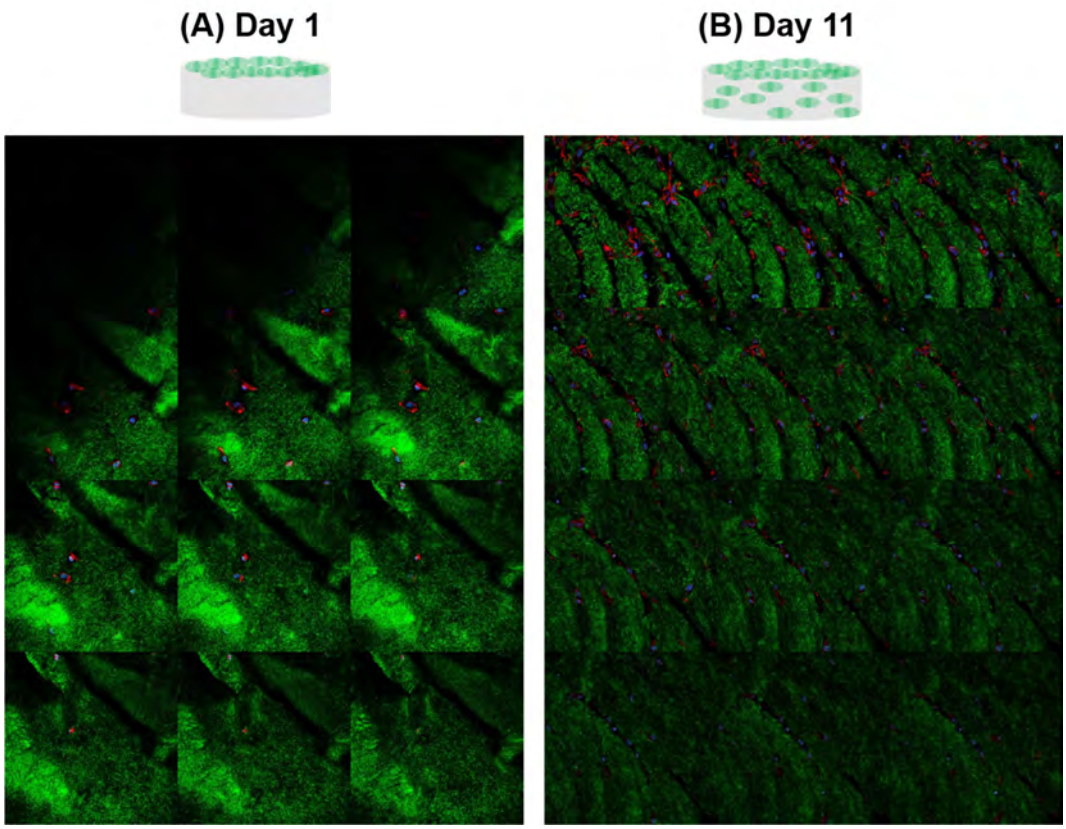

Figure IV-6. Confocal and multiphoton microscopy images of DAPI/Phalloidin staining for collagen hydrogels: **(A)** 1 day of culture and, **(B)** 11 days of culture. Collagen fibers appear green-colored after image processing as result of second harmonic generation imaging. Cell nuclei appear stained blue while actin filaments appear stained red.

Figure IV-7 shows the obtained results for the hydrogels containing both collagen and glycosaminoglycans. As it can be seen, at day 1 of culture (Figure IV-7A), cells are concentrated on the top of the hydrogel and as we move towards the bottom of the hydrogel we can see the collagen fibers. What points out, is the higher number of cells observed for this formulation in comparison with collagen hydrogels, which agrees with the results shown previously in Figure IV-5. At day 11 (Figure IV-7B) cells are spread throughout the entire hydrogel structure. After polymerization, those hydrogels containing glycosaminoglycans are more compact, probably as a result of a higher crosslinking due to the interaction between collagen and glycosaminoglycans. Moreover, because of their highly negative charge and repulsion forces, glycosaminoglycans occupy a large volume into the collagen mesh conferring the hydrogel with high resistance to compression. Thus, when cells are placed on the top of the hydrogel they remain at this position at the initial culture stages. However, as collagen hydrogels are less compacted we hypothesize that once cells are placed on the top of their structure they diffuse by gravity effect through the scaffold, and that is why for collagen hydrogels we observe less cells on the hydrogel surface at day 1 of culture (Figure IV-5A and Figure IV-6A).

Moreover, collagen fiber organization at day 11 has a different appearance in comparison with collagen hydrogels. Again, collagen fiber degree of organization increases from day 1 to day

11, but here instead of creating the characteristic pattern observed previously in Figure IV-6B, collagen fibers appear to be parallel between them.

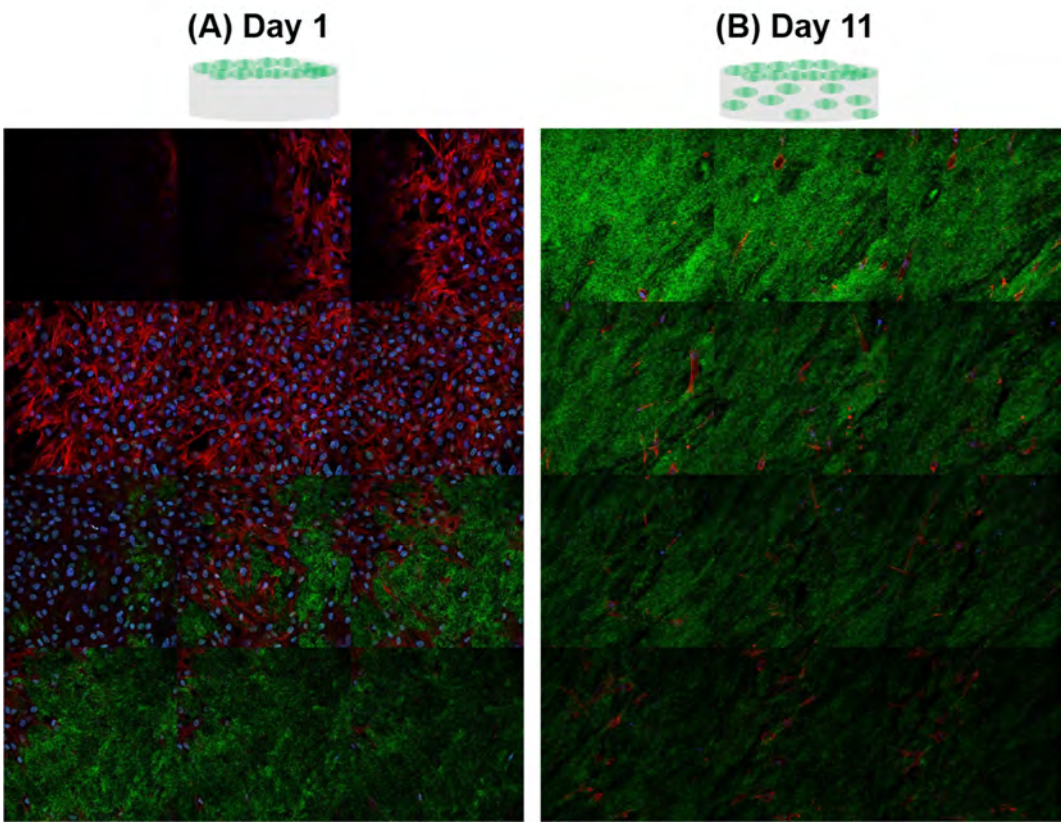

Figure IV-7. Confocal and multiphoton microscopy images of DAPI/Phalloidin staining for collagen / glycosaminoglycans composite hydrogel: **(A)** 1 day of culture and, **(B)** 11 days of culture. Collagen fibers appear green-colored after image processing as result of second harmonic generation imaging. Cell nuclei appear stained blue while actin filaments appear stained red.

Thus, using the vertical experimental setup we have demonstrated how hydrogel colonization does occur, and it is not prevented by the intricate hydrogel network. However, as already mentioned, this setup is subject to gravity effect which it is likely to favor the migration process. Therefore, we have also analyzed cell-homing potential using a horizontal conformation as it is discussed in detail next.

4.3.1.2 Horizontal migration of human adipose-derived mesenchymal stem cells (ADMSCs) towards a cell-free collagen / glycosaminoglycans hydrogel

As already mentioned, it must be noticed that with the vertical setup presented previously, cells are subject to gravity effect which can favor the migration process. Thus, to eliminate the effect of gravity, a horizontal approach was designed. Briefly, a cell-seeded collagen hydrogel was placed at the right side of a 24-well plate and a collagen/glycosaminoglycans hydrogel at the left side (Figure IV-3). Cell migration from the collagen hydrogel towards the collagen/glycosaminoglycans hydrogel was monitored over time using optical microscopy. The assay was performed using adipose-derived mesenchymal stem cells (ADMSCs) and in both growth and chondrogenic medium. The latter contains biochemical cues that trigger ADMSCs chondrogenic differentiation process. Thus, by comparing the process under the two different cell culture media we are able to not only monitor migration process but also to evaluate morphological changes that cells undergo when are under chondrogenesis process.

Figure IV-8 shows how after 16 days of culture in both growth and chondrogenic medium cells have reached the left side of the well, and the colonization of the glycosaminoglycan-containing cell-free hydrogel has begun. The sample cultured in growth medium presents a high degree of confluence (100%) at the center of the plate and cells present a fibroblast-like elongated morphology (Figure IV-8A-B). The dapi/phalloidin staining of the hydrogel reveals how it has been colonized (Figure IV-8D). Cells appear at distinct focal planes, revealing that they have spread through the three-dimensional environment provided by the scaffold. Inside the hydrogel they also present a fibroblastic elongated shape. For those samples cultured in chondrogenic medium (Figure IV-8E-H), with first points out is that at the center of the plate cells present more rounded shape, and they have started to form clusters, meaning that they are under differentiation (Figure IV-8E-F). As it occurred with the samples cultured in growth medium, the dapi/phalloidin staining of the hydrogels (Figure IV-8G-H) show how cells have entered the hydrogel structure. As in the center of the plate, they shape is more rounded in consequence of the differentiation process. It is known that during embryonic development of cartilage, mesenchymal progenitor cells assume a rounded morphology and start to form aggregates[27], and this phenomenon can be reproduced in vitro under the appropriate signaling[28].

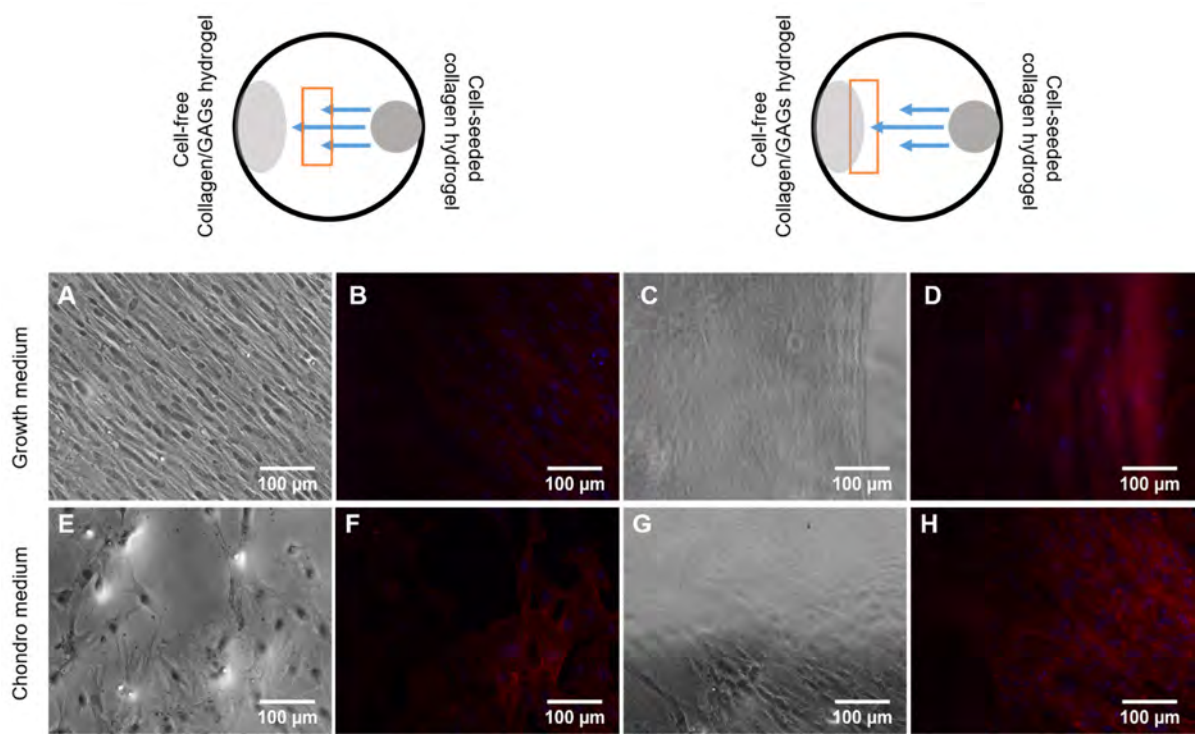

Figure IV-8. Phase contrast images and DAPI/Phalloidin staining of cultures at day 16 both in growth and chondrogenic media.

Therefore, with this horizontal setup we have confirmed how cells are able to colonize a cell-free collagen/glycosaminoglycans hydrogel. Moreover, we have captured morphological changes of cells under chondrogenic induction. Their behavior is similar to that observed during embryonic cartilage development, as they start to form aggregates, which are thought to play a critical role to allow the creation of the proper microenvironment which initiates chondrogenesis[28].

Finally, we have reproduced the previous experiment using Incucyte® S3 Live Cell Analysis System, which allows the automatic acquisition of images over time and the creation of time-lapse sequences that give a better understanding of cell motion. The experimental setups analyzed with Incucyte® have already been described in the materials and methods section. The valuable results are in form of movie and they can be accessed through the link.

After having demonstrated the ability of cells to colonize the hydrogel matrix both in a vertical and horizontal conformation, we proceed with the assessment of both chondrogenic and osteogenic potential of the hydrogel formulation which is critical to obtain a desired cell behavior to induce tissue repair and regeneration. As already mentioned, cartilage and the subchondral bone should be treated as one unit to achieve complete articular regeneration. Thus, we aim to induce different cell behavior depending on its position through the scaffold. Those cells closer to the bioceramic platform should present an osteoblast-like or a hypertrophic phenotype while those cells closer to the hydrogel surface a chondrocyte-like phenotype. Therefore, it is critical to obtain

a control over both differentiation processes through matrix tailoring to provide the appropriate signaling that induces the desired cell response. Chondrogenic potential will be assessed in both human normal dermal fibroblasts (hNDFs), based on previous studies[29], and adipose-derived mesenchymal stem cells (ADMSCs). Osteogenic potential is evaluated solely for ADMSCs based on their easiness to undergo differentiation.

4.3.2 Assessment of the chondrogenic potential of the hydrogel formulation over human normal dermal fibroblasts

As said before, both chondrogenic and osteogenic differentiation processes are critical to the optimal performance of our osteochondral scaffold, thus, once we have demonstrated how cells migrate and colonize the hydrogel scaffold, we proceed with the evaluation of the chondrogenic potential of the hydrogel formulation. As first approach and based on previous research[29], we studied the expression pattern of different chondrogenic markers for human normal dermal fibroblasts (hNDFS) both at protein and gene level. Dermal fibroblasts have gained interest for tissue engineering applications as they present easiness of extraction and several reports have shown their capacity to differentiate into other lineages such as osteogenic[30,31,32,33] adipogenic[30,32,33] and chondrogenic[30,32,34–36] under induction medium.

First, we studied the expression of collagen type II (COL2), a specific chondrogenic marker, at the protein level by western blot analysis (Figure IV-9). The expression was evaluated in both collagen hydrogels (COL) and collagen/hyaluronic acid/chondroitin sulfate (COL/GAGs) hydrogels cultured in growth and chondrogenic medium for 50 days. As mentioned before, chondrogenic medium contains biochemical cues that induce cell differentiation towards a chondrogenic phenotype. As it can be seen, the presence of collagen type II was detected (140kDa) for both formulations when cultured under induction medium. However, the protein was not detected for hydrogels cultured in growth medium. Thus, the presence of hyaluronic acid and chondroitin sulfate is not enough to induce collagen type II expression in hNDFs.

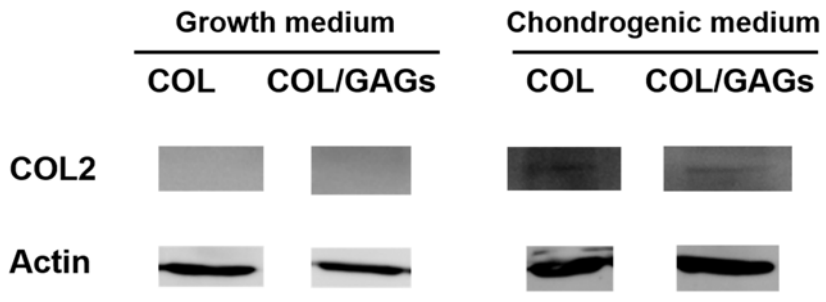

Figure IV-9. Collagen type II expression analysis by western blot after 50 days of culture. Actin expression was used as an internal control. Samples were prepared in triplicate.

As for gene expression, different chondrogenic and hypertrophic markers were analyzed by RT-PCR for hNDFs cultured in both collagen and collagen/hyaluronic acid/chondroitin sulfate hydrogels and in monolayer (2D cultures).

Figure IV-10 shows the expression of the studied genes after 2 and 3 weeks of culture relative to ribosomal protein L22 (RPL22) for three-dimensional cultures, cultured both in growth and chondrogenic medium. From these results, we can analyze if there is expression of the selected markers, as well as determine its peak of expression over the studied time points comparing both types of formulations and cell culture media. First, Table IV-6 summarizes the observed peak of expression of the analyzed genes.

Table IV-6. Peak of expression of chondrogenic genes of hNDFs for both collagen and collagen/glycosaminoglycans hydrogel formulations cultured in both growth and chondrogenic medium.

Gene	Growth medium		Chondrogenic medium	
	Collagen	**Collagen / GAGs**	**Collagen**	**Collagen / GAGs**
COL1	Sustained	Sustained	Sustained	Day 30
ACAN	No expression	No expression	Day 30	Day 30
SOX9	Day 30	Day 30	Day 15	Day 30
COL2	Sustained	Day 15	Sustained	Sustained
COL10	Sustained	Sustained	Sustained	Day 30
RUNX2	Sustained	Sustained	Sustained	Sustained

It can be seen how the expression of collagen type I is sustained for both hydrogel formulations when cultured in growth medium, and for collagen hydrogels when cultured in chondrogenic conditions. Moreover, its expression is higher under chondrogenic conditions for almost all types of sample. However, for the hydrogels containing glycosaminoglycans and cultured in chondrogenic medium it is interesting to see how the expression of COL1 presents a peak at day 30, and that at day 15 its expression is around 10 times inferior to that observed for growth medium. Collagen type I is present in a great amount in fibrocartilage. Thus, it can be hypothesized that the presence of hyaluronic acid and chondroitin sulfate somehow helps to maintain low levels of collagen type I, reducing the amount of fibrocartilage.

Aggrecan, which is one of the main constituents of cartilage ECM together with collagen type II, is only expressed at day 30 for those samples cultured in chondrogenic medium, and there is no statistically significant difference between the two hydrogel formulations. Thus, we can conclude that the presence of glycosaminoglycans alone is not enough to trigger its synthesis. However, as hNDFs have been used for this analysis, and they must undergo a transdifferentiation process, it is possible that longer culture times are required to appreciate its expression.

As for SOX9, which is known to be a regulator of collagen type II synthesis and to be involved in early stages of the differentiation process, it can be seen how for those samples cultured in growth medium it is only observed at after 30 days of culture. When samples are cultured in growth media, a peak of expression at day 15 can be observed for collagen hydrogels, while for those hydrogels containing glycosaminoglycans its expression is only detected at day 30. The higher expression of the gene at day 15 for collagen hydrogels, agrees with the fact that SOX9 is an early marker of MSCs differentiation. Thus, we hypothesize that if hyaluronic acid and chondroitin sulfate present a positive effect over the differentiation process it is possible that we have missed its peak of expression, which could be before 15 days of culture.

Analyzing collagen type II expression, it can be seen how for those samples cultured in growth medium, there is a peak of expression for those hydrogels containing glycosaminoglycans at day 15, which supports the hypothesis presented for SOX9. If SOX9 regulates COL2 expression and the latter is detected, it can be assumed that SOX9 should have been expressed at a certain time point earlier than day 15. For those samples cultured in chondrogenic medium, we can see how COL2 expression is sustained for both collagen and collagen/glycosaminoglycans hydrogels, and that there is no statistically significant difference between the two hydrogel formulations.

As for hypertrophic markers, it can be seen how collagen type X expression is sustained for those samples cultured in growth medium. For those samples cultured in chondrogenic medium the expression of the hypertrophic marker is one order of magnitude superior, which agrees with the fact that chondrogenic induction fastens the differentiation process and subsequently the system reaches a hypertrophic state early. However, it can be appreciated how for those hydrogels containing glycosaminoglycans cultured in chondrogenic medium, the expression of COL10 at day 15 is of the same order of those cultured in growth medium. Thus, the presence of both hyaluronic acid and chondroitin sulfate has an effect over COL10 expression. The latter must be further analyzed using, for instance, histologic studies to assess the quality of the obtained tissue and to confirm whether or not the presence of GAGs helps on obtaining healthier constructs.

Finally, the expression of RUNX2, which is a strong regulator of the expression of type X collagen, is sustained for both culture media and formulations. However, for those hydrogels containing glycosaminoglycans and cultured in chondrogenic medium, its expression is slightly lower than for those hydrogels made of collagen only.

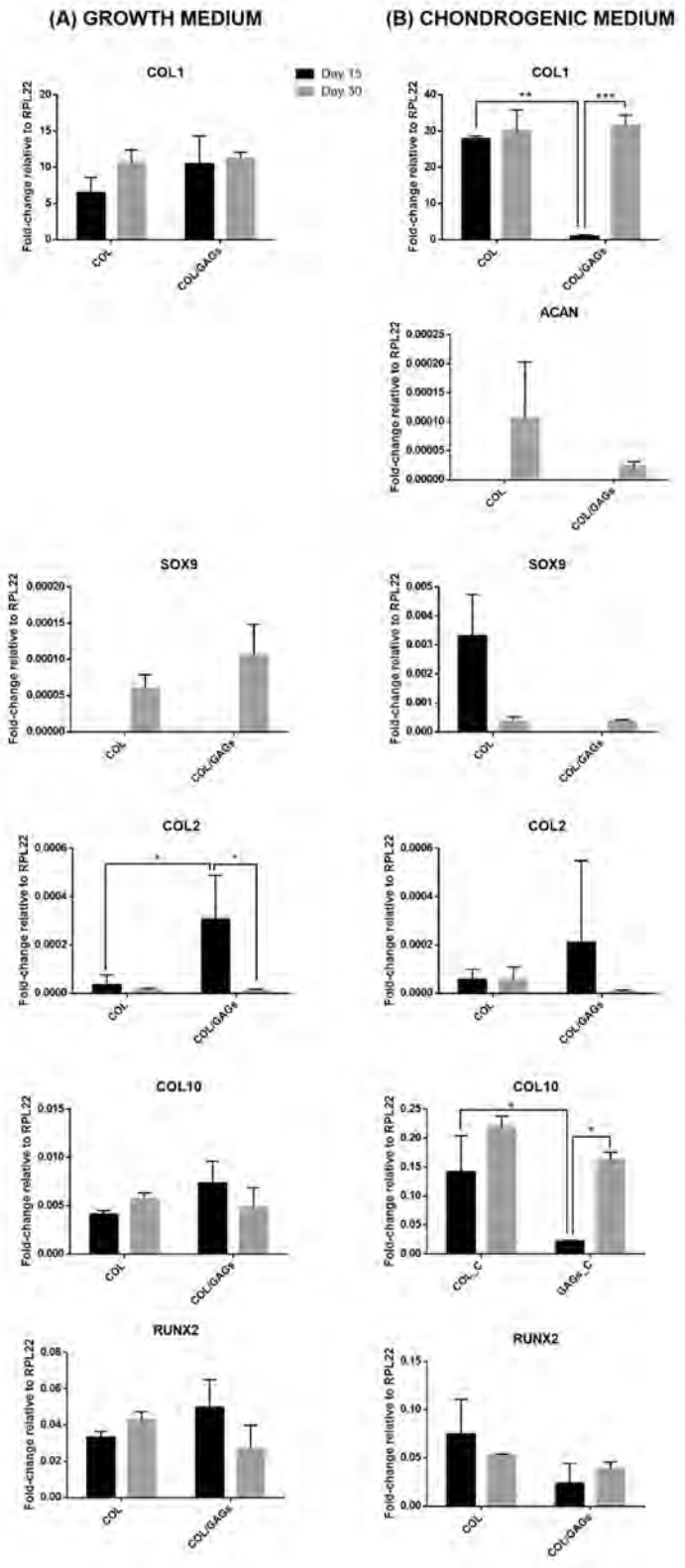

Figure IV-10. Expression kinetics of the analyzed genes: Gene expression in hNDFs cultured for 2 and 3 weeks in both **(A)** growth and **(B)** chondrogenic medium in collagen (COL) and collagen/hyaluronic acid/ chondroitin sulfate (COL/GAGs) hydrogels. C_t values relative to ribosomal protein L22 (RPL22) are represented. (Statistical differences are indicated as: * for $p < 0.05$, ** for $p < 0.01$, and *** for $p < 0.001$, Two-way ANOVA, n = 3).

Thus, we have demonstrated how there is expression of the selected chondrogenic and hypertrophic markers, and how it varies along time and depending on the hydrogel formulation. However, it must be pointed out that to achieve a higher degree of understanding of the kinetics of the differentiation process in our hydrogel formulation, more time points should be analyzed.

Next, in order to evaluate the effect of the presence of glycosaminoglycans in the hydrogel formulation, we have normalized gene expression relative to collagen hydrogels (Figure IV-11).

It can be seen how the expression of collagen type I (COL1) is strongly downregulated for those hydrogels containing glycosaminoglycans cultured in chondrogenic medium at day 15. Moreover, under any circumstances the expression was upregulated for hydrogel formulations containing hyaluronic and chondroitin sulfate. Thus, as already mentioned it can be hypothesized that glycosaminoglycans may help to reduce the amount of fibrocartilage obtained. This effect, if combined with a higher collagen type II expression, could lead to an obtention of a healthier tissue.

Aggrecan synthesis appears to be downregulated for those hydrogels containing glycosaminoglycans. However, as observed previously in Figure IV-10, there is no statistically significant difference between the two studied formulations, and the detected levels of expression are low. Again, this leads to hypothesize that longer culture times may be required to achieve a high degree of expression of cartilage-specific markers for hNDFs. Collagen type II, the other main constituent of cartilage ECM together with aggrecan, is upregulated for those samples containing glycosaminoglycans cultured in growth medium after 15 days. However, it appears to be downregulated with respect to collagen hydrogels at late time points and in chondrogenic medium. The fact that COL2 expression is upregulated in growth medium in the presence of hyaluronic acid and chondroitin sulfate at the earlier time point studied may suggest that glycosaminoglycans present a positive effect over its expression. By analyzing more time points, we could discuss with more criteria the effect of GAGs in the formulation and determine if the downregulation observed when samples are cultured in chondrogenic medium is due to a later expression for collagen hydrogels, and to the fact that we are missing the peak of expression for hydrogels containing GAGs when cultured under chondrogenic induction.

What is more interesting, is the fact that the expression of hypertrophic markers (COL10 and RUNX2) is downregulated for hydrogels containing hyaluronic acid and chondroitin sulfate at both day 15 and day 30 of culture, except for those hydrogels cultured in growth medium at day 15. Thus, it can be hypothesized that the presence of glycosaminoglycans in the hydrogel formulation reduces the expression of hypertrophic markers.

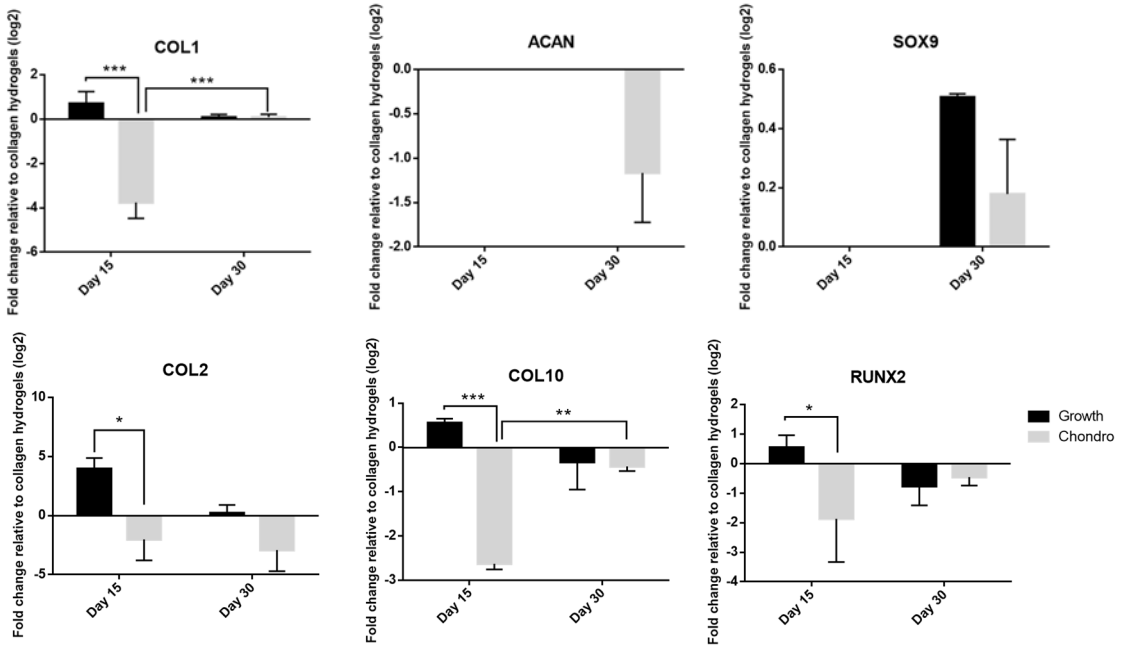

Figure IV-11. Chondrogenic gene expression in human normal dermal fibroblasts (hNDFs) cultured for 15 and 30 days in both growth and chondrogenic medium in collagen/hyaluronic acid/chondroitin sulfate hydrogels. C_t values relative to ribosomal protein L22 (RPL22) were obtained and represented as fold increase ($\Delta\Delta C_t$) relative to collagen hydrogel cultures. (Statistical differences are indicated as: * for $p < 0.05$, ** for $p < 0.01$, and *** for $p < 0.001$, Two-way ANOVA, n=3).

After having studied the expression of both chondrogenic and hypertrophic markers, we considered appropriate analyzing whether hydrogel matrices were mineralized after being cultured in both growth and chondrogenic medium. It must be noticed that mineralization is an undesired effect when trying to obtain engineered hyaline cartilage, as it is an indicator of final stages of hypertrophy. Thus, ideally, mineralization should be avoided to obtain a healthy functional cartilage tissue.

Next, Figure IV-12 shows the result of a von Kossa staining of collagen (COL) and collagen/hyaluronic acid/chondroitin sulfate (COL/GAGs) hydrogels cultured for 21 (Figure IV-12A) and 50 (Figure IV-12B) days in both growth and chondrogenic medium. As it can be seen, at day 21 there is no sign of mineralization (mineral deposits appear black after the staining) for both hydrogel formulations and both culture media. At day 50, after the staining hydrogels show a darker color, which can be attributed to a weak positive von Kossa staining. The obtained results are promising, as they do not show a strong mineralization of the matrix. However, in order to gain a deeper insight into matrix mineralization histologic studies should be performed.

Moreover, we can relate mineralization with the expression of both RUNX2 and collagen type X, studied previously with RT-PCR. RUNX2 is known to be a driver of the expression of terminal differentiation markers[37], such as type X collagen, which is synthesized in areas composed of hypertrophic and degenerative chondrocytes that are associated with increased vascularity and

matrix mineralization[20]. Expression of both genes was detected by RT-PCR, however the weak von kossa staining observed after 50 days of culture may lead to think that both gene levels are not high enough to cause a high degree of matrix mineralization.

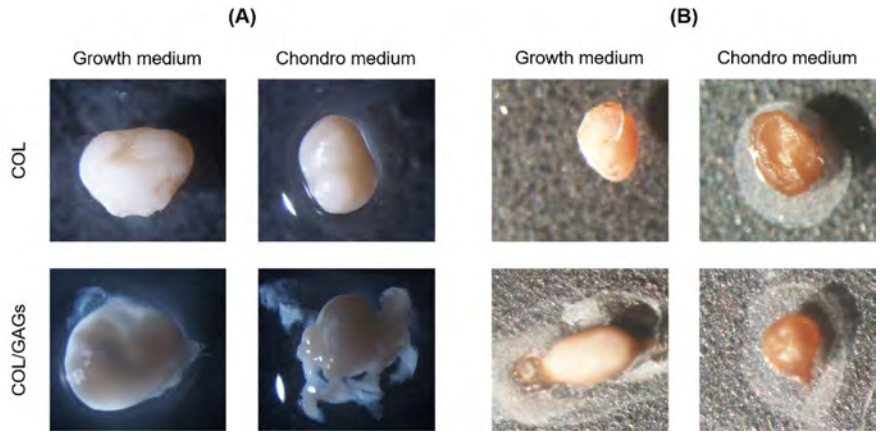

Figure IV-12. Von Kossa staining of hydrogel cultures seeded with hNDFs cultured for **(A)** 21 days and **(B)** 50 days in both growth and chondrogenic medium.

Finally, following with the study of the expression cartilage-related genes by hNDFs we evaluated changes in mechanical properties depending on culture time and culture media. To do so, a compression assay was performed with DMA, and the obtained results are shown in Figure IV-13. As it can be seen, compressive storage modulus (G', kPa) is higher when samples are cultured in chondrogenic medium at both time points. After 30 days of culture, G' has increased two orders of magnitude as a result of the compaction and the stiffening of the hydrogel matrix, caused by the interaction with cells. Although it is difficult to make comparisons in terms of storage modulus, as it is highly dependent on measurements conditions, after 30 days of culture in chondrogenic medium our hydrogel scaffold has reached values near those previously reported. Different studies have measured cartilage mechanical properties under different conditions, and it has been reported that the Young's modulus of articular cartilage, measured under unconfined compression is of the order of 0,5MPa[38].

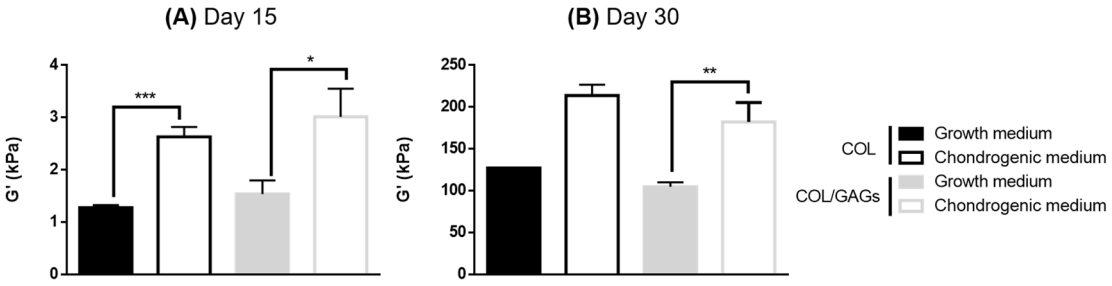

Figure IV-13. DMA analysis of collagen (COL) and collagen/glycosaminoglycans (COL/GAGs) seeded with human normal dermal fibroblasts (hNDFs) at **(A)** day 15 and **(B)** day 30 of culture in both growth and chondrogenic medium. (Statistical differences are indicated as * for $p<0.05$, ** for $p<0.01$, and *** for $p<0.001$, t test, n=3).

4.3.3 Assessment of the chondrogenic potential of the hydrogel formulation over adipose-derived mesenchymal stem cells

After the assessment of the chondrogenic gene expression by human normal dermal fibroblasts, we studied the expression of chondrogenic marker genes in adipose-derived mesenchymal stem cells, as their differentiation process is faster and widely described.

Again, we have evaluated the expression of both chondrogenic and hypertrophic genes by real time RT-PCR in both growth and chondrogenic medium and for the two studied formulations. Figure IV-14 shows the expression of the studied genes after 1, 2 and 4 weeks of culture relative to ribosomal protein L22 (RPL22) for three-dimensional cultures, cultured both in growth and chondrogenic medium. From these results, we can analyze the expression of the selected markers, as well as determine its peak of expression over the studied time points comparing both types of formulations and cell culture media. First, Table IV-7 summarizes the observed peak of expression for the analyzed genes. As it can be seen, the analysis for collagen type II is not presented, as gene expression appeared at high number of PCR cycles, and thus we do not consider the obtained results reliable.

Table IV-7. Peak of expression of chondrogenic genes for both collagen and collagen/glycosaminoglycans hydrogel formulations cultured in both growth and chondrogenic medium.

Gene	Growth medium		Chondrogenic medium	
	Collagen	**Collagen / GAGs**	**Collagen**	**Collagen / GAGs**
COL1	day 27	day 27	day 27	sustained
ACAN	day 27	day 27	day 14	day 14
SOX9	sustained	sustained	sustained	sustained
COL10	day 27	sustained	sustained	day 27
RUNX2	+/- day 27	day 7	sustained	sustained

First, for collagen type I we observe its peak of expression at day 21 for all conditions, except for those hydrogels containing glycosaminoglycans and cultured in chondrogenic medium, for which the expression is sustained along time. As it can be seen in Figure IV-14, the expression is significantly higher, around two times, for those hydrogels cultured in chondrogenic medium, and there are no statistically significant differences between the two formulations.

Aggrecan presents its peak of expression at day 27 for those samples cultured in growth medium and at day 14 for those cultured in chondrogenic medium, reaching also higher levels of expression under induction. The latter demonstrates how a chondro-inductive environment accelerates the differentiation process providing the appropriate biochemical cues required to trigger chondrogenesis. Moreover, its expression is slightly higher for those hydrogels containing glycosaminoglycans.

As for SOX9, as there is no statistically significant difference between the different time points analyzed, strictly it must be said that its expression is sustained along time. However, it seems that its expression is higher at day 7 of culture for all the studied conditions, which agrees with the fact that it constitutes an early regulator of the chondrogenic differentiation process.

Finally, analyzing hypertrophic marker expression, it can be seen how for collagen type X we observe a peak of expression at day 27 for collagen hydrogels cultured in growth medium and for hydrogels containing glycosaminoglycans cultured in chondrogenic medium. This agrees with the fact that hypertrophy occurs at late stages of chondrogenesis. For hydrogels containing glycosaminoglycans cultured in growth medium and for collagen hydrogels cultured in chondrogenic medium, COL10 expression is sustained along time, and it can be seen how its expression is lower for those hydrogels containing GAGs and cultured in growth medium. Thus, collagen type X expression indicates that chondrogenesis is taking place, as its presence is restricted to chondrocyte ECM. It could be considered adding more signaling factors apart from GAGs to the hydrogel matrix, that enhance chondrogenic marker expression in growth medium while maintaining low levels of hypertrophy.

As for RUNX2, its expression is sustained for all the studied conditions except for those hydrogels containing GAGs cultured in growth medium, for which a peak of expression can be observed at day 7. This agrees with the sustained expression of COL10 for this type of formulation when maintained in growth medium. As RUNX2 is a regulator of collagen type X expression, its early expression at day 7 may cause a sustained expression of COL10.

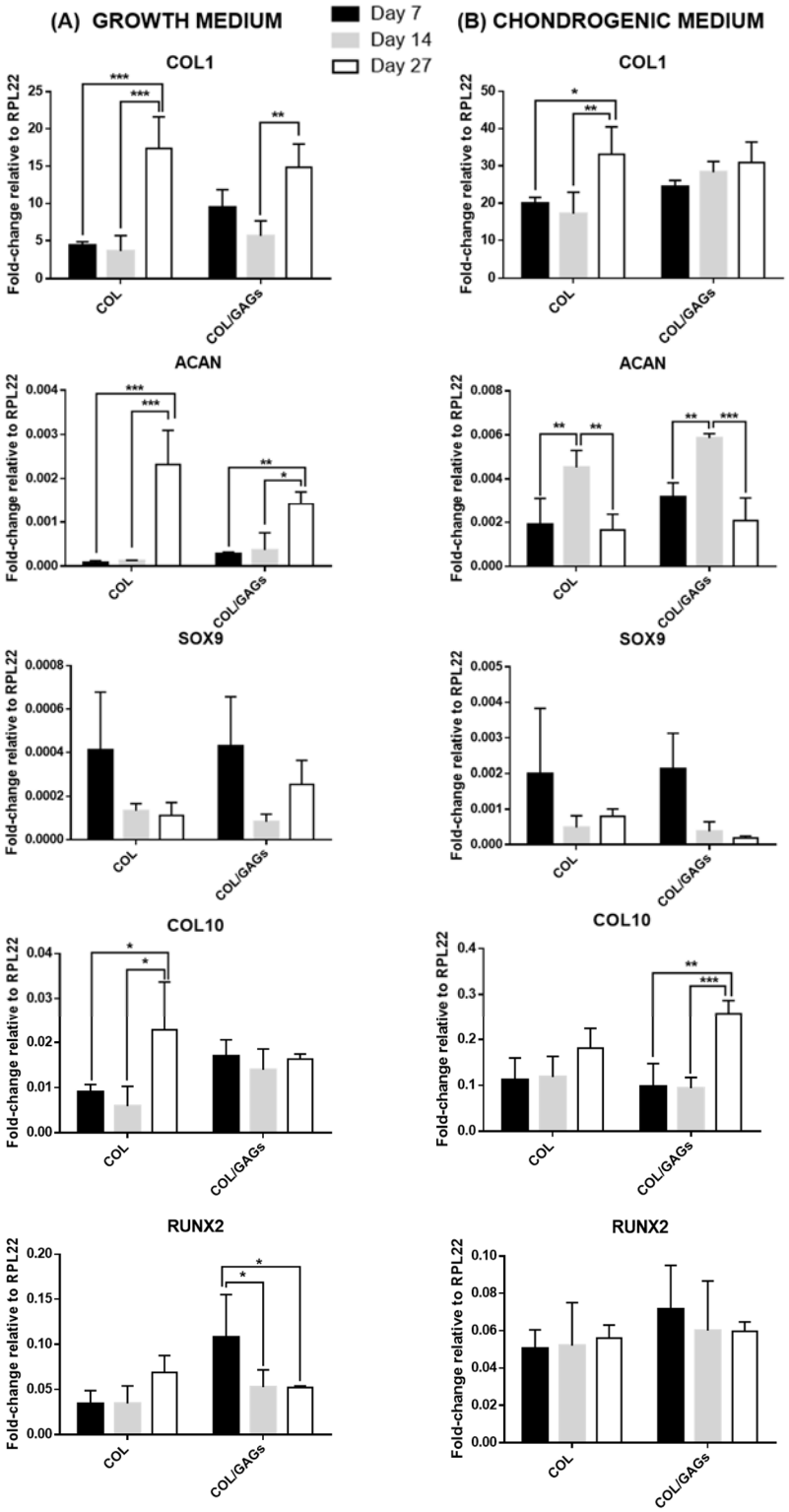

Figure IV-14. Expression kinetics of the analyzed genes: Gene expression in ADMSCs cultured for 1, 2 and 3 weeks in both **(A)** growth and **(B)** chondrogenic medium in collagen (COL) and collagen/hyaluronic acid/ chondroitin sulfate (COL/GAGs) hydrogels. C_t values relative to ribosomal protein L22 (RPL22) are represented. (Statistical differences are indicated as: * for $p < 0.05$, ** for $p < 0.01$, and *** for $p < 0.001$, Two-way ANOVA, n = 3).

Next, we present the results of expression normalized to collagen hydrogels (Figure IV-15), to gain a deeper insight in the effect of the presence of both hyaluronic acid and chondroitin sulfate in the hydrogel formulation.

It can be seen how the expression of collagen type I is overexpressed in hydrogels containing glycosaminoglycans in both growth and chondrogenic medium, except after 27 days of culture. Thus, this provides evidence that for ADMSCs the presence of GAGs is not enough to restrain fibrocartilage formation. The addition of extra signaling biochemical cues could be considered to try to avoid this undesired effect.

Interestingly, aggrecan expression is upregulated for those hydrogels containing glycosaminoglycans, and its effect is more evident for those samples maintained in growth medium. The fact that aggrecan expression is downregulated at day 27 for those samples cultured in growth medium can be attributed at the fact that for collagen hydrogels the differentiation process takes place slowly, and the expression of aggrecan at late points for this type of matrix is higher.

SOX9 appears to be upregulated after 7 days of culture, again, it can be attributed to the fact that it is an early marker of the chondrogenic process. The downregulation observed at later time points can be due to the same reason than aggrecan, as the differentiation process in collagen matrices is slower, it can be expected that the expression of the gene is higher at late culture times.

As for hypertrophic markers, it is interesting that COL10 is downregulated for those samples cultured in chondrogenic medium at both day 7 and day 14. As stated for the results obtained using hNDFs, a further analysis using histologic techniques should be conducted in order to assess the quality of the obtained tissue.

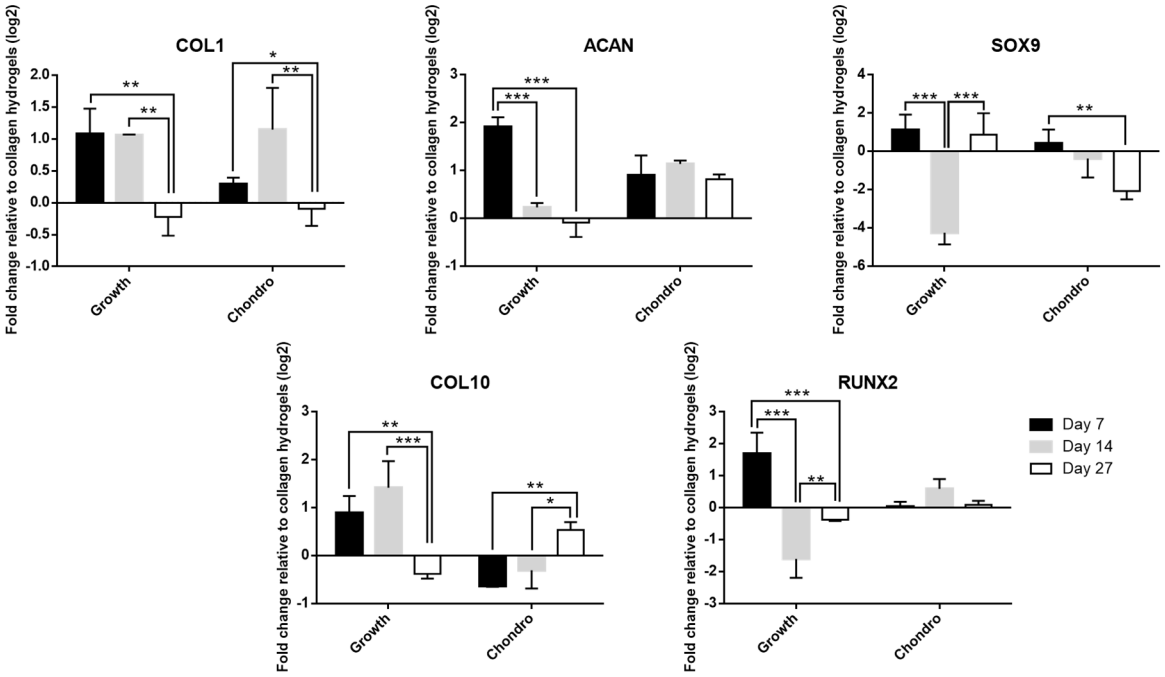

Figure IV-15. qPCR results for chondrogenic markers. Gene expression in ADMSCs cultured for 1, 2 and 3 weeks in both growth and chondrogenic medium in collagen/hyaluronic acid/ chondroitin sulfate hydrogels. C_t values relative to ribosomal protein L22 (RPL22) are represented relative to collagen hydrogel cultures. (Statistical differences are indicated as: * for $p < 0.05$, ** for $p < 0.01$, and *** for $p < 0.001$, Two-way ANOVA, n = 3).

So far, we have demonstrated how the hydrogel formulations not only allow cell migration and colonization, but also allow the expression of chondrogenic markers when cultured under chondrogenic induction, and for some genes, the expression levels reached are significant even when no chemical signaling is added to the culture medium. Therefore, in the following lines we will focus on the study of the osteogenic potential of the hydrogel formulations, the effect of using an induction medium as well as the effect of the presence of glycosaminoglycans in the hydrogel matrix.

4.3.4 Assessment of the osteogenic potential of the hydrogel formulation over adipose-derived mesenchymal stem cells

As already mentioned, in order to achieve a complete regeneration of the osteochondral unit it is critical to enable subchondral bone repair, as well as to promote the creation of a hypertrophic calcified cartilage layer. Therefore, we present a study of the osteogenic potential of the designed hydrogel formulation. From the obtained results, we tailor the hydrogel matrix composition in order to create a signaling gradient and induce a certain cell response depending on cell position through the hydrogel structure.

First, to evaluate the effect of the osteogenic medium over ADMSC's, we studied the presence of calcium deposits after 21 days of culture in monolayer cultures maintained in both growth and osteogenic medium. To do so, we performed an alizarin red staining (Figure IV-16). As it can be seen, when cells are cultured in osteogenic medium (Figure IV-16B), the presence of calcium deposits can be clearly appreciated as reddish spots, while in those cultures maintained in growth medium (Figure IV-16A) mineralization does not occur.

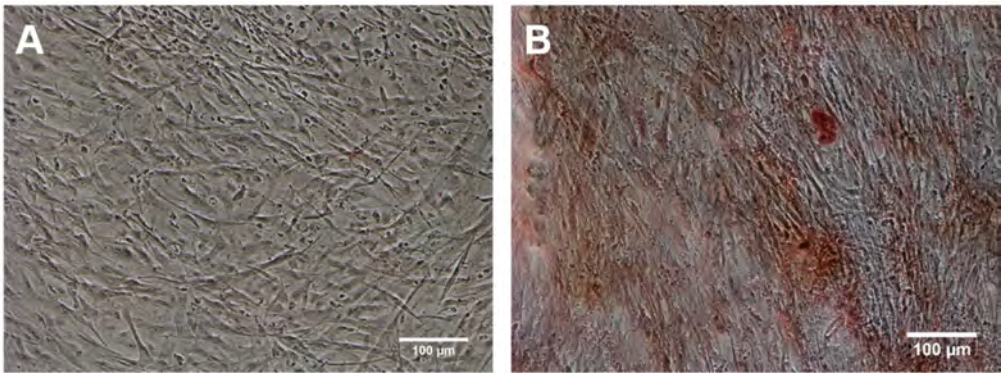

Figure IV-16. Alizarin red staining of a monolayer adipose-derived mesenchymal stem cells in: **(A)** growth medium and **(B)** osteogenic medium after 21 days of culture. (Calcium deposits appear stained red).

Next, an alizarin red staining of 3D cultures in both collagen and collagen/glycosaminoglycans hydrogels and both growth and osteogenic medium was performed (Figure IV-17). As it can be appreciated, both samples cultured in osteogenic medium presented an intense reddish color and calcifications can be clearly appreciated.

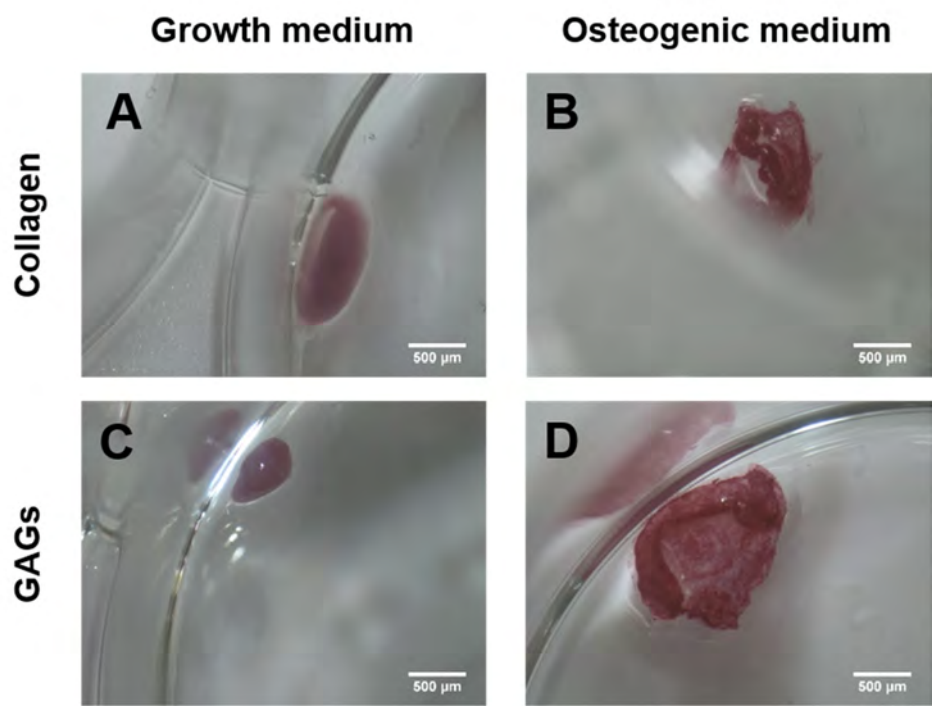

Figure IV-17. Alizarin red staining of an ADMSCs cultures in collagen and collagen / glycosaminoglycans hydrogels cultured in both growth and osteogenic medium at day 21 of culture. (Calcium deposits appear stained red).

The obtained results show how under an osteogenic environment matrix mineralization takes place while when samples are maintained under growth conditions the phenomenon does not occur, as it happened for hNDFs cultures. The fact that we are able to avoid mineralization under growth conditions, enables us to trigger the process only when it is desired. Thus, by using the appropriate signaling we can either trigger or avoid osteogenesis process.

Thus, after having demonstrated that the osteogenic medium is able to induce mineralization, we proceed with the analysis of different osteogenic markers by real time RT-PCR. Figure IV-18 and Figure IV-19 show the expression of the studied genes after 1, 2 and 3 weeks of culture relative to ribosomal protein L22 (RPL22) for three-dimensional cultures, cultured both in growth and osteogenic medium. From these results, we can analyze if there is expression or not of the selected markers, as well as determine its peak of expression over the studied time points comparing both types of formulations and cell culture media. First, Table IV-8 summarizes the observed peak of expression for the analyzed genes.

Table IV-8. Peak of expression of osteogenic genes for both collagen and collagen/glycosaminoglycans formulations cultured in both growth and osteogenic medium.

Gene	Growth medium		Osteogenic medium	
	Collagen	**Collagen / GAGs**	**Collagen**	**Collagen / GAGs**
ALP	day 14	sustained	day 14	Day 14
OSN	Sustained	day 14 / day 21	day 14	day 14
DLX5	Day 21	Day 21	Day 21	Day 21
RUNX2	Sustained	Sustained	Day 7 / day 14	sustained
OSX	Day 21	day 21	Day 21	sustained
OCN	Sustained	Sustained	sustained	Day 14
COL1	Sustained	Day 14 / day 21	Day 14	Day 14

As for alkaline phosphatase expression (ALP), it can be seen how it presents a peak of expression at day 14 for all the studied conditions except for those hydrogels containing glycosaminoglycans maintained in growth medium, for which ALP expression is sustained. It can be seen how its expression is slightly higher for those samples cultured in osteogenic medium. Although alkaline phosphatase is a ubiquitous protein and its presence is not restricted to bone tissue, it has been reported how it may act as an early indicator of cellular activity and osteogenic differentiation.

OSN, is not bone specific either, however constitutes one of the most abundant non-collagenous protein expressed in mineralized tissues[22]. For those samples cultured in osteogenic medium, its expression presents a peak after 14 days of culture, while for the other conditions is nearly sustained. Its level of expression is nearly the same for those samples cultured in growth and those cultured in osteogenic medium. Thus, we can conclude that the presence of chemical signaling has no effect over its expression in the studied hydrogel formulations.

RUNX2 is regarded as the master regulator of osteogenesis, however it is not bone specific. It can be seen how its expression is sustained for all the studied conditions, except for collagen hydrogels cultured in osteogenic medium, for which its expression decreases at day 21.

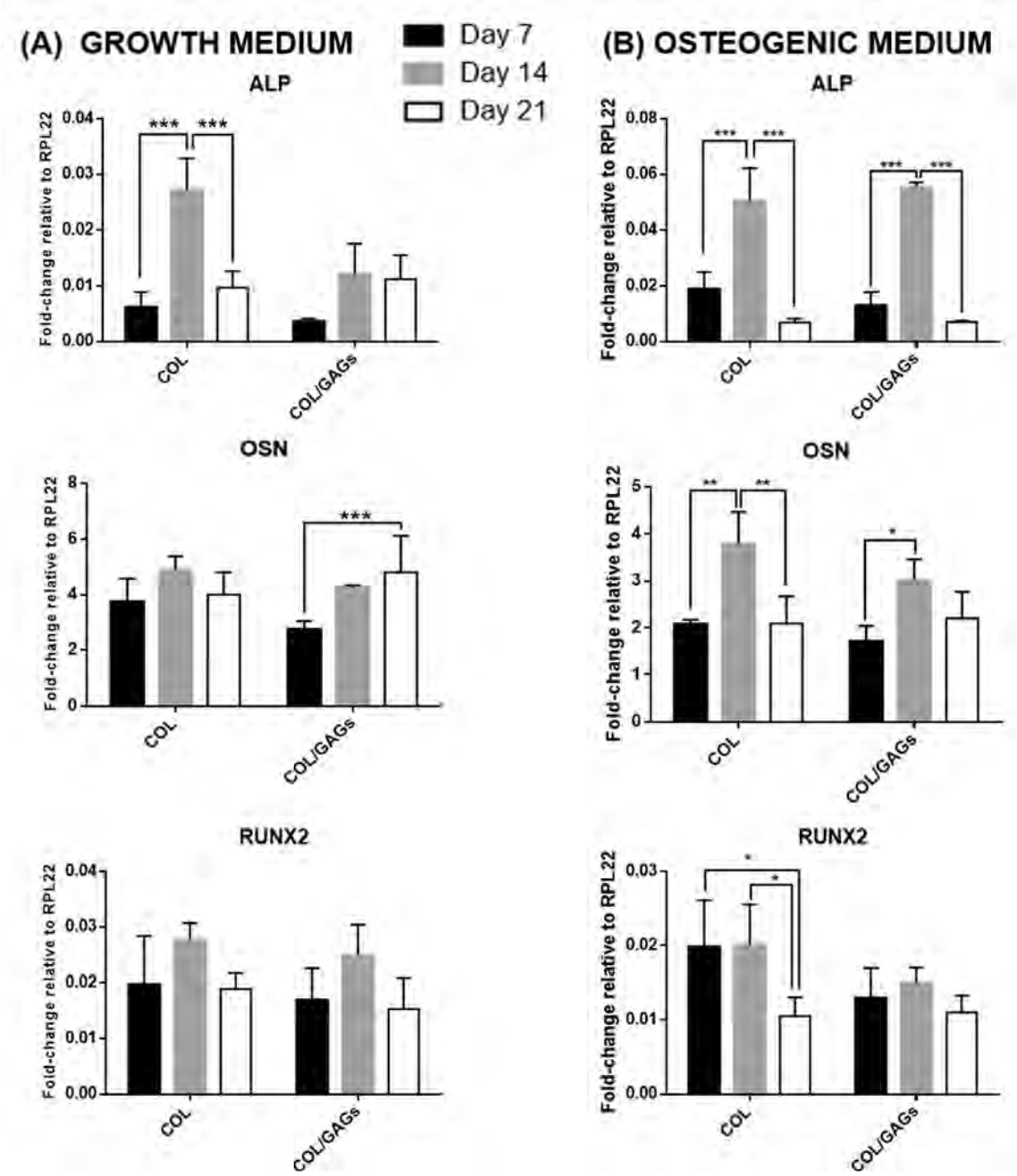

Figure IV-18. Expression kinetics of the analyzed genes. Gene expression in ADMSCs cultured for 1, 2 and 3 weeks in both **(A)** growth and **(B)** osteogenic medium in collagen (COL) and collagen/hyaluronic acid/ chondroitin sulfate hydrogels (COL/GAGs). C_t values relative to ribosomal protein L22 (RPL22) are represented. (Statistical differences are indicated as: * for $p < 0.05$, ** for $p < 0.01$, and *** for $p < 0.001$, Two-way ANOVA, n = 3).

Next, Figure IV-19, shows the expression of osterix (OSX) and osteocalcin (OCN) two bone-specific markers, and of collagen type I (COL1) which, as already mentioned, is one of the main constituents of bone matrix.

As for osterix (OSX), it can be seen how it presents a peak of expression after 3 weeks of culture. It appears to be slightly higher for collagen hydrogels, which may indicate that the presence of glycosaminoglycans in the hydrogel formulation may be detrimental for osteogenic differentiation process. Osteocalcin (OCN) expression is sustained over time except for those samples containing GAGs and maintained in osteogenic medium, for which the expression presents a peak at day 14. The expression is similar for those samples cultured in growth and osteogenic medium. As for, collagen type I it can be seen how its expression is higher for those samples maintained in growth medium, and a peak of expression is observed at day 14 of cultures for almost all the studied conditions.

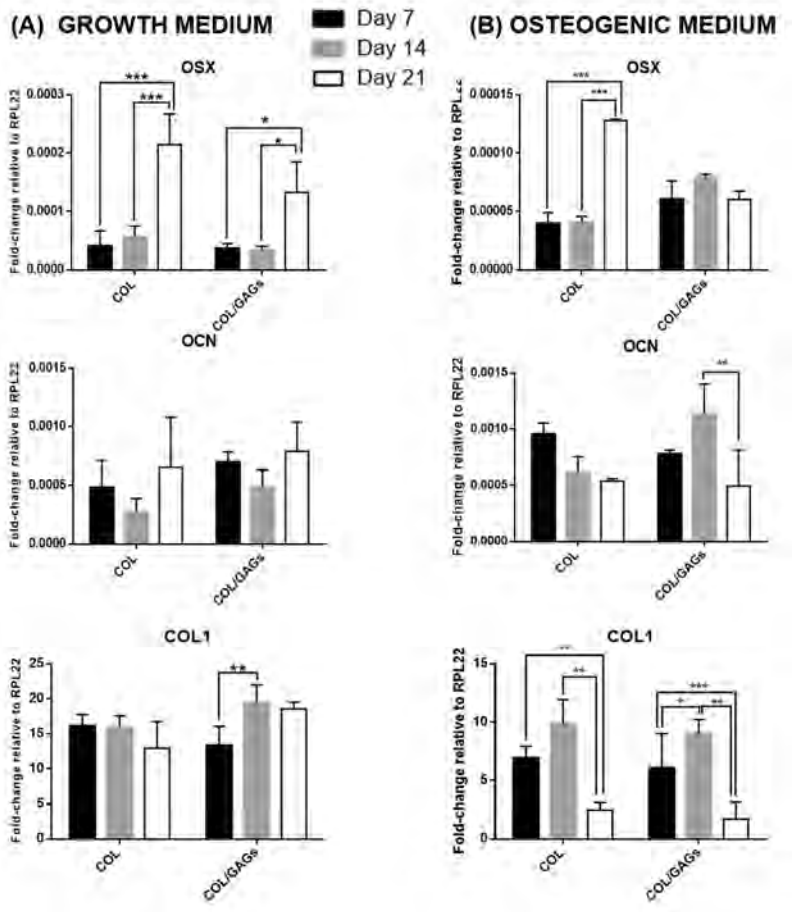

Figure IV-19. Expression kinetics of the analyzed genes (continuation). Gene expression in ADMSCs cultured for 1, 2 and 3 weeks in both **(A)** growth and **(B)** osteogenic medium in collagen (COL) and collagen/hyaluronic acid/ chondroitin sulfate hydrogels (COL/GAGs). C_t values relative to ribosomal protein L22 (RPL22) are represented. (Statistical differences are indicated as: * for $p < 0.05$, ** for $p < 0.01$, and *** for $p < 0.001$, Two-way ANOVA, n = 3).

Next, Figure IV-20 shows gene expression results for the analyzed genes with respect to collagen hydrogels, which give us insight on the effect of the presence of both hyaluronic acid and chondroitin sulfate in the hydrogel formulation. As it can be appreciated, generally we observe downregulation of most of the genes for formulations containing GAGs with respect of hydrogels made of collagen. Thus, it can be hypothesized that the presence of hyaluronic acid and chondroitin sulfate has a negative effect over osteogenesis of adipose-derived mesenchymal stem cells. These results open the doors to achieve a distinct cell behavior along the hydrogel structure by tailoring hyaluronic acid and chondroitin sulfate concentration through the scaffold. Moreover, as the designed hydrogel matrix shows a great versatility and can be easily tuned, the introduction of concentration gradients of more specific signaling biomolecules could be considered.

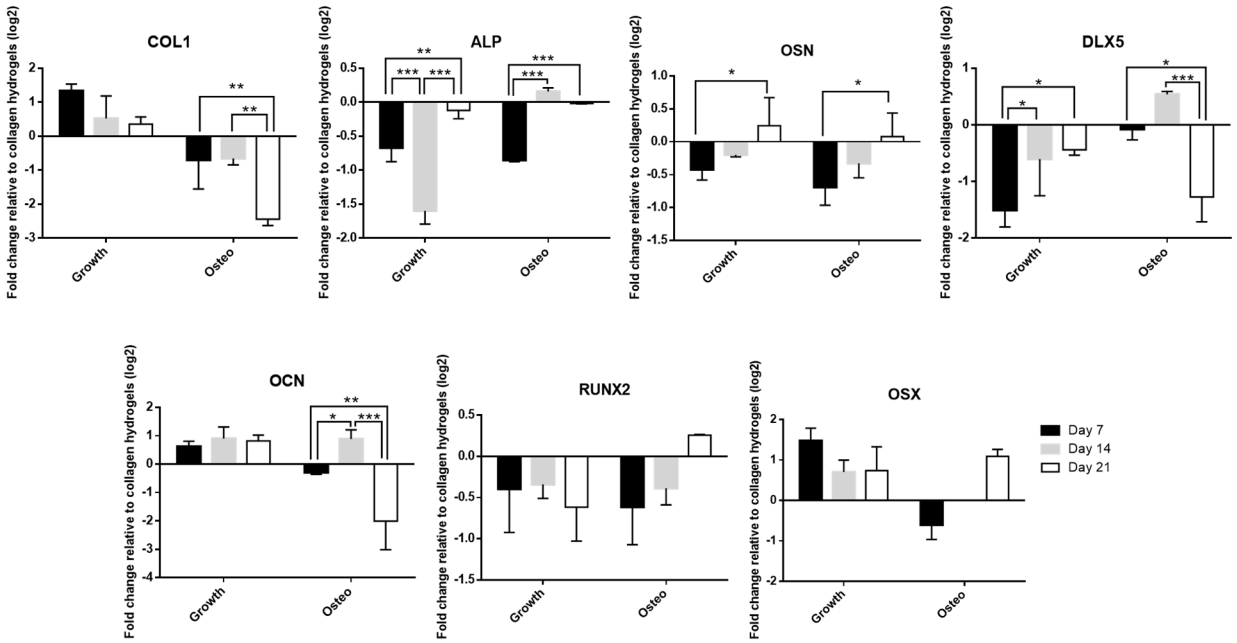

Figure IV-20. qPCR results for chondrogenic markers. Gene expression in ADMSCs cultured for 1, 2 and 3 weeks in both growth and osteogenic medium in collagen/hyaluronic acid/ chondroitin sulfate hydrogels. C_t values relative to ribosomal protein L22 (RPL22) are represented relative to collagen hydrogel cultures. (Statistical differences are indicated as: * for $p < 0.05$, ** for $p < 0.01$, and *** for $p < 0.001$, Two-way ANOVA, n = 3).

To sum up, in the present chapter, we have demonstrated how cell migration and hydrogel colonization can take place through the designed hydrogel matrix. Moreover, it has been seen how the expression of some chondrogenic markers is enhanced by the presence of glycosaminoglycans in the hydrogel formulation, as well as it seems that the addition of GAGs delays hypertrophy. On the contrary, for osteogenic differentiation, it has been seen how both hyaluronic acid and chondroitin sulfate seem to have a negative effect over the process. Thus, a simultaneous chondrogenic and osteogenic differentiation could be achieved by the creation of chemical gradients.

4.4 Concluding remarks

In the present chapter, we have demonstrated the cell homing potential of the designed hydrogel formulation as well as its both chondrogenic and osteogenic potential. As already mentioned, scaffolding techniques for the repair of osteochondral lesions are often combined with subchondral bone stimulation techniques, to promote migration of mesenchymal stem cells from the subchondral plate towards the defect site. Thus, it is critical that the designed scaffold allows cell migration and colonization, and that provides a suitable environment for cell differentiation.

As for cell homing potential, we have presented the results obtained for both a vertical and a horizontal experimental setup. First, we have studied cell migration through collagen and collagen/glycosaminoglycans hydrogels using a vertical setup. Cells were allowed to proliferate for 11 days and images obtained with confocal microscopy show how at the end of the experiment cells were distributed through the hydrogel structure, as migration has taken place. Differences in cell density on the top of the hydrogel at day 1 of culture reveal the higher degree of reticulation of hydrogels containing GAGs. Moreover, thanks to second harmonic generation we have been able to see differences in collagen fiber organization depending on the presence of glycosaminoglycans in the hydrogel formulation. Next, in order to eliminate the effect of gravity we designed a horizontal setup and repeated the experiment in both growth and chondrogenic medium. We demonstrated how cells migrate towards the hydrogel structure and begin its colonization. Cells under chondrogenic induction exhibited morphologic changes as they underwent differentiation.

Moreover, in the present chapter an evaluation of both chondrogenic and osteogenic potential of the hydrogel formulation has been presented.

As first approach, we assessed the transdifferentiation of hNDFs embedded in both collagen and collagen/GAGs hydrogels. Western blot results revealed the presence of collagen type II for collagen and collagen/GAGs hydrogels under chondrogenic induction after 50 days of culture. Moreover, we have analyzed the expression of different chondrogenic marker genes through RT-PCR. We have detected expression of both ACAN and COL2, two of the main constituents of the cartilaginous matrix. It points out that the expression of hypertrophic markers COL10 and RUNX2 is downregulated for those hydrogels containing GAGs, which is a positive effect over the obtention and maintenance of hyaline cartilage. However, further analysis are required to assess the quality of the obtained tissue. Moreover, we have demonstrated how the hydrogel presents a weak mineralization after 50 days of culture in both growth and chondrogenic medium. Mechanical studies performed with DMA show how measured under compression storage modulus (G') reaches values close to those of human hyaline cartilage measured under similar conditions.

Next, the chondrogenic potential of ADMSCs embedded in both collagen and collagen/glycosaminoglycans hydrogel formulation was assessed. The study of the expression of

both chondrogenic and hypertrophic genes has been performed. It has been seen how the presence of GAGs enhances aggrecan expression. Again, as it occurred for hNDFs transdifferentiation process, COL10 expression is downregulated in those hydrogels containing GAGs, which leads us to hypothesize that the presence of hyaluronic acid and chondroitin sulfate could help to maintain hyaline cartilage phenotype and delay the appearance of hypertrophy. However, as already mentioned, the latter has to be confirmed by using, for instance, histologic techniques.

Finally, an assessment of the osteogenic potential of the designed hydrogel formulation has been presented. First, we have demonstrated that we can induce mineralization in both 2D and 3D cultures using an induction medium. Without induction, mineralization does not occur thus, we can trigger the process when desired. Next, different osteogenic marker genes were analyzed by RT PCR. The obtained results show how hyaluronic acid and chondroitin sulfate seem to have a negative effect over osteogenesis, as generally, marker genes appear to be downregulated for those hydrogels containing GAGs.

4.5 References

(1) Yan, L.-P.; Oliveira, J. M.; Oliveira, A. L.; Reis, R. L. Current Concepts and Challenges in Osteochondral Tissue Engineering and Regenerative Medicine. *ACS Biomater. Sci. Eng.* **2015**, *1* (4), 183–200.

(2) Im, G.-I. Regeneration of Articular Cartilage Using Adipose Stem Cells. *J. Biomed. Mater. Res. Part A* **2016**, *104* (7), 1830–1844.

(3) Eslaminejad, M. B. Mesenchymal Stem Cells as a Potent Cell Source for Articular Cartilage Regeneration. *World J. Stem Cells* **2014**, *6* (3), 344.

(4) Xian, C. J.; Foster, B. K. Repair of Injured Articular and Growth Plate Cartilage Using Mesenchymal Stem Cells and Chondrogenic Gene Therapy. *Curr. Stem Cell Res. Ther.* **2006**, *1* (2), 213–229.

(5) Lin, W.; Xu, L.; Zwingenberger, S.; Gibon, E.; Goodman, S. B.; Li, G. Mesenchymal Stem Cells Homing to Improve Bone Healing. *J. Orthop. Transl.* **2017**, *9*, 19–27.

(6) Hoffman, J. K.; Geraghty, S.; Protzman, N. M. Articular Cartilage Repair Using Marrow Stimulation Augmented with a Viable Chondral Allograft: 9-Month Postoperative Histological Evaluation. *Case Rep. Orthop.* **2015**, *2015*, 1–10.

(7) S Dhinsa, B.; B Adesida, A. Current Clinical Therapies for Cartilage Repair, Their Limitation and the Role of Stem Cells. *Curr. Stem Cell Res. Ther.* **2012**, *7* (2), 143–148.

(8) Liu, Y.; Zhou, G.; Cao, Y. Recent Progress in Cartilage Tissue Engineering—Our Experience and Future Directions. *Engineering* **2017**, *3* (1), 28–35.

(9) Stromps, J. P.; Paul, N. E.; Rath, B.; Nourbakhsh, M.; Bernhagen, J.; Pallua, N. Chondrogenic Differentiation of Human Adipose-Derived Stem Cells: A New Path in Articular Cartilage Defect Management? *Biomed Res Int* **2014**, *2014*, 740926.

(10) Walmsley, G. G.; Cheung, A. T. M.; Hu, M. S.; Lorenz, H. P.; Longaker, M. T. Osteogenic Differentiation of Adipose-Derived Stromal Cells: Advancements and Future Directions for Bone Tissue Engineering. *Sci. Proc.* **2016**, 1–6.

(11) Beederman, M.; Lamplot, J. D.; Nan, G.; Wang, J.; Liu, X.; Yin, L.; Li, R.; Shui, W.; Zhang, H.; Kim, S. H.; Zhang, W.; Zhang, J.; Kong, Y.; Denduluri, S.; Rogers, M. R.; Pratt, A.; Haydon, R. C.; Luu, H. H.; Angeles, J.; Shi, L. L.; He, T.-C. BMP Signaling in Mesenchymal Stem Cell Differentiation and Bone Formation. *J. Biomed. Sci. Eng.* **2013**, *6* (August), 32–52.

(12) Calabrese, G.; Giuffrida, R.; Forte, S.; Fabbi, C.; Figallo, E.; Salvatorelli, L.; Memeo, L.;

Parenti, R.; Gulisano, M.; Gulino, R. Human Adipose-Derived Mesenchymal Stem Cells Seeded into a Collagen-Hydroxyapatite Scaffold Promote Bone Augmentation after Implantation in the Mouse. *Sci. Rep.* **2017**, *7* (1), 1–11.

(13) Wang, X.-F.; Song, Y.; Liu, Y.-S.; Sun, Y.-C.; Wang, Y.-G.; Wang, Y.; Lyu, P.-J. Osteogenic Differentiation of Three-Dimensional Bioprinted Constructs Consisting of Human Adipose-Derived Stem Cells In Vitro and In Vivo. *PLoS One* **2016**, *11* (6).

(14) Sun, H.; Liu, Y.; Jiang, T.; Liu, X.; He, A.; Li, J.; Zhang, W.; Liu, W.; Cao, Y.; Zhou, G. Chondrogenic Differentiation and Three Dimensional Chondrogenesis of Human Adipose-Derived Stem Cells Induced by Engineered Cartilage-Derived Conditional Media. *Tissue Eng. Regen. Med.* **2014**, *11* (1), 59–66.

(15) Hamid, A. a; Idrus, R. B. H.; Saim, A. B.; Somasumdaram, S.; Chua, K.-H. Characterization of Human Adipose-Derived Stem Cells and Expression of Chondrogenic Genes during Induction of Cartilage Differentiation. *Clinics* **2012**, *67* (2), 99–106.

(16) Zhang, K.; He, S.; Yan, S.; Li, G.; Zhang, D.; Cui, L.; Yin, J. Regeneration of Hyaline-like Cartilage and Subchondral Bone Simultaneously by Poly(L -Glutamic Acid) Based Osteochondral Scaffolds with Induced Autologous Adipose Derived Stem Cells. *J. Mater. Chem. B* **2016**, *4* (15), 2628–2645.

(17) Horkay, F. Interactions of Cartilage Extracellular Matrix Macromolecules. *J Polym Sci B Polym Phys* **2012**, *50* (24), 1699–1705.

(18) Shi, S.; Wang, C.; Acton, A. J.; Eckert, G. J.; Trippel, S. B. Role of Sox9 in Growth Factor Regulation of Articular Chondrocytes. *J. Cell. Biochem.* **2015**, *116* (7), 1391–1400.

(19) Akiyama, H. Control of Chondrogenesis by the Transcription Factor Sox9. *Mod. Rheumatol.* **2008**, *18* (3), 213–219.

(20) Shen, G. The Role of Type X Collagen in Faciliating and Regulation Endochondral Ossification of Articular Cartilage. *Orthod. Craniofac. Res.* **2005**, *8*, 11–17.

(21) Higashikawa, A.; Saito, T.; Ikeda, T.; Kamekura, S.; Kawamura, N.; Kan, A.; Oshima, Y.; Ohba, S.; Ogata, N.; Takeshita, K.; Nakamura, K.; Chung, U. Il; Kawaguchi, H. Identification of the Core Element Responsive to Runt-Related Transcription Factor 2 in the Promoter of Human Type X Collagen Gene. *Arthritis Rheum.* **2009**, *60* (1), 166–178.

(22) Rosset, E. M.; Bradshaw, A. D. SPARC/Osteonectin in Mineralized Tissue. *Matrix Biol.* **2016**, *52–54*, 78–87.

(23) Tsao, Y.-T.; Huang, Y.-J.; Wu, H.-H.; Liu, Y.-A.; Liu, Y.-S.; Lee, O. Osteocalcin Mediates Biomineralization during Osteogenic Maturation in Human Mesenchymal Stromal Cells.

Int. J. Mol. Sci. **2017**, *18* (1), 159.

(24) Samee, N.; Geoffroy, V.; Marty, C.; Schiltz, C.; Vieux-Rochas, M.; Levi, G.; de Vernejoul, M.-C. Dlx5, a Positive Regulator of Osteoblastogenesis, Is Essential for Osteoblast-Osteoclast Coupling. *Am. J. Pathol.* **2008**, *173* (3), 773–780.

(25) Núñez-Toldrà, R.; Dosta, P.; Montori, S.; Ramos, V.; Atari, M.; Borrós, S. Improvement of Osteogenesis in Dental Pulp Pluripotent-like Stem Cells by Oligopeptide-Modified Poly(ß-Amino Ester)S. *Acta Biomater.* **2017**, *53*, 152–164.

(26) Fernández-muiños, T.; Recha-sancho, L.; Lopez-chicon, P.; Castells-sala, C.; Mata, A.; Semino, C. E. Bimolecular Based Heparin and Self-Assembling Hydrogel for Tissue Engineering Applications. **2015**, *16*, 35–48.

(27) Stott, N. S.; Jiang, T. X.; Chuong, C. M. Successive Formative Stages of Precartilaginous Mesenchymal Condensations in Vitro: Modulation of Cell Adhesion by Wnt-7a and BMP-2. *J. Cell. Physiol.* **1999**, *180* (3), 314–324.

(28) Ghosh, S.; Laha, M.; Mandal, S.; Sengupta, S.; Kaplan, D. L. In Vitro Model of Mesenchymal Condensation during Chondrogenic Development. *Biomaterials* **2009**, *30* (33), 6530–6540.

(29) Bussmann, B. M.; Reiche, S.; Marí-buyé, N.; Castells-sala, C.; Meisel, H. J.; Semino, C. E. Chondrogenic Potential of Human Dermal Fi Broblasts in a Contractile , Soft , Self-Assembling , Peptide Hydrogel. *J Tissue Eng Regen Med* **2013**.

(30) Junker, J. P. E.; Sommar, P.; Skog, M.; Johnson, H.; Kratz, G. Adipogenic, Chondrogenic and Osteogenic Differentiation of Clonally Derived Human Dermal Fibroblasts. *Cells Tissues Organs* **2010**, *191* (2), 105–118.

(31) Hee, C. K.; Nicoll, S. B. Endogenous Bone Morphogenetic Proteins Mediate 1a, 25-Dihydroxyvitamin D3-Induced Expression of Osteoblast Differentiation Markers in Human Dermal Fibroblasts. *J. Orthop. Res.* **2009**, *27* (2), 162–168.

(32) Sommar, P.; Pettersson, S.; Ness, C.; Johnson, H.; Kratz, G.; Junker, J. P. E. Engineering Three-Dimensional Cartilage- and Bone-like Tissues Using Human Dermal Fibroblasts and Macroporous Gelatine Microcarriers. *J. Plast. Reconstr. Aesthetic Surg.* **2010**, *63* (6), 1036–1046.

(33) Blasi, A.; Martino, C.; Balducci, L.; Saldarelli, M.; Soleti, A.; Navone, S.; Canzi, L.; Cristini, S.; Invernici, G.; Parati, E.; Alessandri, G. Dermal Fibroblasts Display Similar Phenotypic and Differentiation Capacity to Fat-Derived Mesenchymal Stem Cells, but Differ in Anti-Inflammatory and Angiogenic Potential. *Vasc. Cell* **2011**, *3*, 1–14.

(34) Singh, M.; Pierpoint, M.; Mikos, A. G.; Kasper, F. K. Chondrogenic Differentiation of Neonatal Human Dermal Fibroblasts Encapsulated in Alginate Beads with Hydrostatic Compression under Hypoxic Conditions in the Presence of Bone Morphogenetic Protein-2. *J. Biomed. Mater. Res. A* **2011**, *98* (3), 412–424.

(35) Nicoll, S. B.; Wedrychowska, a; Smith, N. R.; Bhatnagar, R. S. Modulation of Proteoglycan and Collagen Profiles in Human Dermal Fibroblasts by High Density Micromass Culture and Treatment with Lactic Acid Suggests Change to a Chondrogenic Phenotype. *Connect. Tissue Res.* **2001**, *42* (1), 59–69.

(36) Yates, K. E.; Forbes, R. L.; Glowacki, J. New Chondrocyte Genes Discovered by Chondroinduced Human Fibroblasts. **2004**, *02115*, 41–53.

(37) Chen, S.; Fu, P.; Cong, R.; Wu, H. S.; Pei, M. Strategies to Minimize Hypertrophy in Cartilage Engineering and Regeneration. *Genes Dis.* **2015**, *2* (1), 76–95.

(38) Park, S.; Hung, C. T.; Ateshian, G. A. Mechanical Response of Bovine Articular Cartilage under Dynamic Unconfined Compression Loading at Physiological Stress Levels. *Osteoarthr. Cartil.* **2004**, *12* (1), 65–73.

This page left blank intentionally

Chapter VII

Chapter V. Conclusions

This page left blank intentionally

Conclusions

In this thesis, a collagen-based hydrogel immobilizing technology has been developed and applied to build a heterogeneous osteochondral scaffold with great potential to be used in the treatment of osteoarthritis. The heterogeneous scaffold is composed of a cartilage-like collagen-based hydrogel attached to a bone-like bioceramic platform through a polymeric coating obtained by PECVD. With the developed scaffold we intent to mimic the whole joint structure, from the subchondral bone to the articular surface.

Firstly, in order to gain insight into the bone-like platform design, different commercial bone substitutes have been analyzed and characterized, focusing on their composition and degree of crystallinity. Moreover, both the presence of a PFM coating over hydroxyapatite bioactivity and its ability to covalently bind collagen molecules to form a protein monolayer have been evaluated. The latter is critical to guarantee a stable bond between the bone-like platform and the hydrogel, which will self-assemble onto the bioceramics using the collagen monolayer as anchoring point.

- It has been demonstrated how both composition and degree of crystallinity play a critical role in the bioactivity of the studied bioceramics. It has been seen how bioceramics bioactivity can be tailored by the modification of its β-TCP/HA ratio.

- A hydroxyapatite bioceramic has been successfully coated with PFM by PECVD. It has been demonstrated how the presence of the polymeric coating not only does not prevent the crystallization of calcium phosphates, but also seems to provide nucleation points that promote precipitate formation.

To study the ability of the polymeric coating to bind collagen molecules, QCM-D technique has been used. QCM-D studies of collagen adsorption onto different substrates, stainless steel, hydroxyapatite and PFM-coated stainless steel, have demonstrated how PFM allows the immobilization of a higher amount of collagen molecules. Besides, thanks to the presence of highly reactive ester groups and their high reactivity towards amines, collagen molecules are covalently attached to the PFM coating, and its interaction is not affected by physiological changes such as ionic exchange.

Secondly, it has been demonstrated how collagen fibrillation process can be monitored using QCM-D technique. The effect of the presence of a PFM coating over fibrillation process has been analyzed, as well as the interaction of collagen with both hyaluronic acid and chondroitin sulfate.

- Fiber formation is reflected by dissipation changes while frequency signal remains nearly unaffected. This phenomenon is attributed to the fact that the adsorbed collagen fiber mesh

is not fully coupled to the sensor surface due to its high viscoelasticity and it does not follow sensor's oscillation preventing changes in frequency signal.

- To trigger fibril formation onto non-treated sensors both temperature change and the introduction of a fresh collagen solution are required. When working with PFM-coated sensors, fibrillation process is detected right after the change of temperature, without the need of flowing a fresh collagen solution through the QCM-D chamber. The presence of the PFM-coating allows the immobilization of higher amount of collagen molecules, enabling fiber formation when the temperature reaches physiologic value.

- It has been observed how there is a strong interaction between positively charged collagen molecules and negatively charged GAGs. The QCM-D data shows how a previously adsorbed collagen thin film collapses after the flow of GAG solutions, as the ionic interaction causes the expulsion of water molecules.

In vitro studies to assess the toxicity of both the hydrogel formulation and the immobilization methodology have been performed.

- It has been demonstrated how the composite hydrogel formulation has no toxic effect over cells, as well as the designed encapsulation procedure.

- As for the linking interface, it has been proved that the immobilization protocol does not affect cell viability as the procedure enables the elimination of the cytotoxic group pentafluorophenol.

Moreover, we have demonstrated the versatility of the designed immobilization procedure, as it can be applied over substrates very different in nature such as a collagen membrane, a PTFE membrane and a hydroxyapatite disk.

Finally, we have demonstrated the cell homing capacity of the designed hydrogel formulation as well as its both chondrogenic and osteogenic potential.

- Using a vertical setup, we have demonstrated how cells are able to proliferate and migrate through the hydrogel structure. Thanks to confocal microscopy with multiphoton, and second harmonic generation we have seen how the presence of both hyaluronic acid and chondroitin sulfate lead to a different collagen fiber organization.

- Next, using a horizontal experimental we eliminate the gravity effect, which facilitates cell migration, present in the vertical conformation presented previously. We have demonstrated that cells can migrate and colonize the hydrogel formulation even when they come from a bidimensional culture.

The chondrogenic potential of the hydrogel formulation has been studied using both hNDFs and ADMSCs.

As first approach, we studied the hydrogel potential to induce hNDFs transdifferentiation, and:

- Initial western blot results show how collagen type II, one of the main constituents of the cartilage matrix, is detected when cells are maintained in a chondro-inductive environment, with and without the presence of glycosaminoglycans.

- RT-PCR results reveal that glycosaminoglycans seem to have a positive effect in reducing the expression of hypertrophic markers COL10 and RUNX2 which appear to be downregulated for those formulations containing GAGs. Moreover, mineralization studies reveal how after 50 days of culture constructs are weakly mineralized when cultured both in growth and chondrogenic medium.

- DMA compression studies show how after 30 days of culture G' reach characteristic values of human cartilage tissue, obtained under similar experimental conditions.

Next, due to their potential to be used a stem cell source for regenerative purposes, we assessed the chondrogenic differentiation of ADMSCs embedded in the hydrogel formulation.

- RT-PCR results show how the presence of GAGs enhances aggrecan expression, one of the main constituents of the cartilage matrix.

- As it occurred with hNDFs, the expression of the hypertrophic marker COL10 is downregulated in the presence of hyaluronic acid and chondroitin sulfate.

Finally, an evaluation of the osteogenic potential of the hydrogel formulation over ADMSCs is presented:

- It has been demonstrated how mineralization occurs both in 2D and 3D culture under osteo-inductive conditions. Without induction, mineralization does not take place which is interesting as it gives us control to trigger the process when desired.

- RT-PCR analysis of osteogenesis marker genes reveals how the presence of GAGs seem to have a negative effect over osteogenesis. Generally, osteogenic marker genes appear to be downregulated in the presence of both hyaluronic acid and chondroitin sulfate.

This page left blank intentionally

List of Publications and Presentations

Publications and Patents

Anna Mas-Vinyals, Salvador Borrós, **"Cell homing, chondrogenic and osteogenic potential of the collagen-based hydrogel formulation"**. Advanced healthcare materials. (Prepared for submission)

Anna Mas-Vinyals, Joan Gilabert-Porres, Salvador Borrós, **"Improving the linking interface between collagen-based hydrogels and bone-like substrates"**. Langmuir. (Prepared for submission)

A. Mas, S. Borrós, **"Bioactivity evaluation of commercial calcium phosphate-based bioceramics for bone regeneration"**. Afinidad LXXII. Vol. 73, No. 575, pp. 170-174, June – September 2016

Seminars and Courses

Anna Mas-Vinyals, Laura Figueras-Esteve, Salvador Borrós. **"Specific Differentiation of Adipose Derived Mesenchymal Stem Cells in a Structured Scaffold"** 2018 eCM XVIII: Cartilage & Disc: Repair and Regeneration. June 2018. Davos, Switzerland. Poster presentation.

Anna Mas-Vinyals, Salvador Borrós. "**Scaffold design proposal for osteochondral tissue engineering"**. 19th. World Congress of the International Cartilage Repair Society. September 2016. Sorrento, Italy. Poster presentation.

Anna Mas-Vinyals, Salvador Borrós. **"New design proposal for mimic de joint structure between bone and hyaline cartilage"**. 9ª Trobada de Joves Investigadors dels Països Catalans. February 2016. Perpignan, France. Oral presentation.